9950-426

UNIVERSITY OF ARKANSAS

Evaluation of Aircraft Microwave Data For Locating Zones For Well Stimulation and Enhanced Gas Recovery

Final Report

by

H. MacDonald
W. Waite
C. Elachi
R. Babcock
R. Konig
J. Gattis
M. Borengasser
D. Tolman

University of Arkansas
Fayetteville, Arkansas 72701

January, 1980

(NASA-CR-163710) EVALUATION OF AIRCRAFT MICROWAVE DATA FOR LOCATING ZONES FOR WELL STIMULATION AND ENHANCED GAS RECOVERY Final Report (Arkansas Univ.) 130 p HC A07/MF A01 CSCL 08G G3/43
N81-11437
Unclas
29176

Prepared for the

JET PROPULSION LABORATORY,
CALIFORNIA INSTITUTE
OF TECHNOLOGY

Under JPL Contract No. 955048

EVALUATION OF AIRCRAFT MICROWAVE DATA FOR LOCATING ZONES FOR WELL STIMULATION AND ENHANCED GAS RECOVERY

FINAL REPORT

By

H. MacDonald, W. Waite, C. Elachi, R. Babcock, J. Gattis
R. Konig, M. Borengasser, and D. Tolman

January 1980

University of Arkansas
Fayetteville, Arkansas

This work was performed for the Jet Propulsion Laboratory,
California Institute of Technology under Contract No. 955048

CONTENTS

I. INTRODUCTION 1

II. LOCATION AND GEOLOGY OF ARKOMA BASIN 4

III. PREVIOUS INVESTIGATIONS 9

A. Linear Terminology 9

B. Linear Analysis and Geologic Significance . . 11

IV. SURFACE JOINT STUDIES 14

A. Data Collection 14

B. Fracture System Origins 16

C. Joint Parameter Analysis 20

V. LINEAR REMOTE SENSOR ANALYSIS 24

A. Side-Looking Airborne Radar (SLAR) and Stereo Photography 25

1. Existing Radar Data (SLAR) 25

2. Aerial Photography 25

B. Radar (SAR) and Enhanced Landsat 28

1. Computer Processing and Enhancement . . . 28

a. Radar Image Processing 28

b. Landsat Image Processing 35

c. Radar/Landsat Composite 38

2. Evaluation of Enhancement Techniques . . . 38

a. Landsat-Band Comparison 38

b. Enhanced Color--Standard Color Comparison 41

c. Synthetic Aperture Radar--L-Band . . . 42

d. Radar/Landsat Merge 44

CONTENTS--Continued

e. Radar and Radar/Landsat Evaluation . . 46

f. Operator Variability 52

VI. PROXIMITY ANALYSIS--LINEARS 53

A. Southern Region 58

1. Density Analysis 60

2. Proximity Analysis 61

B. Northern Region 63

1. Density Analysis 68

2. Proximity Analysis 73

C. Practical Application 79

1. Batson Field 79

2. Rock Creek Field 81

3. Data Anlaysis 84

VII. GEOPHYSICAL STUDIES 87

A. Gravity and Magnetic Studies 87

1. Location and Data Collection 88

2. Data Analysis 90

B. Results 91

VIII. SEASAT 92

IX. SUMMARY AND CONCLUSIONS 92

X. RECOMMENDATIONS 96

XI. REFERENCES 98

XII. APPENDIX 105

LIST OF TABLES

Table

1. Landsat winter--Gaussian stretch 39
2. Landsat winter--uniform distribution stretch . . . 39
3. Landsat summer--Gaussian stretch 40
4. Landsat summer--uniform distribution stretch . . . 40
5. Landsat winter 42
6. Landsat summer 42
7. Linear-operator variation 43
8. Enhanced radar 44
9. Radar plus Landsat 45
10. Modified area histograms 45
11. Induced hydraulic fracturing linear density comparison 61
12. Comparison of linear areas 64
13. Half-quads and density measurements 69
14. Data used for Pearson correlation coefficient for linear density 71
15. Pearson correlation coefficient - density 72
16. Data used for Pearson correlation coefficient for linear distance 74
17. Pearson correlation coefficient - distance 78

LIST OF ILLUSTRATIONS

Figure

1. Location of Arkoma basin 5
2. Location of test site 6
3. Landsat mosaic, winter scene showing prominent northeast-southwest-trending topographic lineaments 8
4. Joint orientations--Arkoma basin 15
5. Examples of orthogonal jointing in the Arkoma basin 17
6. Examples of plumost structures on systematic joint faces 17
7. Joint provinces of Arkoma basin 21
8. Results of operator variability study--stereo photography 27
9. Landsat winter scene, ID 5261-15490 48
10. Landsat summer scene, ID 0861-15515 49
11. SAR swath configuration, April, 1978 imagery . . 51
12. SAR swath configuration, May, 1977 imagery . . . 51
13. Linears from Landsat winter scene, band 7, IPCOF (initial production calculated open flow) indicated 54
14. Linears from SAR L-band radar and well locations with IPCOF (initial production calculated open flow) indicated 56
15. Format for rectangular window computer output 62
16. Half-quad subdivision, northern region. Linears from Landsat winter scene band 7 65
17. Linears detected from Landsat analysis, well locations with initial production, Batson field 80

LIST OF ILLUSTRATIONS--Continued

Figure

18. Structure contour map for the top of the Boone Formation, Batson Field 82

19. Linears detected from Landsat analysis, well locations with initial production, Rock Creek field 83

20. Structure contour map for the top of the Boone Formation, Rock Creek field 85

21. Geophysical survey site locations, Landsat mosaic, winter scene 89

This report contains information prepared by the University of Arkansas under JPL sub-contract. Its content is not necessarily endorsed by the Jet Propulsion Laboratory, California Institute of Technology, or the National Aeronautics and Space Administration.

ABSTRACT

The purpose of this investigation is to evaluate imaging radar as an adjunct to conventional petroleum exploration techniques, especially linear mapping. Linear features were mapped from several remote sensor data sources including stereo photography, enhanced Landsat imagery, SLAR radar imagery, enhanced SAR radar imagery, and SAR radar/Landsat combinations. Linear feature maps were compared with surface joint data, subsurface and geophysical data, and gas production in the Arkansas part of the Arkoma basin.

The best Landsat enhanced product for linear detection is found to be a winter scene, band 7, uniform distribution stretch. Of the individual SAR data products, the VH (cross-polarized) SAR radar mosaic provides for detection of most linears; however, none of the SAR enhancements is significantly better than the others. Radar/Landsat merges may provide better linear detection than a single-sensor mapping mode, but because of operator variability the results are inconclusive. Radar/Landsat combinations appear promising as an optimum linear mapping technique, if the advantages and disadvantages of each remote sensor are considered.

Although interpreters generally agreed on the orientation of major linear trends, they differed greatly on other parameters, such as total number, average length, and coincidence of linears. Mapping of relative concentrations of linears (density) appears to be somewhat less influenced by operator variability.

In the southern region of the Arkansas Arkoma basin, little relationship is discernible between surface structure and gas production, and no correlation is found between gas production and linear proximity or linear density as determined from remote sensor data. However, in the northern Arkoma basin, a positive correlation is found between linear density and gas production from a high-chert-content carbonate reservoir. Linear density analysis should not be the single basis for petroleum exploration on the northern flank of the Arkoma basin. Regional and local structural position and surface joint orientation are equally important data sets to be evaluated in an exploration program. However, the probability of economic savings in the exploration for fractured reservoirs in other parts of the work can be significant if linear density maps, derived from radar and Landsat merges, are used to target prospects for further geological and geophysical investigations.

I. INTRODUCTION

The space program has confirmed that most remote sensing techniques previously proved useful from aircraft altitudes have equal or greater value from orbital altitudes. Landsat imaging systems have been used to demonstrate that earth observations from space can provide valuable information for the exploration and management of energy and mineral resources. However, even a brief review of the present state-of-the-art of earth resource exploration from space shows that an improvement must be made in spaceborne observing and measuring techniques. Present remote sensor technology for geologic exploration is simply inadequate to aid in the discovery of sufficient new reserves to satisfy the accelerating demand for petroleum and natural gas. NASA has recognized this fact and several satellites and space missions are being readied for launch during the next few years to take advantage of new sensor technology. New sensors are being designed that are adapted more specifically to the earth resources applications. Spaceborne microwave systems appear to have immediate application for geologic mapping.

During the past two decades the petroleum industry has shown increasing interest in fractured reservoirs because many of the world's oil and gas fields have reservoirs in which porosity and, perhaps more important, permeability

are fracture controlled. Knowledge of fracture control in a reservoir not only aids the primary recovery of hydrocarbons but also guides the design of well stimulation and enhanced recovery programs. Because fractures are commonly propagated upward and reflected at the earth's surface as subtle linears, detection of these surface features is extremely important in many phases of petroleum exploration and development.

As an adjunct to field investigations, various remote sensor techniques have been used for fracture analysis and geologic reconnaissance surveys. Photography has been the most useful survey system because its application has been refined, and a great number of people are experienced in analyzing the images obtained. From the vantage point of the aerial camera, geologists have been able to obtain fracture information that is not readily discerned from the ground. However, within the last decade, a variety of more sophisticated remote sensors have been used in geologic studies. More recently, Landsat satellites have provided the impetus for renewed interest in linear tectonics.

Very little research has been devoted to assessing the geologic linear mapping capability of radar imagers, though such mapping has received considerable attention in relation to visible and near-visible spectrum sensors. The linear mapping potential of multifrequency imaging radars from satellites appears to be very promising for petroleum

exploration, especially in the United States. Active remote sensors such as multifrequency imaging radars now are being recognized as the next logical and perhaps the most sophisticated sensor package to be placed in space. These microwave remote sensors could have a significant impact on petroleum exploration in the next decade.

To document the utility of microwave analysis for petroleum exploration, the Arkansas part of the Arkoma basin was selected as a prime test site. The research plan included comparison of aircraft microwave imagery, stereo photography, and Landsat imagery in an area where significant subsurface borehole geophysical data were available. The test site provides contrasting rock types and structures in an area where surface cover includes cropland and deciduous, coniferous, and mixed forest types. There is little discernible relationship between structure and gas production in the area, and stratigraphic entrapment appears to be the primary factor influencing the presence of gas.

Space imaging radar systems will provide the longest wavelengths of the family of instruments used for sensing the electromagnetic radiation reflected or emitted from the earth's surface. These microwave systems should yield unique terrain data to facilitate geologic interpretation and thus will provide an important new technique for petroleum exploration. In anticipation of Space Shuttle programs for the 1980s, radar systems should be evaluated as an adjunct

to conventional petroleum exploration techniques, especially linear-lineament mapping. Such an evaluation is the overall objective of the program described in this report.

Subobjectives include:

1) Compilation of linear features maps from appropriate remote sensor data sets.

2) Comparison of linear features maps with surface joint data, subsurface structure and geophysical data, and gas productivity.

3) Determination of the relationship between remote sensor linear proximity and density to gas productivity.

4) Definition of optimum remote sensor data set for linear enhancement.

5) Evaluation of the role of operator variability in linear feature mapping.

II. LOCATION AND GEOLOGY OF ARKOMA BASIN

The test site is in northwestern Arkansas, generally within a rectangle bounded by latitudes 35°45'N and 35°07'N and longitudes 94°30'W and 92°45'W, encompassing approximately 11,000 km^2. It includes all of the major gas fields in the Arkansas part of the Arkoma basin. The Arkoma basin is an arcuate structural trough 400 km long extending east-west across central Arkansas and northeast-southwest in eastern Oklahoma (Fig. 1). The basin is typified by imbricate thrust faults in the south and normal faults, monoclines, and east-west-trending anticlines and synclines in the north.

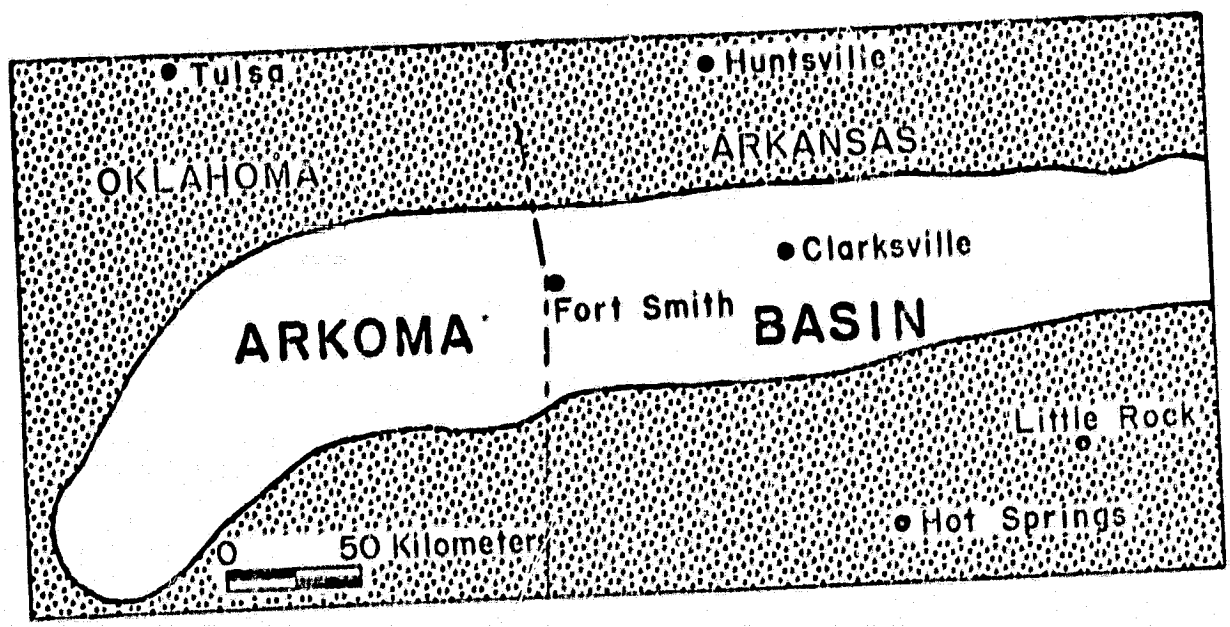

Figure 1. Location of Arkoma basin.

The Arkoma basin ranges in width from 32 to 70 km measured from north to south. It is bounded on the north by the northern Arkansas structural platform and on the south by the Ouachita Mountains (Fig. 2).

The northern Arkansas structural platform, composed of essentially horizontal strata of Mississippian and Pennsylvanian age, trends generally east-west across northwestern Arkansas. Structural features of the platform include low amplitude east-west-trending folds, northeast-southwest-trending normal faults, and east-west-trending faults along the southern margin. Other prominent features of the platform are a series of regional northeast-southwest-trending topographic lineaments (aligned straight stream valley

ORIGINAL PAGE IS
OF POOR QUALITY

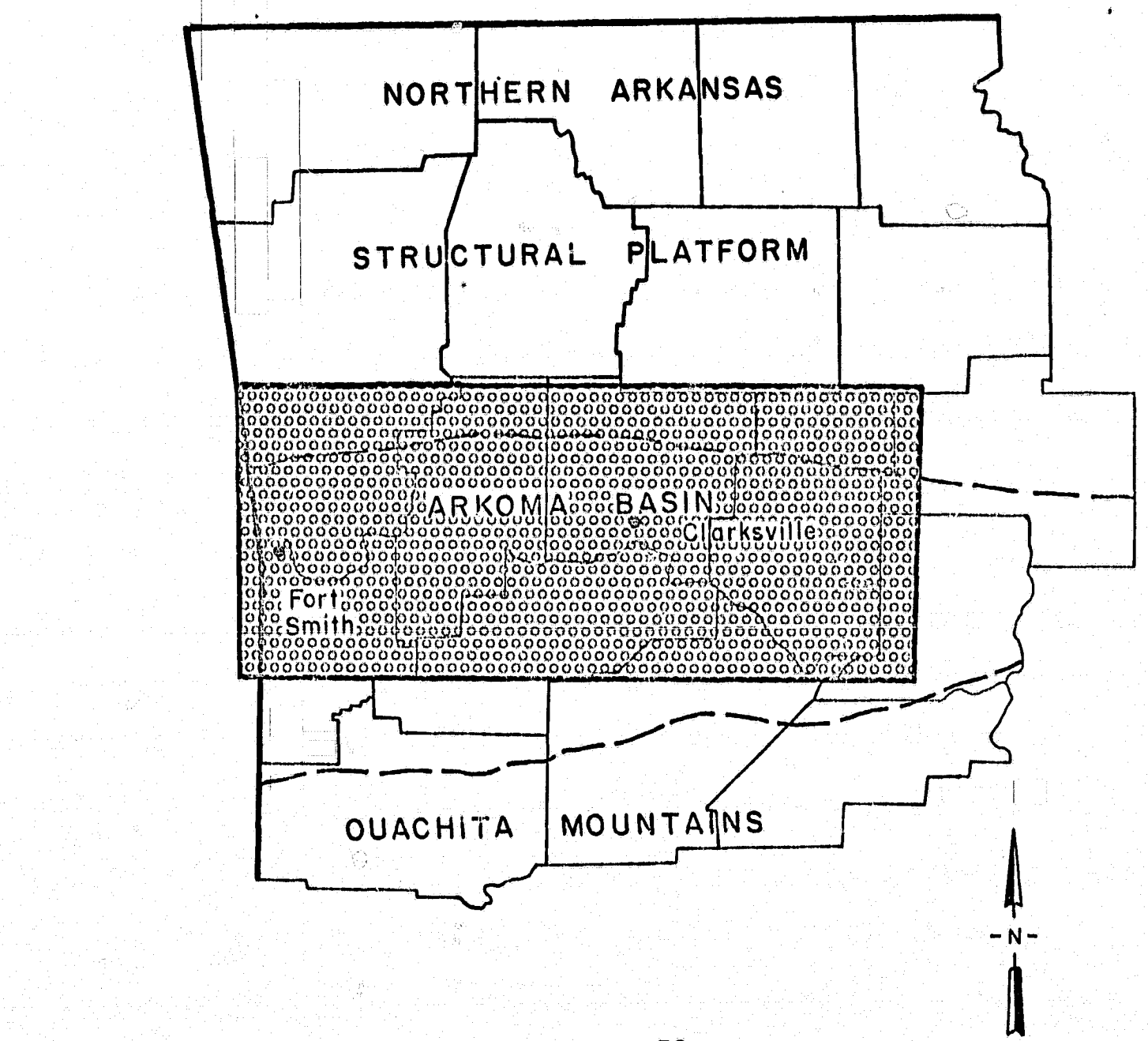

Figure 2. Location of test site.

ORIGINAL PAGE IS
OF POOR QUALITY

segments) which, on the west, are coincident in part with mapped normal faults (Fig. 3).

The Ouachita Mountain fold belt, which is south of the Arkoma basin, is characterized by contorted imbricate thrust plates, intense folding with thrust faults, moderate folding without thrust faults, and gentle folding (Diggs, 1961).

All rocks exposed within the test site are of early and middle Pennsylvanian age and are within the Atokan, Des Moinesian, and Morrowan Series. The Atoka Formation of the Atokan Series is essentially a sandstone, siltstone, and shale sequence and comprises 95 percent of the surface exposures within the test site. In the subsurface at least 35 different gas-bearing zones have been recognized, ranging in age from early Pennsylvanian to late Ordovician; however, the principal gas-bearing zones are sandstone units within the Atoka Formation.

Although much of the early drilling and production (early 1900s) was associated with surface-expressed structural traps (anticlines), more recent drilling and subsurface studies provide evidence that, at least for the Atoka gas-bearing zones in the central part of the Arkansas part of the Arkoma basin, there is little discernible relationship between structure and gas production. Variation in porosity and permeability, i.e., stratigraphic entrapment, appears to be the primary factor influencing the presence of gas. Structure is generally of only secondary importance.

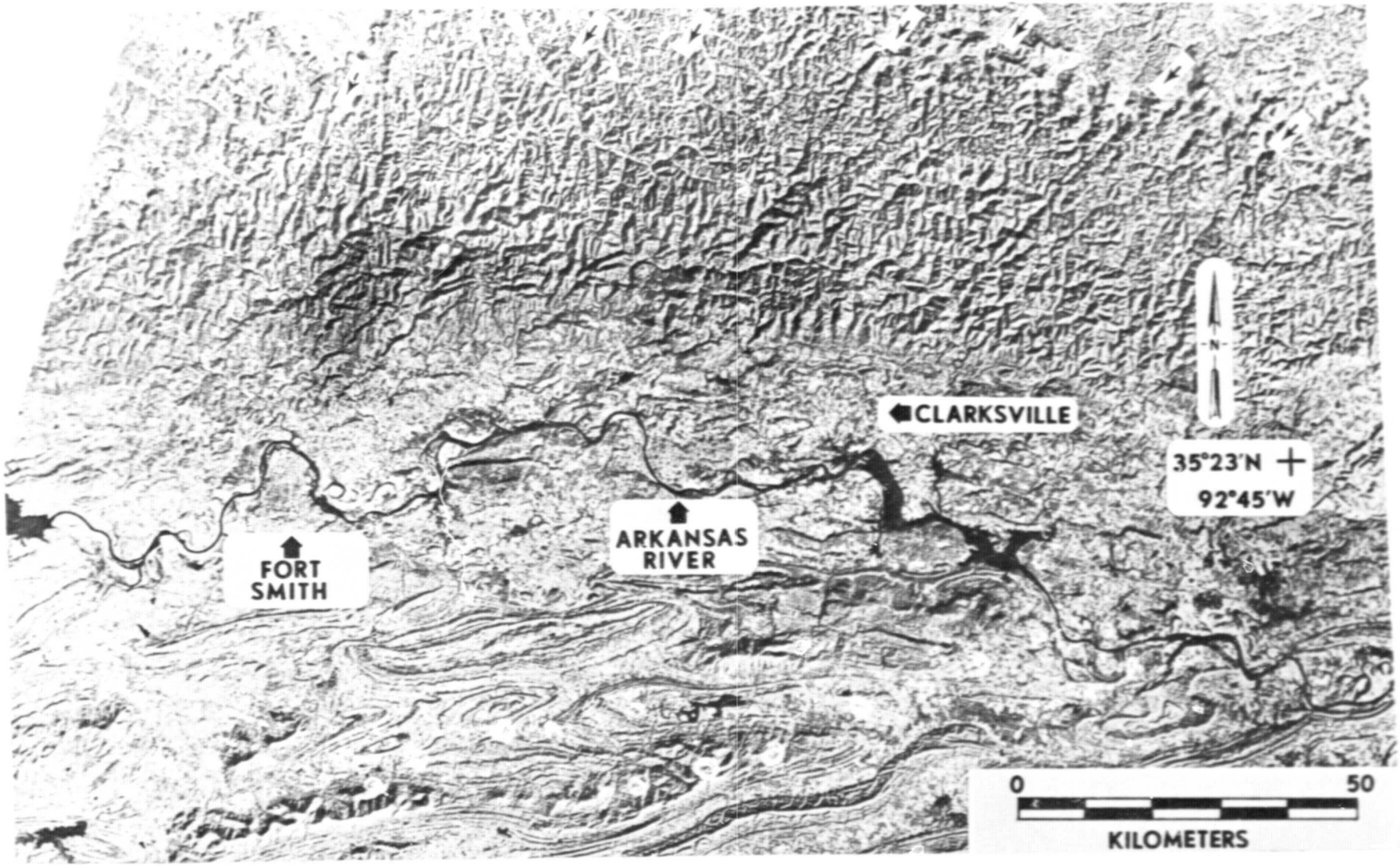

Figure 3. Landsat mosaic, winter scene showing prominent northeast-southwest-trending topographic lineaments.

The Arkoma basin is essentially a dry gas province (no liquid hydrocarbons associated with gas production), the gas being composed of approximately 95 percent methane by volume. At the end of 1978, there were 71 gas fields in the Arkansas part of the Arkoma basin. During 1978, 89,373,839 MCFG (1000 cubic feet of gas) was produced from an estimated reserve of 1,542,789,839 MCFG (Arkansas Annual Oil and Gas Report, 1978).

III. PREVIOUS INVESTIGATIONS

A. Linear Terminology

Fractures, fracture traces, microfractures, mesofractures, macrofractures, megajoints, lineations, linears, and lineaments are some of the names given to naturally occurring, straight-line, aligning features observable by remote sensing. Many investigators have classified linear features according to their length (Blanchet, 1957; Lattman, 1958; Haman, 1961; Hoppin, 1974; Johnson, 1974). These investigators found that the relatively long linear features are regionally significant whereas the relatively short features are more closely related to local conditions.

Blanchet (1957) describes fractures as "generally abundant, natural lineations discernible on aerial photographs." Fracture traces are defined by Lattman (1958) as natural linear features that have less than 1.6 km continuous expression. Lattman terms fractures longer than 1.6 km "lineaments." Haman (1961) uses the term

"microfracture" to describe linear features less than 3.2 km long and the term "macrofracture" for features more than 3.2 km long. Johnson (1974) describes regional lineaments as relatively long linear features which have been propagated upward from the basement rock. His boundary or local lineaments, in contrast, are relatively short and were generated by differential compaction along the flanks of a subsurface anomaly. Hoppin (1974) differentiates between linears and lineaments: "Linears are single rectilinear elements commonly, but not necessarily, of structural origin. Lineaments are generally rectilinear lines or zones of structural discordance of regional (100 km or longer) extent."

An excellent terminological reappraisal of lineaments and linears is provided by O'Leary et al. (1976). These authors suggest that "lineament" be used instead of "linear" for describing simple or composite linear features. Werner (1976) similarly summarizes the use and misuse of linear and lineament terminology. He suggests that a linear is similar to a fracture trace or lineament that is continuous, whereas a lineament can be composed of an alignment of discrete features and short segments of lines.

The term "linear" is used in this investigation because, by definition, it does not apply to composite features whose parts may be aligned. A linear, as used in this report and inferred from remote sensor data, is a

naturally occurring, continuous straight-line features, regardless of length, which may be manifested as a tonal, vegetative, stream pattern, or landform alignment. Two aligned but distinctly separate linears would be mapped as two entities (linears), having the same azimuth (compass orientation) and perhaps different lengths.

B. Linear Analysis and Geologic Significance

Since the launch of Landsat-1 in 1972, considerable interest has been generated in linear feature tectonics, especially as related to regional fracture patterns. Studies conducted throughout the world have been reported in two International Conferences on New Basement Tectonics (Hodgson, 1976; and Podwysocki and Early, 1976). Geologic applications of fracture, linear, and lineament analyses derived from various remote sensing techniques have had varied success.

Many workers involved in geologic remote sensing analyses would agree that global patterns of regional linear features are related to pre-existing zones of weakness reflected into younger sedimentary strata by upward propagation, probably from the basement complex, whereas "local" linear features result from nonregional stress conditions indicative of subsurface discontinuities (Blanchet, 1957; Mollard, 1957; Hodgson, 1961a,b; Wobber, 1967; Wise, 1968, 1969; Rumsey, 1971; Haman, 1972; Johnson, 1974; Kowalik and Gold, 1975;

Sanders and Hicks, 1976). Similarly, most structural remote sensing studies reveal that linear features are commonly associated with zones of increased joint or fracture concentration (Hobbs, 1911; Lattman, 1958; Lattman and Matzki, 1961; Lattman and Parizek, 1964; Overbey et al., 1974). The degree of success and geologic utility of remote sensor linear feature analysis, however is, a subject of considerable debate. Fracture trace, linear, and lineament analyses for groundwater exploration have been moderately successful in specific geologic environments. Significantly greater yields were obtained from water wells located in proximity to linear features mapped from remote sensor data (Lattman and Parizek, 1964; Setzer, 1966; Sonderegger, 1970; Siddiqui and Parizek, 1971; Moore, 1976). However, not all hydrologic studies produced positive correlation between linear features and water yields (Whitesides, 1971; Ogden, 1976).

Several articles have outlined the importance of recognizing linear features as a possible petroleum prospecting tool; however, the success or failure rates of actually using features identified by remote sensing techniques is an exploration program have not been well documented. Saunders and Hicks (1976) provide a summary of articles showing the importance of wrench faults in creating potential petroleum traps. These authors suggest the application of satellite lineaments in prospecting for

concealed wrench faults or other basement faults which may control massive reef growth. Attempts to predict petroleum-bearing rock fractures from surface linear feature analysis have had mixed success. Some authors (Overbey and Rough, 1971; Alpay, 1973) suggest that linear feature analysis used in conjunction with joint strike measurements and borehole data can provide significant information on the orientation of natural fractures in a reservoir. The mapping of linear features has been shown to be helpful in exploration for some fracture reservoirs (Rumsey and Gelnett, 1976; Ryan, 1976; Zirk and Lahoda, 1978). However, other authors support the contention that although linear feature analysis may serve at least partially to predict subsurface fracture orientation, the additional step of predicting a relationship between petroleum production and proximity to subsurface fractures is less certain (Overbey et al., 1974; Werner, 1978). Jones and Rauch (1978) and Beebe and Rauch (1979) give evidence that Landsat lineaments are associated with low yields from gas wells into Devonian shales, yet short photolineaments have a positive correlation with high gas yields. Jackson et al. (1979) could find no basis for the validity of remote sensing in the exploration for shale gas in West Virginia.

Fractures and faults in hydrocarbon-bearing strata have been recognized as factors affecting migration, accumulation, and production of hydrocarbons. Carbonate and less permeable

sandstone reservoirs are particularly susceptible to fracturing. Efforts to determine the nature and extent of subsurface fracture systems and their effect on hydrocarbon reserves and reservoir flow during production have generally been unsuccessful. The complexity of establishing an acceptable relationship between surface and subsurface features is presumably due in part to operator variability, different tectonic regimes in various study areas, differences in remote sensor data sets, non-standardization of analysis techniques, marked scale differences in imagery data bases, and probably most important, lack of understanding of the possible origin of the mechanisms responsible for the observed features (Podwysocki and Gold, 1976).

IV. SURFACE JOINT STUDIES

A. Data Collection

Joint data were collected at 67 different stations throughout the 11,000 km^2 study area. In addition to joint orientation and frequency, bedrock lithology, thickness, and inclination were recorded at each station. At most of the stations the dip of the joints is essentially vertical. As illustrated in Figure 4 the regional orientation of surface joints within the study area is generally nearly north-south and east-west; however, deviation from the regional pattern can be seen at stations 19, 27, 28, 45, 46, and 62.

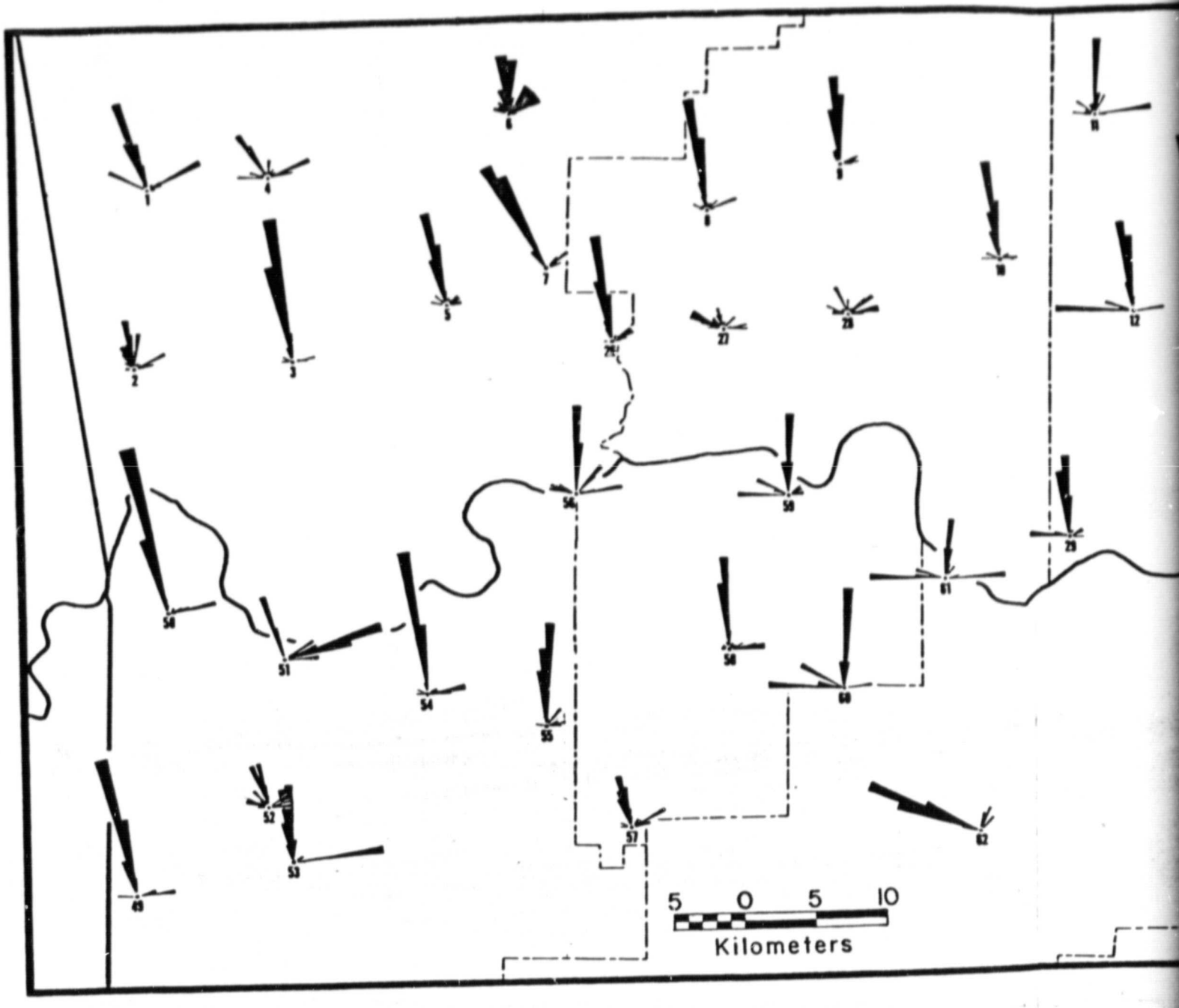

ORIGINAL PAGE IS
OF POOR QUALITY

FOLDOUT FRAME

IENTATIONS— ARKOMA BASIN

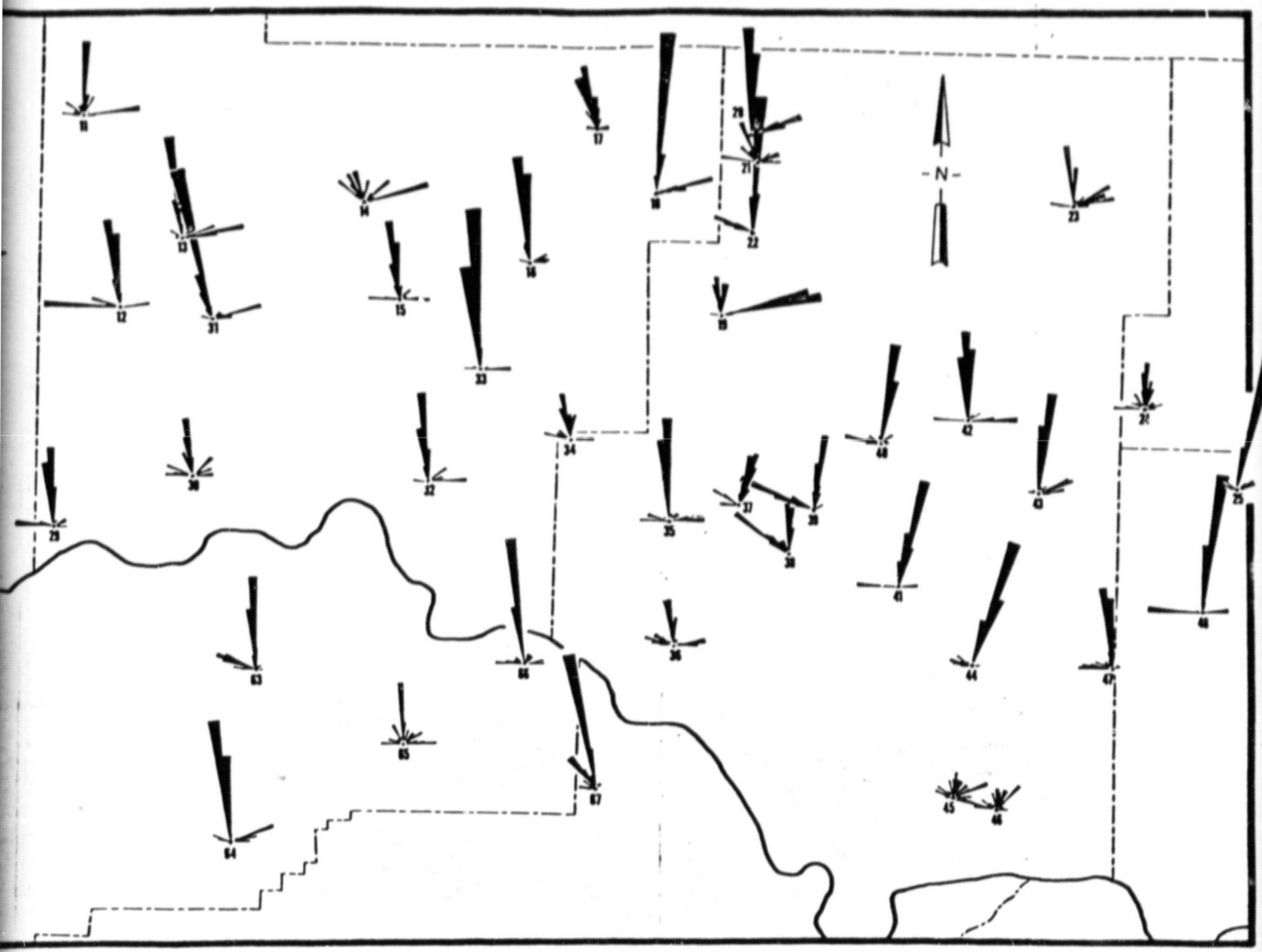

Figure 4

FOLDOUT FRAME 2

The characteristic two sets of orthogonally oriented joints found at each outcrop are illustrated in Figure 5. One set, composed of straight, through-going joints, is designated the systematic set; its average orientation is N10°W. The other set, which is more irregular and contains joints that commonly terminate against the systematic joints, is designated the non-systematic set; its average orientation is N86°E. This terminology is modified from that used in previously published reports by Hodgson (1961a,b). Plumose structures were observed on the surfaces of numerous systematic joints (Fig. 6); however, plumose structures were not observed on the non-systematic joint surfaces. Plumose structures are believed to be indicative of tensional stress conditions (Gramberg, 1966).

B. Fracture System Origins

Many areas such as the Colorado Plateau, Vinta basin, and Piceance Creek basin are characterized by one or more sets of regional orthogonal fracture patterns (Stearns and Friedman, 1972). Several authors have discussed the possible origins of regional orthogonal joint or fracture systems (Blanchet, 1957; Price, 1959; Hodgson, 1961; Gramberg, 1966). Stearns and Friedman (1972) summarize the various opinions.

Although there is some variation in the trend of the axial traces of folds along the Ouachita Mountain fold belt (Fig. 3), the general east-west trend of folding indicates

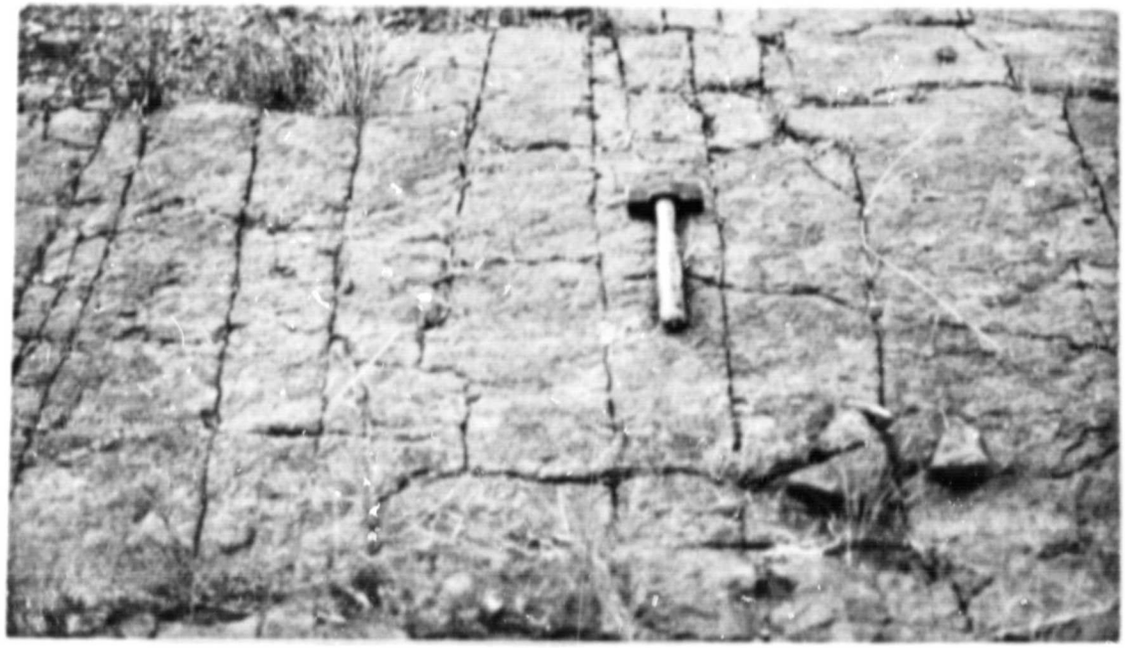

Figure 5. Examples of orthogonal jointing in the Arkoma basin.

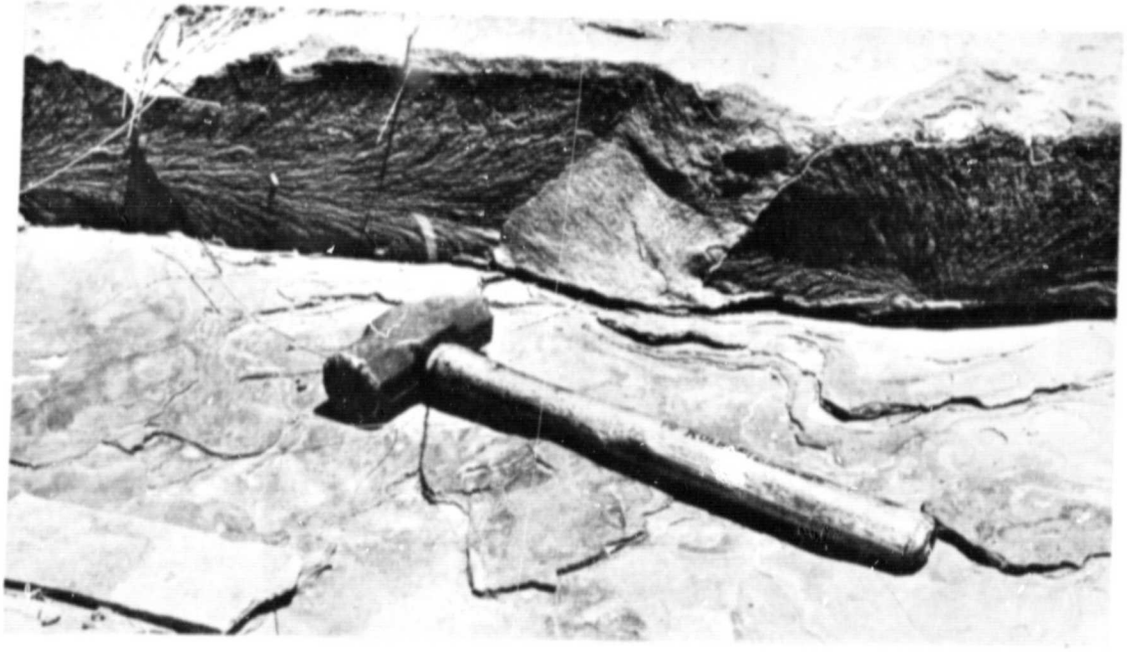

Figure 6. Examples of plumose structures on systematic joint faces.

ORIGINAL PAGE IS
OF POOR QUALITY

a northerly compressive stress. If this hypothesis is correct, the systematic joint sets in the study area are oriented parallel with the major Ouachita compression and the non-systematic joint sets are oriented perpendicular to the compressive stress. This pattern conforms well with theoretical models for vertical fracturing presented by Price (1959) and Gramberg (1966). According to the studies of Price and Gramberg, the stress conditions needed to form joints similar to those of the Arkoma basin are: (1) vertical major principal stress, (2) north-south intermediate principal stress, and (3) east-west least principal stress.

The basic mechanism for joint formation in the Arkoma basin is suggested to be tensional stress caused by burial and later northward compression attributable to the Ouachita orogeny. The theories of Price (1959) and Gramberg (1966) each require the strata containing the joints to have been buried relatively deeply during the compressive phase of the Ouachita orogeny. According to Diggs (1961), major Ouachita compression was not active until late Pennsylvanian time. The thickness of sedimentary rock within the Atoka Formation (early Pennsylvanian) ranges upward to at least 6,000 m (Branan, 1968). In some areas where erosion has not yet taken place, the Atoka Formation is overlain by more than 900 m of younger sedimentary rock. It therefore seems probable that, at the time of major Ouachita compression, the strata comprising much of the Arkoma basin were subjected

to a very great vertical load, sufficient to qualify as a major principal stress. Obviously, under certain conditions of extreme Ouachita compression, the major principal stress may have been reoriented north-south. However, this situation would have been conducive to the formation of regional shear fractures trending north-northwest and north-northeast (Price, 1959); consequently, as soon as shear fracturing occurred, it would have reduced the north-south stress and restored the major principal stress to vertical.

The evidence indicates that the basic mechanism for joint formation in the Arkoma basin was tensional stress caused by burial and later northward compression by the Ouachita orogeny. Increased pore pressure also may have helped to initiate fractures by decreasing the effective stress in all directions, which would have resulted in a north-south tension fracture perpendicular to the east-west least principal stress. In addition, subsequent uplift and erosion of the Arkoma basin may have generated vertical tensional fractures as a result of the "residual stresses" stored in the rock in the manner described by Price (1959).

The non-systematic set of joints may have formed because of changes in the principal stress orientations resulting from the formation of systematic fractures. However, another explanation for the non-systematic joints is documented by Hodgson (1961a), who states: "Any warping or bending of the strata subsequent to the formation of the systematic joint

should generate stresses and, consequently, fractures in the blocks between the joints. The common occurrence of a right-angle or nearly right-angle juncture between the traces of non-systematic and systematic joints indicates some control exerted by the systematic joint on the forces producing the non-systematic joint."

C. Joint Parameter Analysis

Initial measurements were taken from each joint station on nine parameters:

(1) Thickness of the bed that contains the measured joints (THICK).

(2) Dip of the beds (DIP).

(3) Orientation of dip (DIPDIR).

(4) Lithology of the joint medium (LITH).

(5) Frequency of the systematic joint set per 30 m of traverse measured perpendicular to the systematic jointing (SFREQ).

(6) Frequency of the non-systematic joint set per 30 m of traverse measured perpendicular to the non-systematic jointing (NSFREQ).

(7) Orientation of the systematic joint set (SORIENT).

(8) Orientation of the non-systematic joint set (NSORIENT).

(9) Relative stratigraphic position of each joint station outcrop (ROCKUNIT). (Older or lower rock units were assigned lower numbers.)

From four of the parameters, numbers 5, 6, 7, and 8, three other parameters are generated:

(10) Overall averaged frequency of the systematic and non-sysmatic sets (AVEGREQ).

(11) Ratio of the systematic frequency of the non-systematic frequency (FREQDIF).

(12) Angle between the systematic and non-systematic sets (ORIENDIF).

Each joint station was categorized into one of three provinces within the study area (Fig. 7). From north to south, they are:

Province 1: Area of high relief along the Boston Mountain escarpment--characterized by growth faulting and minor folding.

Province 2: Area of low relief between the Boston Mountain escarpment and the Arkansas River--characterized by growth faults and folding.

Province 3: Area south of the Arkansas River--characterized by intense folding and some thrust faulting.

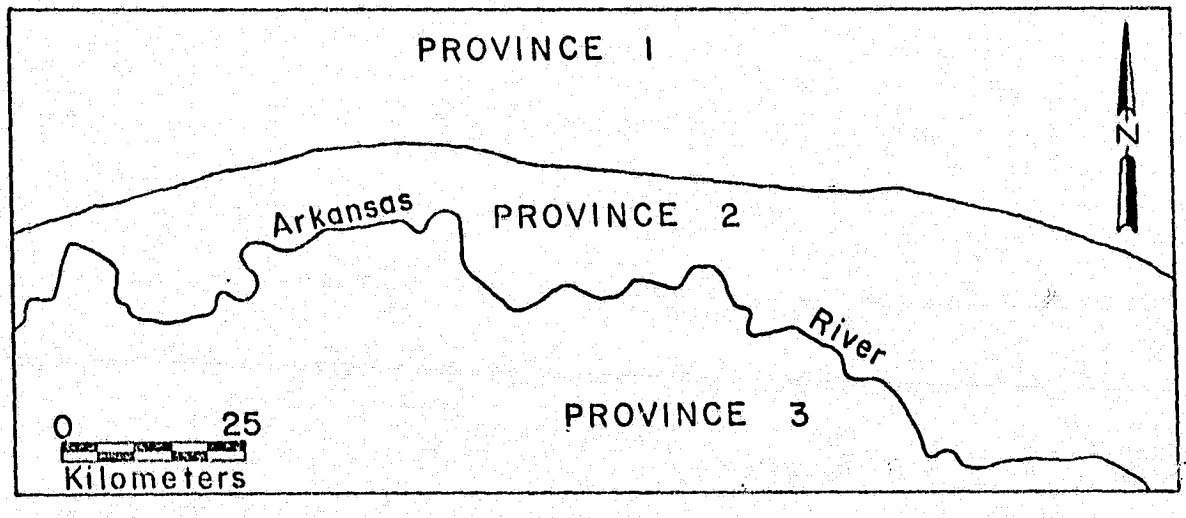

Figure 7. Joint provinces of Arkoma basin.

A correlation coefficient and significance probability level (α) were generated for each combination of the 12 parameters. A correlation was assumed to be present if a relationship had a significance probability level greater than 95 percent ($\alpha \leq .05$). Previous investigations have shown a correlation between joint frequency and other parameters such as stress, lithology, or bed thickness (Price, 1959; Harris et al., 1960; Knoring, 1965; McQuillan, 1973). Consequently, the relationships of major interest in this investigation are between the joint frequency parameters (SFREQ, NSFREQ, and AVEFREQ) and the rock parameters (THICK, LITH, or DIP). DIP is interpreted as an indicator of stress levels in most instances.

Correlations are found between joint frequency and two other parameters--dip and, more significantly, stratigraphic position. No correlation is found between joint frequency and lithology or bed thickness. The dip of the beds has a positive correlation with the average joint frequency at an α level of 0.043. One can infer from this relationship that the non-systematic joint set has a better correlation ($\alpha = 0.024$) with dip than does the systematic set ($\alpha = 0.087$). This relationship supports Hodgson's (1961a) theory that non-systematic joints are created by the bending or warping of the strata after the formation of the systematic joints, which produces fractures that are usually perpendicular to the systematic set.

According to the joint origin theory of Gramberg (1966), great depth with high confining pressure is characterized by a high frequency of relatively short, regularly spaced joints. As confining pressure is reduced (i.e., at higher levels), the joints become less frequency and longer, and commonly are in multi-fracture zones. In this study the relative stratigraphic position of each joint station outcrop shows a negative correlation with joint frequency ($\alpha = 0.012$). In other words, the joint frequency increases in the lower part of the stratigraphic succession. This finding corresponds to the result predicted by the Gramberg (1966) model.

Another relationship of significance is the very good correlation ($\alpha = 0.0001$) between joint frequencies of the systematic and non-systematic sets. This finding implies that the two sets are probably genetically related. A negative correlation ($\alpha = 0.006$) between average joint frequency and province indicates that joint frequency decreases southward. This finding was not expected because the compressional stress component increases southward. However, joint stations in the southern part of the test site, on the average, are higher in the stratigraphic succession than joint stations in the north. Therefore, the shift in joint frequency may be due to differences in the stratigraphic units measured, rather than the location of joint stations within the study area.

In summary, joints in the Arkoma basin consist of two orthogonally oriented sets of vertical joints. One set (systematic), trending N10°W, consists of straight, planar, through going joints. Its orienation perpendicular to the fold axes of the Ouachita Mountains on the south indicates that this joint set formed parallel with the major horizontal compressive stress. Plumose structures on many of these joints suggest a tensional origin. The other set of joints (non-systematic) has an average orientation of N86°E and consists of short and commonly curved joints which cut the rock between the systematic joints. The non-systematic joints probably formed after systematic jointing in response to subsequent warping of the strata as indicated by a significant increase in non-systematic joint frequency with increasing dip.

V. LINEAR REMOTE SENSOR ANALYSIS

The end points of each linear from primary remote sensor data sets were digitized on a latitude (X)--longitude (Y) coordinate system. Digitization was accomplished by means of a Tektronix model 4954 digitizing tablet which has a 40-inch by 30-inch sensitive surface area and provides resolution of 0.01 inch. The tablet was attached to a Tektronix 4015 graphics terminal which, in turn, was linked to an IBM 370-155 host computer. Data stored on magnetic tapes were used to produce linear and well location plots on a Zeta 3653 plotter.

A. Side-Looking Airborne Radar (SLAR) and Stereo Photography

1. Existing Radar Data (SLAR)

Parts of the study area had previously been imaged at various times by military APS-73 (X-band) and Westinghouse AN/APQ-97 (Ka-band) systems. Variations in flight direction (radar look-direction), altitude, and scale precluded the mosaicking of these flight lines. Similarly, because of marked differences in radar depression angles among the various flight lines and "spotty" coverage within the test site proper, linears obtained could be compared only in a visual, nonstatistical manner.

2. Aerial Photography

Stereo black and white photographs (generally 1:20,000 scale) were obtained from various government, state, and private agencies. Approximately 1600 photographs were needed to provide stereo coverage. Unfortunately, the photography spanned some 20 years and the quality was not uniform. Mapped linears were transferred from the photographs to 7.5' orthophoto-quad bases and then digitized.

Because of the large area involved (11,000 km^2), different parts of the test site were assigned to different interpreters. In areas of interpreter overlap, considerable interpreter variability was apparent, especially in those areas in the low-relief Arkansas River valley. To provide an indication of the extent of interpreter variability, four interpreters were selected to analyze stereo photographs

in two different areas (three 7.5' quadrangle maps) of contrasting terrain configuration. The terrain of the Mountainburg and Mountainburg S.W. quadrangles is characterized by high relief (>200 m) because of dissection of the nearly flat-lying strata. The Alma quadrangle, in contrast, is characterized by much less relief (<50 m) and includes part of the Arkansas River floodplain.

Rosette diagrams for each quadrangle and operator (Fig. 8) indicate the number of linears mapped (n), the average length of each linear ($\bar{x}$), and the percentage of linears mapped by more than one operator. The rosette diagrams drawn by each operator show considerable variation. However, in the Mountainburg and Mountainburg S.W. quadrangles, the variation was less than in the Alma quadrangle. For example, in the Mountainburg quad all four of the operators identified a major linear set trending N42°W and three of the operators approximated two other linear sets trending N23°E and N54°E. There is somewhat less agreement among rosettes constructed from the Mountainburg S.W. quad where three operators agreed on two linear sets trending N5°E and N25°E. Very few linears were mapped in the Alma quadrangle and the linear trends recognized by different operators show no agreement. The number of linears mapped by all operators is by far the lowest in the Alma quadrangle. This finding may indicate that operators are more likely to distinguish

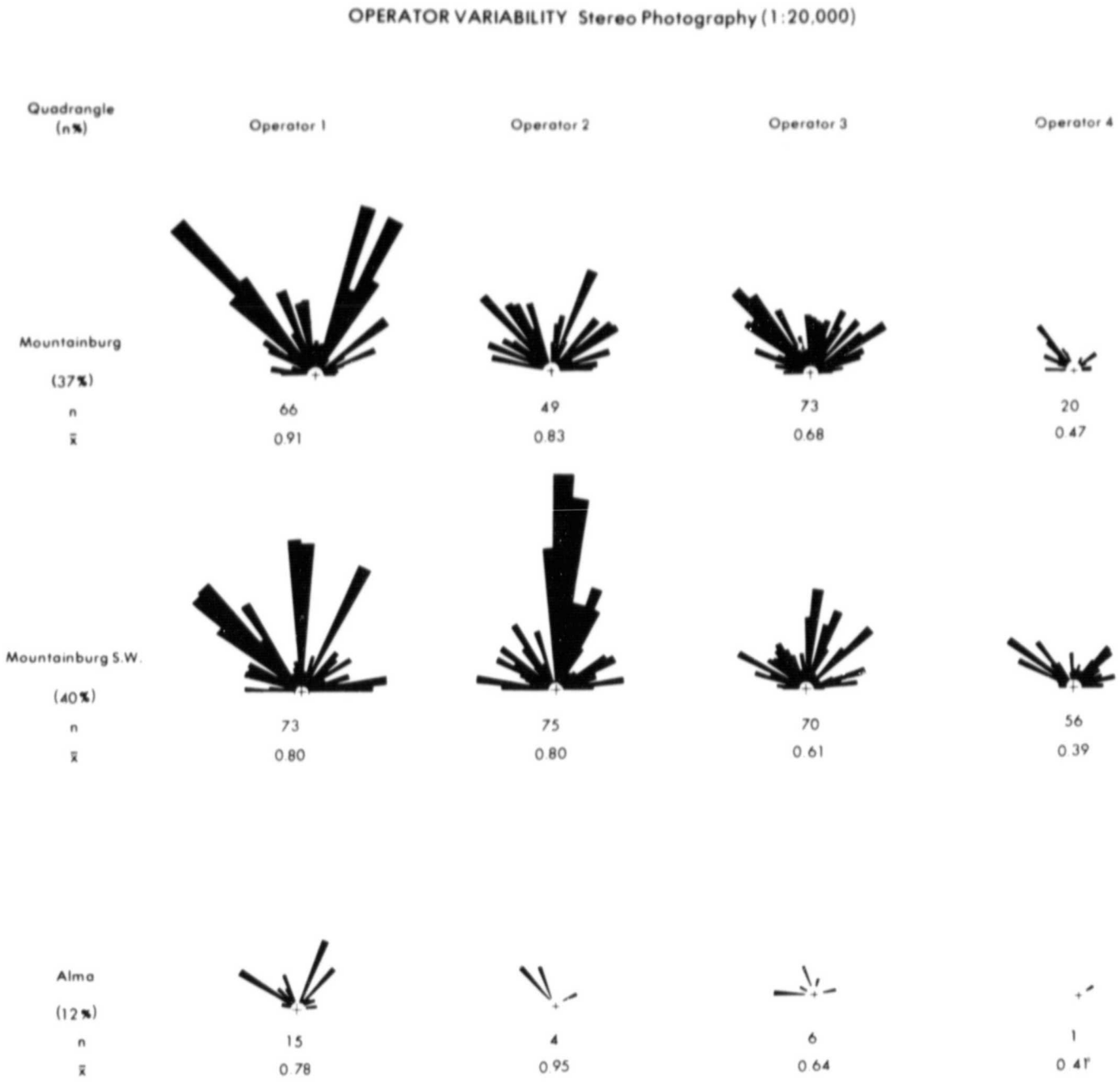

Figure 8. Results of operator variability study--stereo photography.

topographic linears than tonal or vegetation-related linears caused by soil moisture variations.

B. Radar (SAR) and Enhanced Landsat

1. Computer Processing and Enhancement

In support of this reserach effort, the Jet Propulsion Laboratory provided SAR imagery of the test site obtained during May of 1977 and April of 1978. Because of funding limitations, only the 1978 data set was digitally processed. This L-band (23-cm wavelength) imagery was obtained in a series of north-south flight lines with approximately 8-km swath widths and providing dual-polarization coverage. Two different Landsat scenes (winter and summer) were selected to provide maximum changes in solar illumination (elevation) and terrain cover. Both radar and Landsat imagery was subjected to various computer enhancement and analysis procedures performed at the Image Processing Laboratory of the Jet Propulsion Laboratory.

a. Radar Image Processing

Strips of radar imagery which had been converted from raw data to image format by the JPL optical processing system were digitized on the IPL microdensitometer. Samples of film density were taken with a 50-micron aperture at intervals of 50 microns, corresponding to dimensions of 15 and 25 m in the range and azimuth directions, respectively. The resulting density measurements were scaled to teger

values, although in any strip considerably fewer than this number of levels were usually occupied. A typical strip of sampled imagery yielded a digital array of approximately 500 samples in the range direction by 3500 lines in the azimuth direction.

Removal of gain variation

The radar system which generated the imagery produces a perceptible gain variation with range. This effect is the result of three phenomena: the normal spreading loss of power density with increased path length, the decrease in differential backscattering cross section (σ°) as incidence angle increases, and antenna gain variations over the imaged swath. To combat this problem the system incorporates the capability to increase the gain as a function of range. The system is only partially effective in compensating for these effects, leaving a noticeable average intensity variation with range in the data. Such a residual effect is particularly apparent in a mosaic where the near range of one strip is adjacent to the far range of its neighboring strip. There is an obvious average intensity discontinuity at the strip boundary.

To reduce the intensity descrepancy between adjacent strips, a scene-dependent gain correction was applied to each strip. The procedure consisted of applying a gain and offset to each line of constant range in the imagery to force the mean and variation (i.e., ABS $[x_i - \bar{x}]$ where x_i is an

image sample value, and $\bar{x}$ is the average of x_i over a line of constant range) at each range to predetermined constant values. This process is admittedly inferior to a true calibration operation, but the information available was inadequate for a meaningful calibration. A major drawback of the technique is the fact that the applied gain and offset might reflect the feature content of the imagery rather than correct for true gain variations. To reduce undesirable feature-cued gain modification, the process was controlled by using statistics obtained only from uniform-appearing areas in the mountainous regions. This method was generally successful in reducing apparent intensity jumps between strips in the regions where the statistical estimates were obtained. However, intensity discontinuities did appear in areas of low return where the gain attenuation was limited by the low signal strength. Because these areas were not of primary interest in the investigations, the artifacts were deemed acceptable.

Conversion from range to surface distance

Because the side-looking radar system records the returned signal from each pulse as a function of time, the imagery obtained from the raw data displays distance along the flight path in one coordinate (azimuth direction) but line of sight distance to the surface in the perpendicular coordinate (range direction). A difference in range between two points nearly beneath the sensor corresponds to a much

greater separation on the surface than does an equal range difference between points located to the side of the flight path. As a result, features appear greatly compressed in the near range areas of the imagery.

This basic distortion is complicated by the fact that the range to a surface point is dependent upon its elevation. Without exact knowledge of the topography and the position of the sensor, an accurate conversion to distance on the surface cannot be made. The near range compression effect, however, is sufficiently pronounced that application of an approximate "first-order" correction is often warranted. Such was the case in this project where the radar strips were to be incorporated in a mosaic and registered to Landsat imagery. The presence of gross local distortions would confuse the analyses and significantly degrade registration accuracy. Therefore, each strip of imagery was subjected to a geometric transformation to accomplish an approximate conversion from slant range to distance on the surface. The altitude was assumed constant over the strip. A simple trigonometric conversion from measurement along the hypotenuse of a right triangle to distance on the horizontal side was made with the assumption that the topography was absolutely flat.

Mosaic generation

Radar strips which had been processed to remove gain variations and to convert from measurement of range to

distance on the surface were ready for incorporation into a mosaic. A mosaic was constructed by combining neighboring image pairs into two-component mosaics. These two-component mosaics were then merged in pairs to form four-component mosaics and the process was repeated to generate the completed mosaic. At each step a pair of images were combined by deforming the right component to spatially match the left component at the boundary between the two images. Identical features were located manually in bands across the overlapping areas of both images. Typically, five bands of such "tiepoints" were obtained at equally spaced intervals down the strip of overlap. To avoid compounding the complexity of subsequent mosaicking steps, the right-side component was subjected to a strictly controlled geometric transformation to achieve alignment with its left-side counterpart. The transformation was performed in such a manner that each line of constant azimuth (a horizontal row in a component strip) was translated only in the horizontal direction and was translated as well as rescaled in the vertical direction. Between the bands of tiepoints the deformations were computed by linear interpolation between those indicated by direct observation at the tiepoints. The two-element mosaics were formed by truncating the left and registered right-side components at the boundary and abutting the resulting strips.

Brightness transformations

To provide image displays in which features of various textures and dimensions could be easily discerned, the mosaics were subjected to two brightness transformations. Providing the lower contrast was a transformation to produce an approximately Gaussian distribution of intensity. A transformation table was constructed to change the original brightness levels to the set of new values which produced the closest approximation to a Gaussian distribution with mean at midrange and six standard deviations spanning the 256 available shades of gray.

A more dramatic contrast enhancement was achieved by the second procedure. As in the first method, a transformation table was generated to produce a specified distribution in the transformed image. In this case that distribution was uniform. The algorithm operated by the equilvalent method of forcing the cumulative distribution function to be linear.

Spatial filtering

The nature of the investigations conducted in this project required the clear visibility of fine detail in the imagery. To increase the apparent sharpness of the pictures, a spatial filtering operation was performed. This procedure increased the contrast of small scale brightness changes and reduced brightness differences between large scale features. If the low frequency (large scale) components had been completely removed, the filter would have been a

"high-pass" filter. In this project contrast was 80 percent attenuated in features larger than approximately 2500 m and smaller dimension variations were left unchanged. This contrast corresponded to the average of a "high-pass" filtered version with 20 percent of the original image.

Registration to Landsat

Any combined analysis of radar and Landsat imagery is facilitated if a specific feature appears at the identical coordinates in each type of image. Such spatial alignment (registration) also makes possible the generation of numerical composites of the images. To achieve registration in this project the radar scene was geometrically manipulated to coincide with the Landsat scene. The transformation was controlled by approximately 80 tiepoints manually obtained by locating identical features in both images. A polynomial geometric transformation was used to describe the distortion. It was "fit" to the tiepoints by adjusting its coefficients to minimise the sum of the squared error in its predictions of thetiepoint locations. To speed computation the polynomial transformation was applied only at a sparse grid of locations in the image. Movements of points falling between the grid intersections were obtained through bilinear interpolation between those of the four surrounding grid locations.

b. Landsat Image Processing

Landsat imagery was obtained from the U.S. Geological Survey in standard digital form. Each scene consisted of images in four spectral bands sampled with a spacing of approximately 60 m across the scene and 80 m down the scene. Sampled at these intervals, the roughly 190 km square area imaged in a scene comprised a digital array of about 2300 lines each containing approximately 3200 samples.

Geometric correction

The standard format of the USGS-supplied digital data is incompatible with much of the software in the Image Processing Laboratory. Therefore, it was necessary to reformat the data as the initial processing step. During this "logging" process it was convenient and computationally efficient to undertake a set of geometric corrections which could be performed independently on each image line. Included were the following geometric manipulations:

(a) correction for the earth's rotation during the elapsed time between imaging the first and last lines,

(b) resampling to achieve equal horizontal and vertical sampling spacing,

(c) removal of synthetic samples introduced by NASA to ensure equal line lengths,

(d) correction for non-uniform sensor scan mirror velocity,

(e) correction for panorama effect, and

(f) adjustment of sample coordinates to compensate for variation in alignment of the sensors of each spectral band.

Brightness transformations

As in radar imagery, the distribution of brightness in the original Landsat images did not necessarily provide sufficient contrast and average level to produce useful photographic representations. To generate more informative visual displays, the individual spectral band images were subjected to the same intensity transformations that were applied to the radar imagery, producing Gaussian and uniform distributions of brightness.

Spatial filtering

Edges and fine structure in the Landsat scenes were enhanced by the same filtering procedures that were applied to the radar imagery.

Color composites

Two types of color composites, referred to as standard and enhanced versions, were generated from Landsat imagery. The standard version was obtained by modulating each of the three primary colors (red, green and blue) with a single spectral band image. To ensure that spectral variations in all the bands were equally displayed, the images were first subjected to the Gaussian brightness transformation. This process produced equal first- and second-order statistics in the color component images and eliminated the possibility that a single hue would dominate the scene.

The enhanced color composite was produced to display even small spectral variations as marked color differences. The color enhancement procedure was designed to spread the distribution of brightness, causing it to occupy a broad region in the color space. This effect was accomplished by rotation to the space of eigenvectors of the original R, G, B (red, green, blue) distribution. Statistically independent images were formed by assigning brightness based on coordinates along axes aligned with each of the eigenvectors. Therefore, when a Gaussian brightness transformation was subsequently applied to each of the new component images, a roughly spherical distribution was produced, generating a broader range of colors than the cigar-shaped original distribution. To maintain general color similarity to the standard color composite, the inverse rotation back to the original color space was performed to generate the tri-stimulus components of the color image.

Registration of multiple scenes

To facilitate temporal comparisons of Landsat imagery, scenes obtained at different times were registered. The procedure was identical to that used to register radar to Landsat imagery. The accuracy of the Landsat registration, however, was considerably greater because the geometric differences were less severe and more continuous than the rather disjoint distortions generated by mosaicking independently correct radar strips.

c. Radar/Landsat Composite

Registration of a radar mosaic to a Landsat scene made possible point-by-point manual comparisons of the two data types. It also allowed numerical combinations to be undertaken. For this project composites were produced by using Landsat data to provide color information and radar imagery to supply brightness modulation. The enhanced color tri-stimulus components were transformed to a spherical coordinate system known as hue saturation and intensity (HSI) space. The intensity coordinate is a distance along a vector forming equal angles with the orthogonal R, G, B (red, green, blue) axes. Hue is the angular rotation in a plane perpendicular to the intensity vector. Saturation is the angular displacement at the R, G, B origin away from the intensity vector. In this system brightness information is contained in the intensity coordinate and color in the hue and saturation dimensions. To form the composite, the Landsat intensity image was simply replaced by the registered radar mosaic. The inverse transformation from HSI to RGB space was then performed to obtain the tri-stimulus components of the color composite.

2. Evaluation of Enhancement Techniques

a. Landsat-Band Comparison

The first evaluation is for the four bands of each enhancement and scene combination. For this evaluation, total number of linears detected by each of three different

operators (A, B, C) is used. The Landsat scene-enhancement combinations are:

Landsat winter - Gaussian stretch

Landsat winter - uniform distribution stretch

Landsat summer - Gaussian stretch

Landsat summer - uniform distribution stretch

Tables 1, 2, 3, and 4 show the number of linears drawn by each operator (A, B, C) for each band and the band and histogram numbers (Appendix). The highest number for each operator is indicated by * and the lowest number by x.

Table 1. Landsat winter--Gaussian stretch.

	(1) Band 4	(2) Band 5	(3) Band 6	(4) Band 7
A	127	178	101	229*
B	108	212*	84x	103
C	33	28x	62	63*

Table 2. Landsat winter--uniform distribution stretch.

	(5) Band 4	(6) Band 5	(7) Band 6	(8) Band 7
A	133	155*	119x	127
B	114	209	113x	269*
C	47x	54	53	75*

Table 3. Landsat summer--Gaussian stretch.

	(9) Band 4	(10) Band 5	(11) Band 6	(12) Band 7
A	74	59[X]	86*	86*
B	130	147	95[X]	102
C	16	15[X]	62*	40

Table 4. Landsat summer--uniform distribution stretch.

	(13) Band 4	(14) Band 5	(15) Band 6	(16) Band 7
A	58[X]	124*	100	93
B	143*	126	134	124[X]
C	21	20[X]	30	51*

For the Landsat winter scene, with both Gaussian and uniform distribution stretch, two of the three operators found the greatest number of linears on band 7. For the Landsat summer--Gaussian stretch combination, two of the three operators found the greatest number of linears on band 6. None of the operators agreed on which band had the greatest number of linears for the Landsat summer--uniform distribution stretch combination.

For the Landsat winter scene, regardless of enhancement technique, two of three operators found the greatest number of linears on band 7. There was less agreement among the

operators for the Landsat summer scene. In one case, band 5 was the best and in the other case there was no agreement.

In two of four cases the least number of linears was found on band 6. However, in three of four cases, band 6 showed the least variation in the number of linears drawn by the three operators.

Also, from Tables 1, 2, 3, and 4 it is apparent that the Landsat winter scene detects more linears than the Landsat summer scene. The uniform distribution stretch consistently detects more linears than the Gaussian stretch. The best combination to find the greatest number of linears is Landsat winter, band 7, uniform distribution stretch.

b. Enhanced Color--Standard Color Comparison

For this evaluation, the number of linears detected with enhanced color Landsat imagery is compared with the number of linears detected on standard color Landsat imagery. The Landsat scene-enhancement combinations are:

Landsat winter--enhanced color
Landsat winter--standard color
Landsat summer--enhanced color
Landsat summer--standard color

Table 5 and 6 show the number of linears drawn by each operator (A, B, C0 for each scene and the histogram number (Appendix). The highest number for each operator is indicated by *.

Table 5. Landsat winter.

	(17) Enhanced Color	(18) Standard Color
A	178	203*
B	191	192*
C	51	62*

Table 6. Landsat summer.

	(19) Enhanced Color	(20) Standard Color
A	143*	129
B	148	167*
C	37	41*

The standard color Landsat imagery detects more linears for both the summer and winter scenes. Also, a greater number of lineras is detected with the winter scene.

C. Synthetic Aperture Radar--L-band

The images from which histograms 21 and 22 were produced are uncontrolled mosaics whereas the images from which histograms 23 and 27 were produced are controlled mosaics (response range dependence removed). Histograms 21 and 22 were obtained from the 1977 data set. Table 7 compares the number of linears from each of the three operators (A, B, C)

with the histograms indicated (Appendix). The greatest number of linears found by each operator is shown by * and the lowest number by x.

Table 7. Linear-operator variation.

	(21) (HH)	(22) (HV)	(23)$_1$ (HH)$_1$	(27)$_1$ (VH)$_1$
A	65	50^x	85	111*
B	54	49^x	137*	87
C	23	4^x	41	100*

[1]Response range dependence removed.

Table 7 shows that two of the three operators found the greatest number of linears on the (VH) (response range dependence removed) image and all three operators found the least number of linears on the (HV) uncontrolled image. More linears are detected by mosaicked (response range dependence removed) April 1978 imagery than uncontrolled imagery (May 1977).

Enhancement comparison

Three SAR (L-band) enhancements--uniform distribution stretch, high-pass filtering, and high-pass filtering with 20 percent added back are evaluated. As before, the evaluation is based on the number of lineras detected.

Table 8 compares the number of linears from each of the three operators (A, B, C) with the histograms indicated

(Appendix). The greatest number of linears found by each operator is shown by *.

Table 8. Enhanced radar.

	(24) Uniform Distribution Stretch	(25) High Pass Filtering	(26) High Pass 20% Added Back
A	60	109*	80
B	143	72	196*
C	82*	80	79

Although none of the operators agreed on which type of enhancement detects the most linears, the high-pass filtering shows a very small variation in number of linears found by the three operators.

d. Radar/Landsat Merge

The parallel-polarized (HH) (response range dependence removed) image was registered to the winter and summer Landsat scenes. Table 9 compares the number of linears from each of the three operators (A, B, C) with the histograms indicated (Appendix). The greatest number of linears found by each operator is shown by *.

All three operators found more linears on the radar/Landsat winter scene than on the radar/Landsat summer scene. Unfortunately, because of the size limitation of the color playback device, the area generated for the radar/Landsat

Table 9. Radar plus Landsat.

	(28) Winter Scene	(29) Summer Scene
A	69*	40
B	60*	46
C	74*	33

analysis was smaller than that used for other linear analyses and histogram generation. Table 10 indicates modified area histograms for comparable areas derived from the radar/ Landsat input combinations that provided histograms 28 and 29. The greatest number of linears found by each operator is shown by *.

Table 10. Modified area histograms.

	(30) Landsat Summer Enhanced Color	(31) Landsat Winter Enhanced Color	(32) HH-Response Range Dependence Removed
A	95	162*	49
B	79	138*	130
C	27	42*	30

When histograms 28 and 29 (winter and summer radar/ Landsat combinations) are compared with the original data (histograms 30-32), it is obvious that the Landsat winter

enhanced scene provided for the detection of most linears. The radar/Landsat merge appears to improve the confidence of operators in interpreting relatively longer linears. The average length of linears on the radar/Landsat merge shows a moderate increase for two of the three operators, but the total number of linears is smaller. Operator C was able to detect more linears using the radar/Landsat merge than with either the radar or Landsat alone. However, the other two operators show marked disagreement. Again, operator variability was considerable.

Although the VII mosaic provided for the detection of relatively more linears, none of the SAR enhancement techniques is significantly better than the others.

e. Radar and Radar/Landsat Evaluation

From the preceding discussion it is apparent that L-band radar imagery provided for detection of fewer linears than the optimum data set, that is, the Landsat winter scene. This conclusion is not surprising, however, if one examines the contrast in terrain displays provided by the two remote sensor data sets. The dominant linear features inferred by all interpreters on both the Landsat and radar imagery were topographic linears, i.e., usually alignment landforms or straight valley segments. Topographic linears are enhanced on the Landsat winter scene because of the relatively low solar illumination (21° solar elevation) which causes

highlighting and shadowing on many of the terrain elements oriented toward and away from the southeastern solar azimuth (142°, measured clockwise from north). This low sun angle enhancement is especially evident if the winter scene (Fig. 9) is compared with a high sun angle (56° solar elevation) summer scene (Fig. 10). The contrasting terrain information in the two Landsat scenes is striking, but not a new observation. In recent years many Landsat investigators have found that the winter months' lower sun angles enhance topographic detail. However, the similarity between low solar illumination and radar illumination is most important in analyzing the SAR imagery linear detection.

The L-band radar imagery was obtained along north-south flight lines, with two separate but overlapping swaths providing flight line coverage (Fig. 11). This flight line configuration allowed for a continuous change in incidence angles from 43° (near range) to 71° (far range), or 47° to 19° depression angle, respectively. In contrast, the Landsat winter scene provided a constant solar elevation (equates to radar depression angle) of 21° across the entire swath. Only in the extreme far range part of each radar swath does the radar depression angle approximate or equal the solar elevation of the Landsat winter scene. The enhancement of topographic linears on the radar imagery is a function of two parameters, one related to the imaging system and the other related to terrain. The system parameters

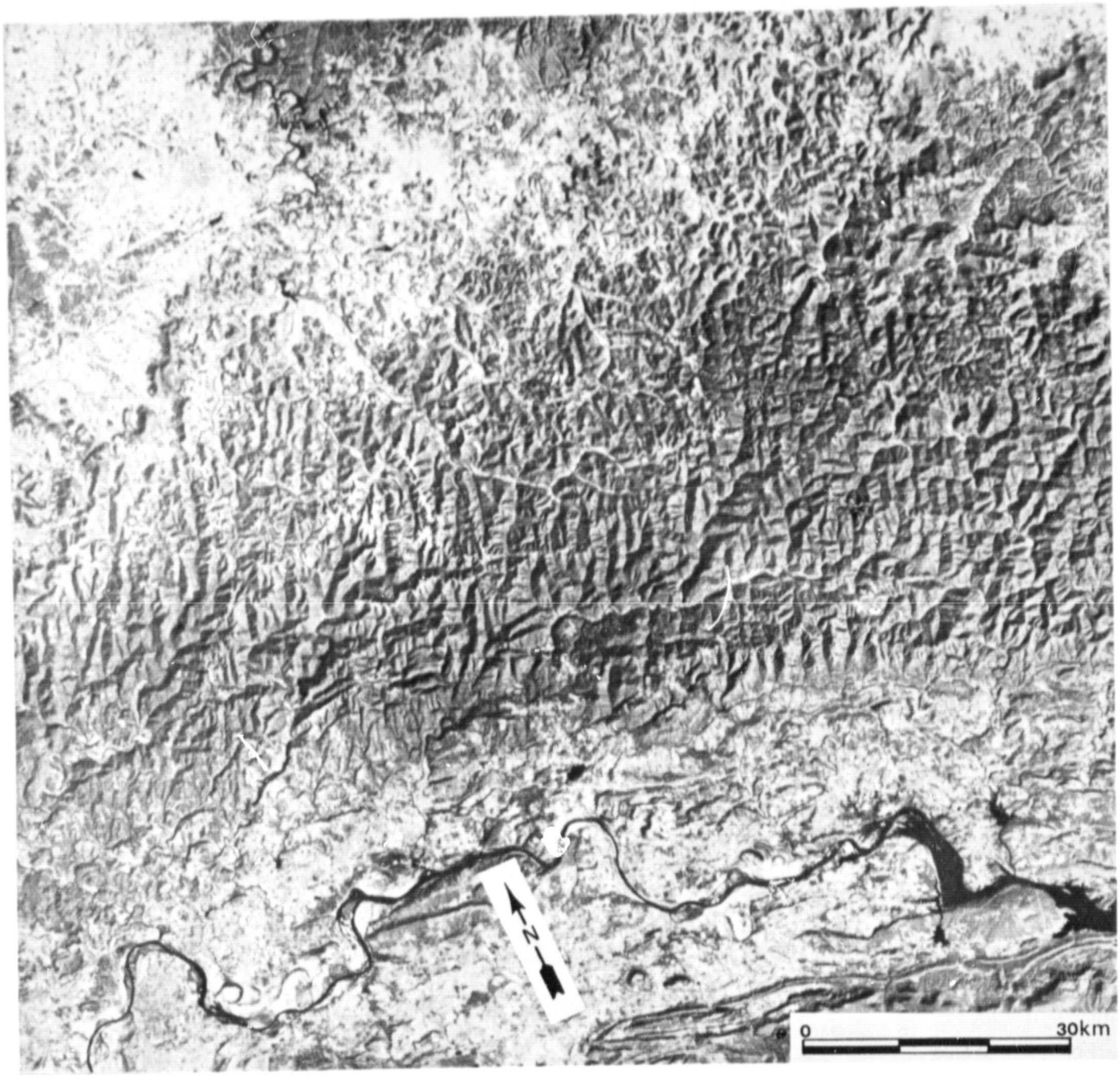

Figure 9. Landsat winter scene, ID 5261-15490.

ORIGINAL PAGE IS
OF POOR QUALITY

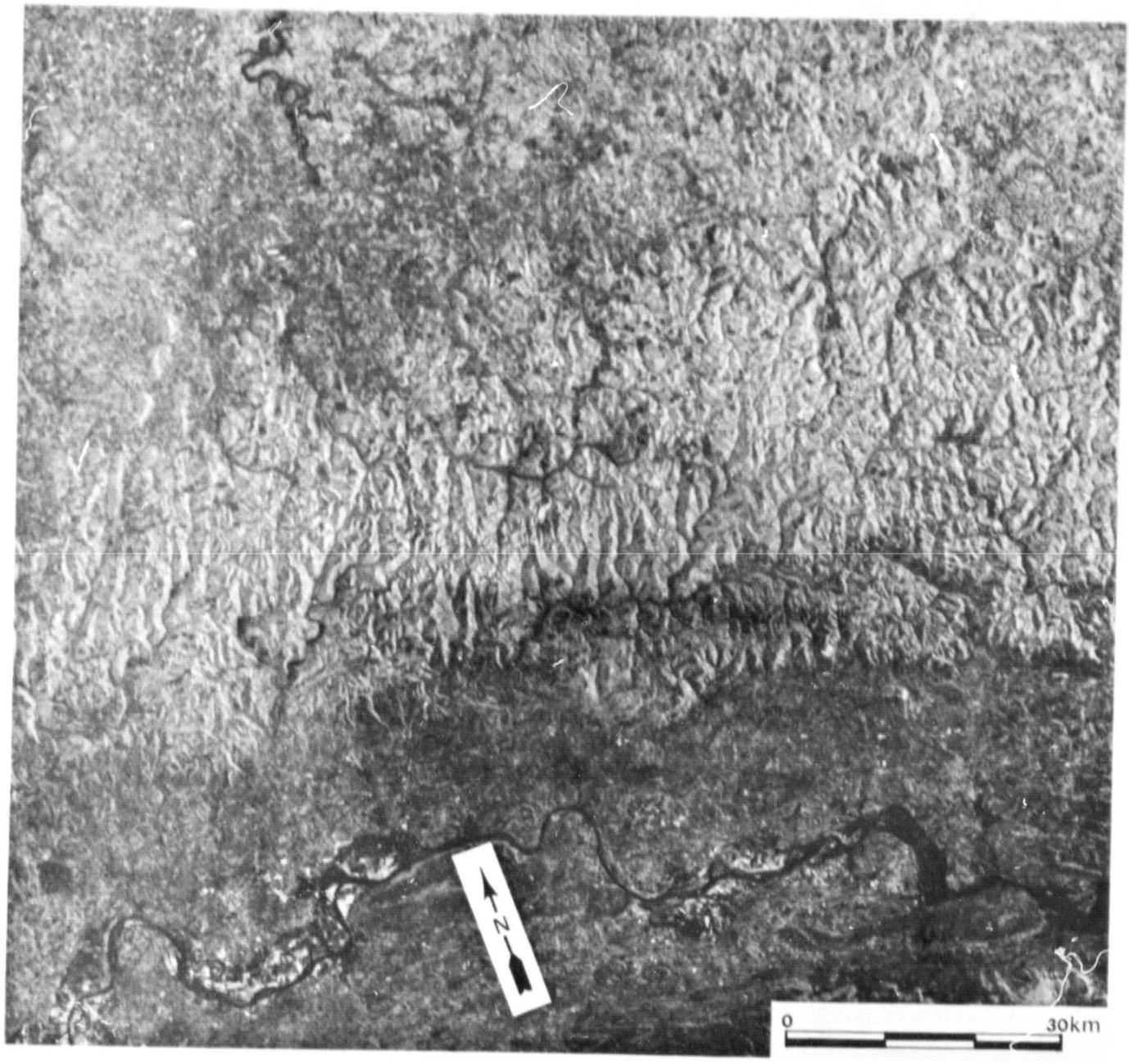

Figure 10. Landsat summer scene, ID 0861-15515.

are radar depression angle and look-direction. Changing the depression angle can have a significant effect on the enhancement of topographic linears. The May 1977 L-band imagery was obtained using a swath configuration that provided for much larger (steeper) depression angles across the swath (Fig. 12). Although the imagery was not processed in the same way as that of 1978, and was not analyzed in a controlled mosaic format, histograms 21 and 22 (Appendix, 1977 data) show significantly fewer linears detected with 1977 than with 1978 data (histograms 23, 24, 25, 26, 27).

Other researchers have recognized this relationship (MacDonald et al., 1969; Gelnett, 1977). Gelnett (1977) provides a summary of articles emphasizing the importance of considering radar depression angle and look-direction when attempting linear analysis from radar surveys. It should be noted, however, that because of east and west look-directions of the radar flight lines, some linears oriented parallel or nearly parallel with the flight lines were more easily detectable on the radar than on the Landsat imagery. Thus, in a way similar to radar, Landsat is also look-direction dependent (single solar azimuth illumination angle). Gelnett (1977) reports that single-look radars provide only about 70 percent of the available geologic data. Therefore, because of radar's operational capability of selectable look-angles and depression angles, radar surveys should complement any topographic linear survey using Landsat.

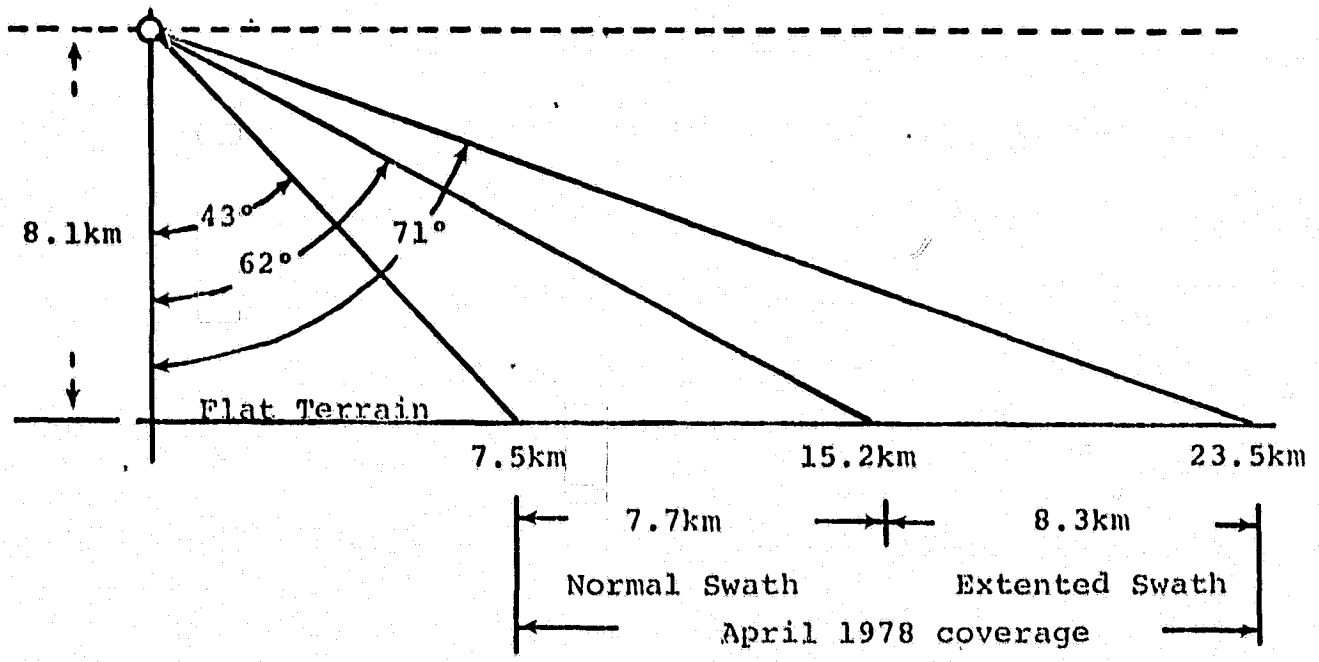

Figure 11. SAR swath configuration, April, 1978 imagery.

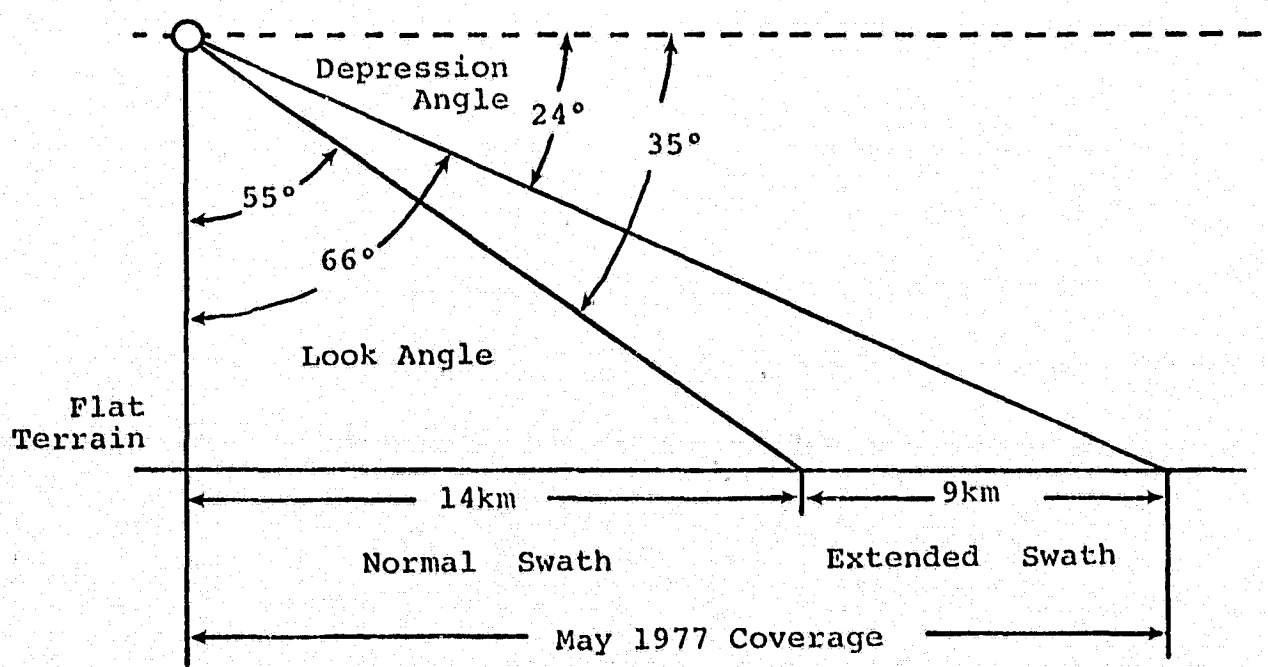

Figure 12. SAR swath configuration, May, 1977 imagery.

From the complementary aspects of Landsat and radar, intuitively one might expect the radar/Landsat merge to provide better linear mapping capability than a single-sensor mapping mode. Comparison of histograms 28 and 29 (winter and summer radar/Landsat merge, respectively) with histograms 30, 31, and 32 (original imagery used for Landsat-radar merge) provides no evidence of an overall improved linear detection capability for the merged data sets. Although each operator was able to detect linears of greater average length than those detected in the original data sets, the merge of the two data sets tends to "mask" the relatively smaller and more subtle linears. The enhanced color of the Landsat, for example, suppresses subtle radar linears that are relatively distinctive by demarcation between black and white tonal contrasts on the original imagery. A black and white radar/Landsat merge of Landsat uniform distribution stretch, band-7, winter scene with the VH radar appears to be an ideal data set. Such a black and white combination was not generated for this study.

f. Operator Variability

The problem of operator variability in the mapping of linears and lineaments has been addressed recently by Podwysocki et al. (1975), Siegal (1977), and Huntington and Raiche (1978). All found significant discrepancies in both coincidence and directions of linears drawn by different operators on the same Landsat image. Podwysocki et al.

report that of all linears mapped among four operators, only 0.4 percent were recognized by all four operators, 4.7 percent by three, 17.8 percent by two, and 77 percent by one operator. Siegal (1977), using five operators and a single Landsat scene, found that only 4 percent of the lineaments were consistently delineated by all five operators. Huntington and Raiche (1978) suggest that differences between two interpretations, by two observers looking at the same scene, can be of the same order as would be expected for one person interpreting two scenes with entirely different geology.

Differences between linear interpretations of the same scene can be extraordinary. Even when the operator variables are minimized, contrasts between remote sensor data sets may produce significant differences in interpretations. However, maps derived from linear density analysis are found to be somewhat less influenced by operator variability. Generally, conservative linear "mappers" tend to infer fewer linears per unit area, but relative concentrations are sometimes agreed upon among operators.

VI. PROXIMITY ANALYSIS--LINEARS AND GAS YIELDS

Production or gas yield data (initial calculated open flow) combined with well locations and linears from various remote sensor data sets were called up simultaneously from the Zeta 3653 plotter. Figures 13 and 14 are representative

PRODUCTION PLOT

LEGEND

+ = NON-PRODUCING WELL

△ = < 2 MILLION CUBIC FEET

◇ = 2 < 5 MILLION CUBIC FEET

○ = 5 < 15 MILLION CUBIC FEET

□ = 15 MILLION CUBIC FEET OR MORE

NUMBER OF PRODUCING WELLS = 1059

Figure 13. Linears from Landsat winter scene, band 7, IPCOF (initial production calculated open flow) indicated.

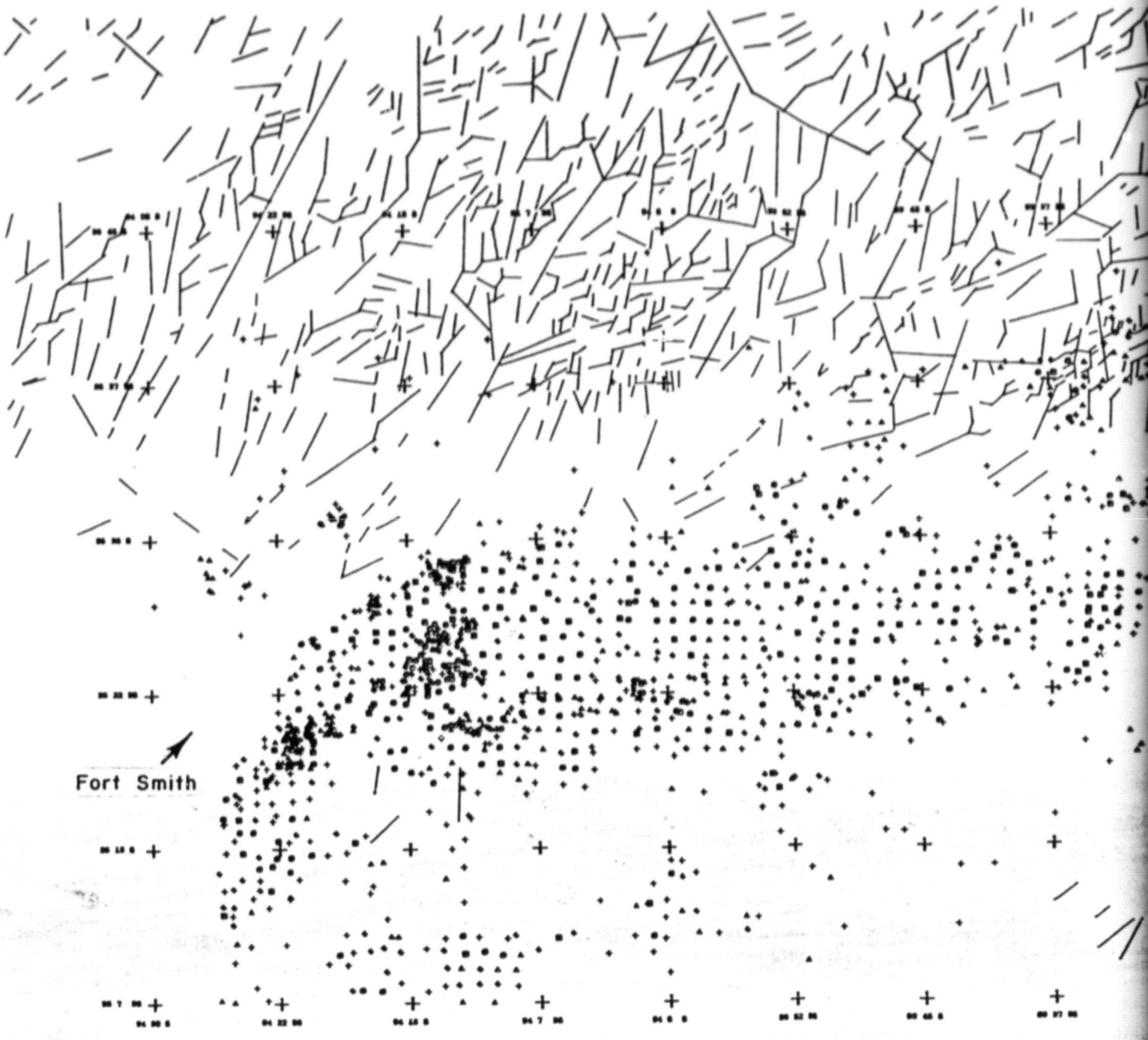

FOLDOUT FRAME

ORIGINAL PAGE IS
OF POOR QUALITY

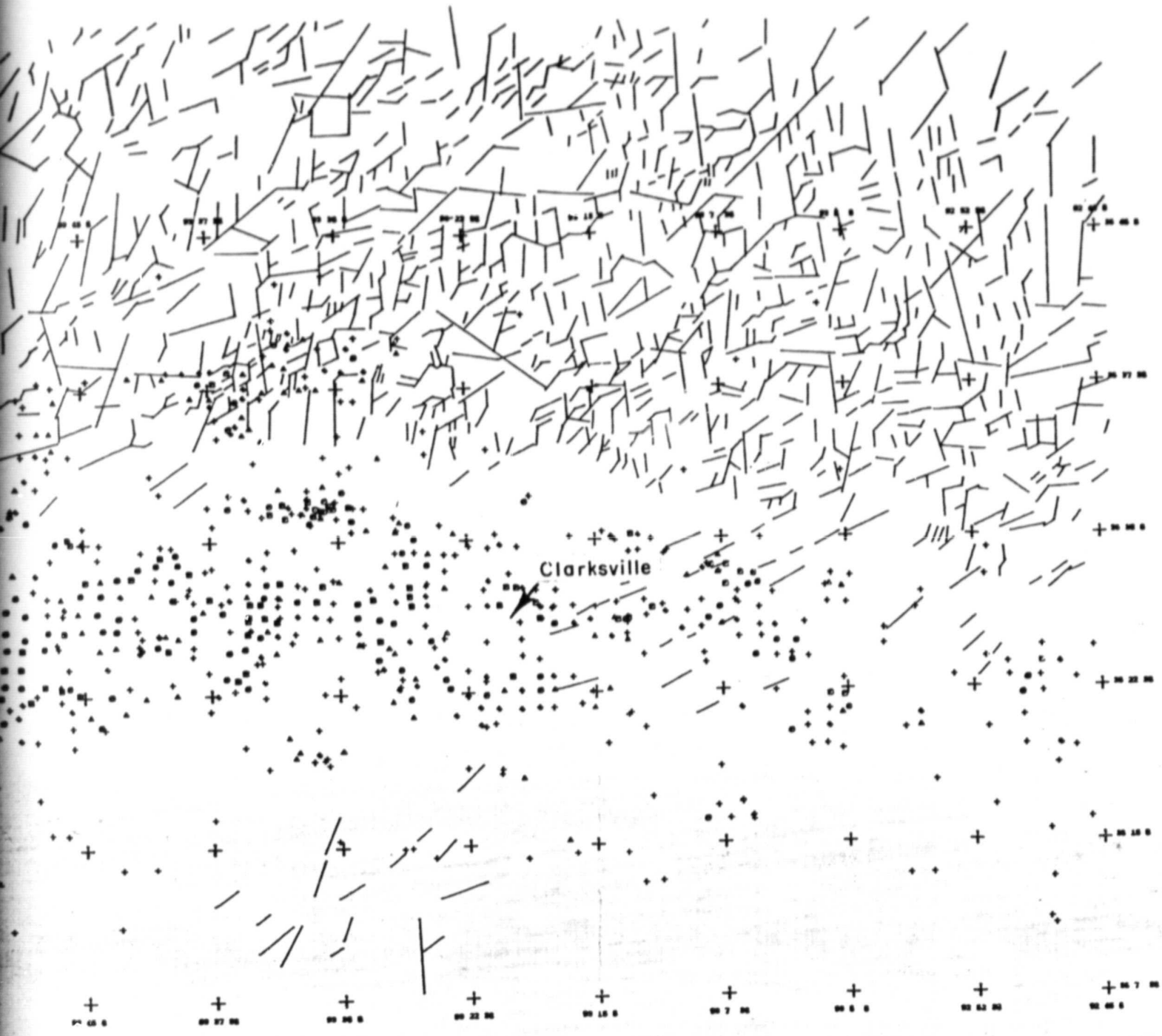

FOLDOUT FRAME 2

Figure 13

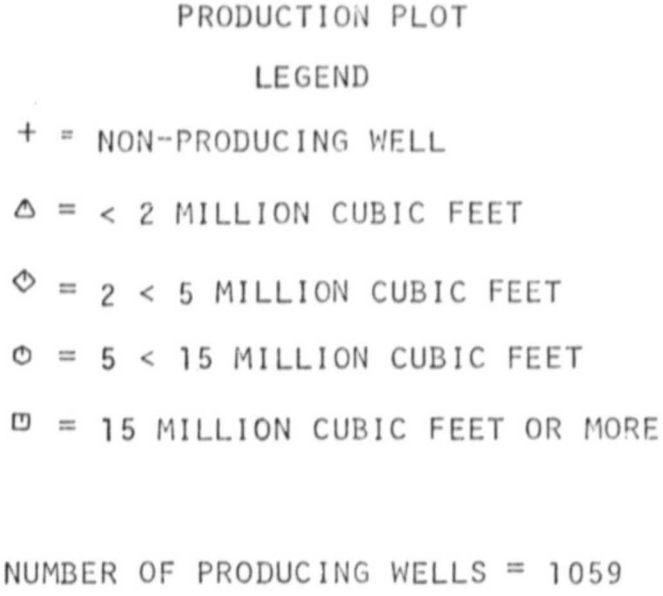

Figure 14. Linears from SAR L-band radar and well locations with IPCOF (initial production calculated open flow) indicated.

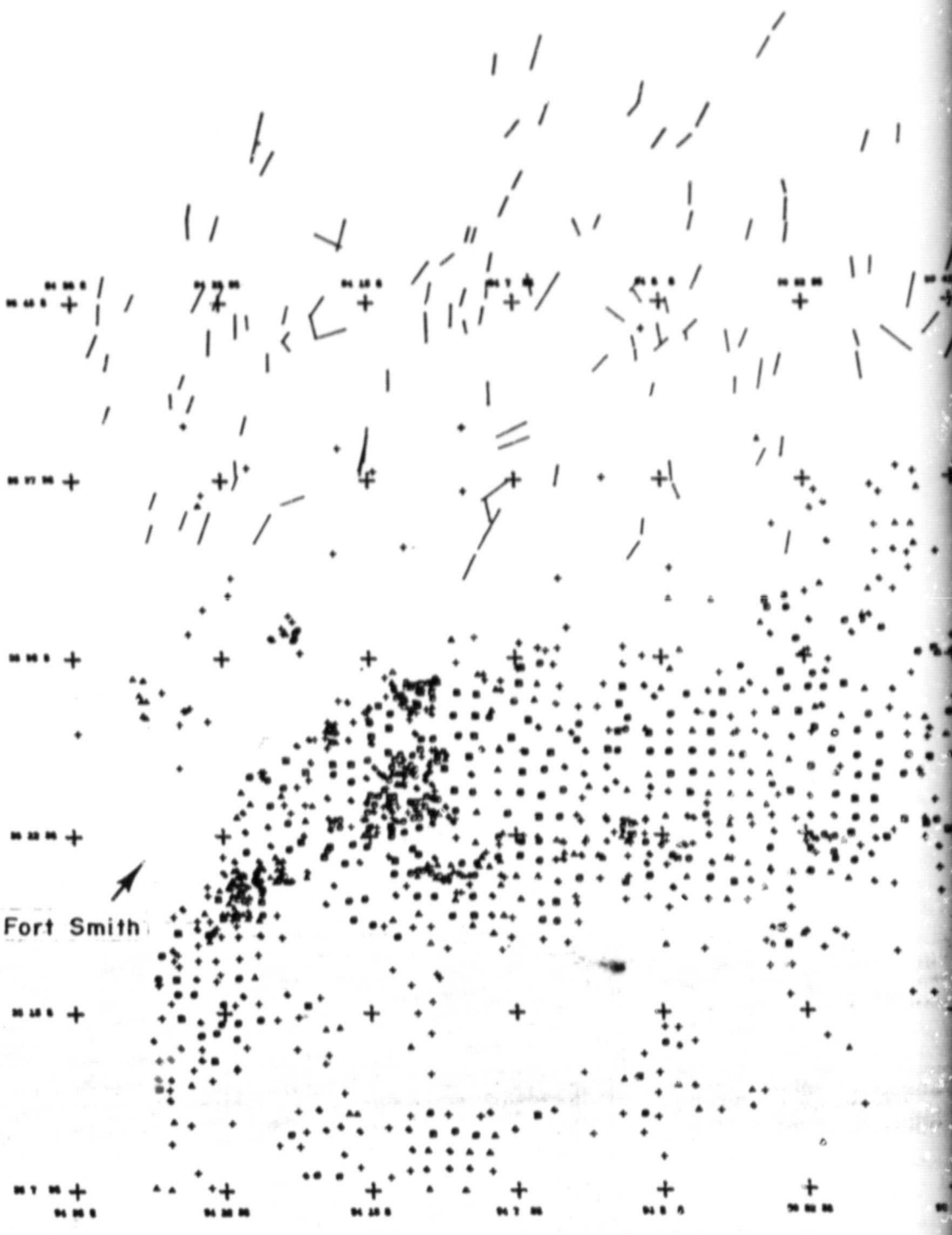

FOLDOUT FRAME

ORIGINAL PAGE IS
OF POOR QUALITY

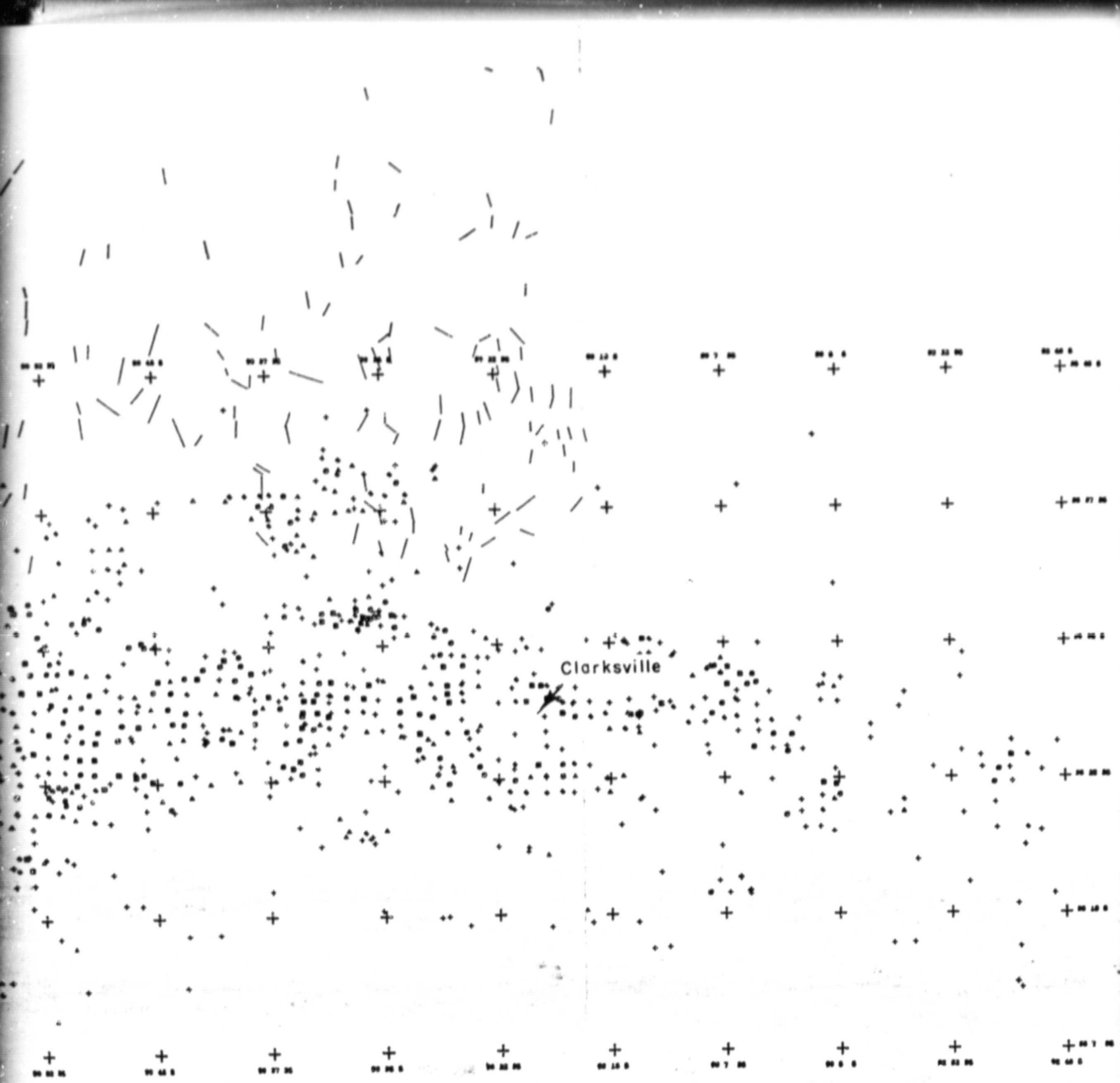

FOLDOUT FRAME 2

ORIGINAL PAGE IS
OF POOR QUALITY

Figure 14

sample plots from the Landsat band 7 winter scene and L-band respectively. The superimposed plots provide an overall comparison of poor, average, and good gas well yields with respect to linear position, clustering, and density. Regardless of the remote sensor data set used, it was apparent that the test site could be subdivided into two contrasting regions: the southern two-thirds of the test site which is characterized by an overall lack of linears in an area where producing wells are most numerous, and the northern third of the test site which has a relative abundance of linears where gas wells are nearly absent. An attempt is made to define the relationship between gas production and linear proximity in both of these regions.

A. Southern Region

Within the southern region or Arkoma basin proper, where wells are numerous and linears sparse, all attempts (linear regression analysis) to establish a relationship between well productivity and linear proximity proved futile. However, two additional methods of analysis were tried with well stimulation (hydraulic fracturing) data. Hydraulic fracturing, first introduced in 1949, is a process of injecting fluid into a wellbore under sufficient pressure to induce a vertical or horizontal fracture in the well formation. Continued injection of fluid after formation "breakdown" has occurred extends the fracture laterally from

the wellbore. Eventually an equilibrium is reached in which the filtration fluid losses through the walls of the fracture are equal to the fluid injection rate, and lateral extension of the fracture ceases. It is generally assumed that if the fracture area so generated is to remain open to flow a proppant must be simultaneously injected into the fracture area. The most common propping agent is 20-40 mesh sand (0.42-0.84 mm), though other propping agents are used such as glass beads, plastic particles, and ground walnut hulls. Various completion data (amount of proppant, proppant size, and fluid injection volume) from well completion cards were used to evaluate hydraulic fracturing effectiveness. This effectiveness was then compared with linear proximity or linear density in a manner somewhat similar to that reported in shale-gas studies where surface joints or fractures were used as predictors of the orientation of induced fracturing in the subsurface (Overbey et al., 1974; Jones and Rauch, 1976). Initially, a computerized data system was generated having the following information taken from completion cards for each of the producing wells in the study area.

Well Name	Producing Formation (up to 3
Field Name	different zones)
Legal Description	Open Flow Potential
Longitude/Latitude	Perforation Interval
County	Acidizing Volume
Spud Date	Sand Proppant Weight
Completion Date	Hydraulic Fracturing Volume
Total Depth	After Fracture Test Production (not always available)

Two different methods of anlaysis were applied with well stimulation data, one method for linear density and the second for individual linear proximity. The first method was an attempt to "generate" additional linears by use of the Ronchi grating in the area of maximum well density. The Ronchi grating or square wave transmission grating consists of a set of opaque parallel lines (normally 200/inch) separated by equal-width spaces on a transparent backing such as glass or plastic. Light is diffracted by the Ronchi grating in a direction perpendicular to the direction of the lines on the grid. When an image is viewed through the Ronchi grating the diffracted light will be spread out in one direction, but undisturbed in the perpendicular direction. This diffraction tends to blur out linears on the image that are parallel with the lines of the grid, thus accentuating the linears that are perpendicular to the lines of the grid (Pohn, 1970; Bench et al., 1977; Jackson, 1979).

1. Density Analysis

A contour map of linear density based on the Landsat-2 (winter scene) imagery was prepared. No significant trend or correlation could be established from this analysis. The percentage distribution of fractured and non-fractured wells was almost identical for each contour interval (see Table 11). Also, no trend could be established with respect to the volume of fracturing fluid injected and the linear density.

Table 11. Induced hydraulic fracturing linear density comparison.

Linear Density (m/sq km)	Fractured Wells		Non-Fractured Wells	
	No. of Wells	%	No. of Wells	%
0-176	318	73	452	72
176-353	91	21	119	19
353-529	17	4	30	5
529-706	3	1	8	1
706-882	2	-	9	2
882-1059	3	1	7	1
	434	100%	625	100%

2. Proximity Analysis

The second method provided the opportunity to call up wells in a given localized "window" enclosing a particular linear field or section of a field. The latitude and longitude of the two terminal points of a linear were read into the computer to create a rectangular window based on specified distances from these end points (Fig. 15). All wells within this window were plotted with an accompanying printout of the data parameters shown in Figure 15. Wells also could be called up by any one or combination of the five major geological zones known to yield gas in the areas selected.

Four separate areas were examined in detail by this method in terms of contrasting linear densities, proximity of gas wells to major linears, and contrasting linear orientations.

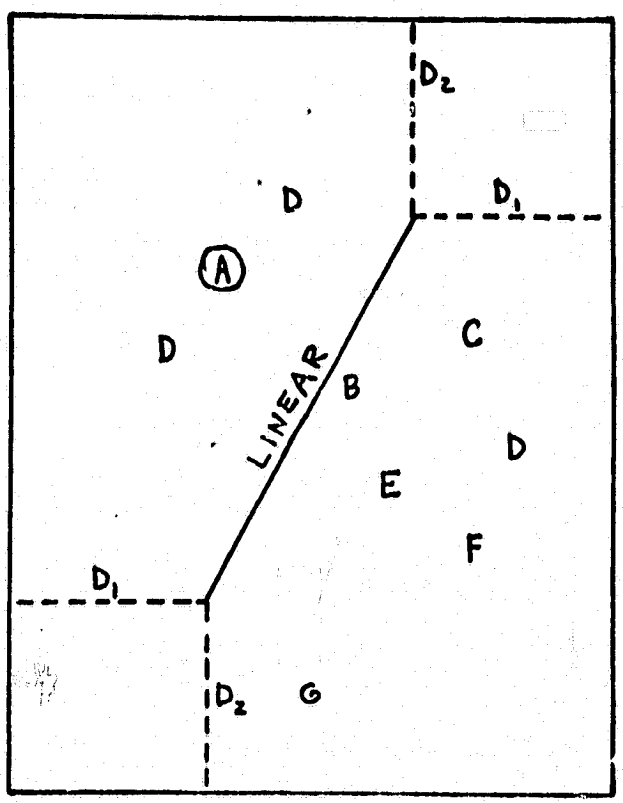

DATA INPUT: Longitude/latitude of linear end points, D_1, D_2, and scale choice, formation key.

DATA OUTPUT: Plot shown above with well record printout as shown below. (D - denotes dry hole, other letters denote coding for producing wells.)

```
WELL NAME = WILSON PROD CO. #1 SYDNEY JOHNSON          FLD NAME = DOVER
LEGAL DESCRPT =      SEC 2-9N-20W,1320'FNL,2600'FEL
SPUD DATE= 02-01-74     LONG= 93DEG  5Min 24SEC     LAT= 35DEG 27MIN 45SEC
COMP DATE= 03-01-74       TOTAL DEPTH= 3971'        COUNTY= POPE
GAS WELL
PRODUCTION FORMATION1: A-JENKINS          PRODUCTION FORMATION2:
        IPCOF=   6939.000 MCF                    IPCOF=       0.000 MCF
        IPF=        0.000 MCF                    IPF=         0.000 MCF
        INTERVAL1= 3177-3187                     INTERVAL1:     0-   0
        INTERVAL2=    0-   0                     INTERVAL2:     0-   0
        ACID          0 GALLONS                  ACID=          0 GALLONS
        SAND=         0  #                       SAND=          0  #
        GALLONS=      0                          GALLONS=       0
        FRAC PRODUCTION=      0 MCFGPD           FRAC PRODUCTION=       0 MCFGPD

NO.    1              CUMULATIVE PRODUCTION+  6939.000 MCF              CODE= (A)
```

Figure 15. Format for rectangular window computer output.

Analysis of the well stimulation data provides little evidence to support the hypothesis that surface linears can be related to subsurface reservoir fracturing. Although approximately 40 percent of the producing wells in the entire study area are hydraulically fractured, the average open flow potential for these wells is not significantly higher than the average for non-stimulated wells. Within the four separate areas selected for detailed analysis (Table 12), there appears to be no relationship between the open flow potential of hydraulically fractured wells and linear density, nor can a relationship be established between the open flow potential of stimulated wells and linear proximity.

B. Northern Region

In parts of the northern region well control and linear density contrast are sufficient for use in examining the relationship between well yield and linear trends. To facilitate computer analysis, the northern one third of the test site was subdivided into half-quad (7.5' quad maps) areas (Fig. 16). In addition, the various gas-bearing zones within the stratigraphic column were consolidated into manageable groups based on their stratigraphic position and reservoir and lithologic similarities: Upper Atoka, Lower Atoka, Sandstone Group, and Carbonate Group.

Table 12. Comparison of linear areas.

Area & Location	Fields Involved	No. Prod. Wells	No. Dry Wells	% Prod.	No. of Wells Hyd. Fractured	Average Open Flow (Not Fractured)	Average Open Flow (Fractured)	Major Linear Length (km)	Linear Density (m/sq. km)	Orthogonality	Formation Zones Involved
Johnson County Long. 932820 934010 Lat. 352523 352827	Spadra, Union City Scranton 102.3 sq. km	34	16	68	21	15.6MM	18.6MM	8.72	0-176 with intermittent zones of 176-353	Low	Upper & Lower Atoka Sandstones
Johnson County Long. 933000 933730 Lat. 353730 354115	Batson 79.0 sq. km	13	5	72	2	7.20MM	0.5MM	6.84	529-706	Strong	Cherty & Carbonate & Atoka Sandstones
Pope County Long. 930450 931510 Lat. 352508 353052	Dover New Hope 183.4 sq. km	24	31	44	10	10.6MM	10.4MM	10.62	=353 with intermittent zones up to 529. One streak of zero.	Strong	Lower Atoka Sandstones
Crawford County Long. 941000 941500 Lat. 352600 353000	Alma, Kibler, and Hollis Lake 56.2 sq. km	18	9	67	15	10.36MM	10.57MM	None	=176	Moderate	Upper Atoka Sandstones

PRODUCTION PLOT

LEGEND

+ = NON-PRODUCING WELL

△ = < 2 MILLION CUBIC FEET

◇ = 2 < 5 MILLION CUBIC FEET

○ = 5 < 15 MILLION CUBIC FEET

□ = 15 MILLION CUBIC FEET OR MORE

NUMBER OF PRODUCING WELLS = 1059

Figure 16. Half-quad subdivision, northern region. Linears from Landsat winter scene band 7.

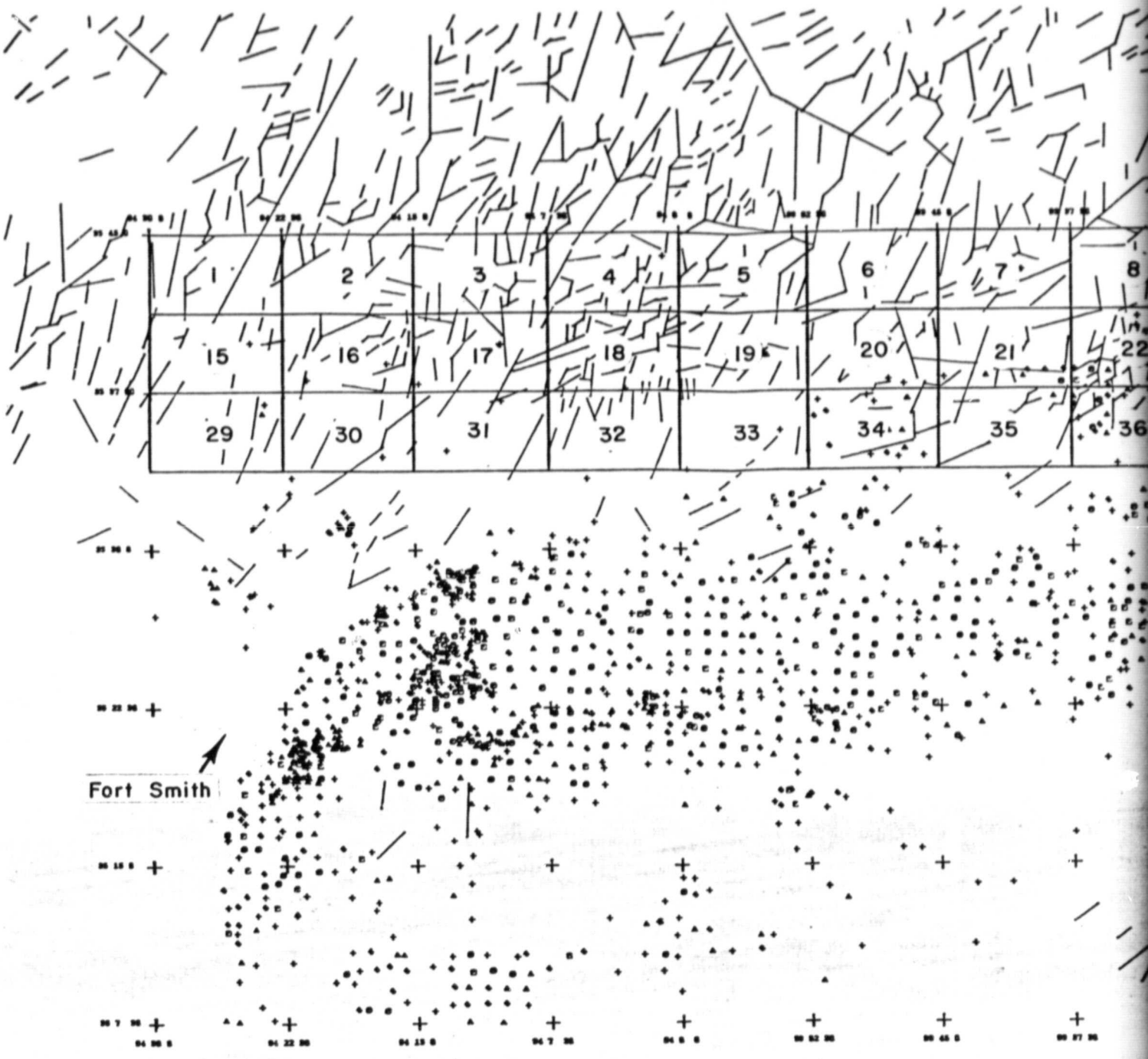

FOLDOUT FRAME

ORIGINAL PAGE IS
OF POOR QUALITY

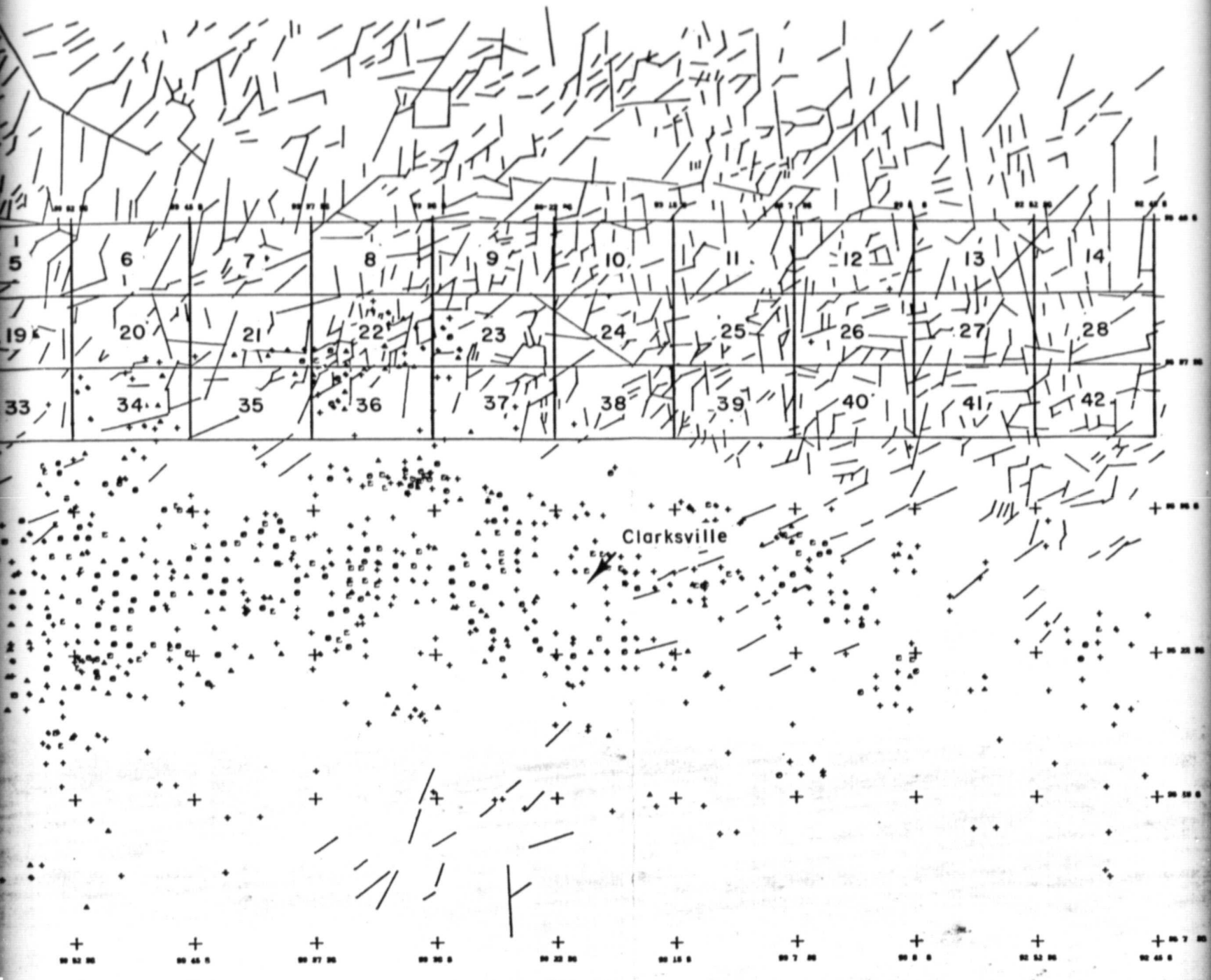

ORIGINAL PAGE IS
OF POOR QUALITY

FOLDOUT FRAME 2

Figure 16

The Atoka Formation, which accounts for a large part of the gas production, contains a laterally persistent shale horizon between the Vernon and Sells sands. This shale is chosen as a boundary between the Upper Atoka and the Lower Atoka (LATOKA). The upper Atoka units are very thin or absent in the northern margin of the test site and therefore are omitted from the analysis. The sandstone units in the Lower Atoka are:

Lower Atoka (LATOKA)

Sells	Cecil Spiro
Jenkins	Patterson
Dunn C	Spiro
Paul Barton	

The remaining productive horizons can be grouped by lithology and demarcated by unconformities. In descending stratigraphic order, the next group is predominantly sandstone and is referred to as the Sandstone Group (SANDST). The Sandstone Group, bounded by unconformities, is from Pennsylvanian to Mississippian in age. It includes the following units

Sandstone Group (SANDST)

Kessler	Upper Hale
Cannon	Middle Hale
Pitkin	Lower Hale
Wedington	

The Carbonate Group (CARB), the lowermost group, is predominantly limestone and dolomite and ranges in age from

Mississippian to Ordovician. The Carbonate Group is also bounded by unconformities and includes the following units.

Carbonate Group (CARB)

Boone	Everton-Simpson
Penters	Arbuckle
Hunton	

Another parameter, referred to as Total (TOTAL), is needed to represent the total production from the three groups for any certain well.

1. Density Analysis

For the density values, each linear within a half-quad was measured and the lengths were added to obtain a total linear length for the half-quad. This value is referred to as DENS1. Linears (or any part thereof) within a half-quad are hypothesized to have an effect on gas production and linears outside the half-quad are not. The total number of linears within the half-quad was calculated and is referred to as DENS2 (Table 13).

By means of the Statistical Analysis System (SAS) (Barr et al., 1976), the Pearson correlation coeffieicnt test is used for a relationship between the production values and the density functions.

DENS1 - TOTAL
DENS1 - LATOKA
DENS1 - SANDST
DENS1 - CARB
DENS2 - TOTAL

Table 13. Half-quads and density measurements.

Half-Quad Number	DENS1 (Total Length-Meters)	DENS2 (Total Number)
1	35305	13
2	26890	17
3	42409	29
4	48445	35
5	45854	25
6	29268	17
7	39909	21
8	43689	26
9	52378	38
10	44055	30
11	40274	25
12	44024	31
13	38994	22
14	32896	18
15	19878	13
16	42226	23
17	43567	20
18	60396	48
19	36189	19
20	32805	22
21	26402	14
22	58079	47
23	44726	38
24	50732	29
25	51707	34
26	44695	30
27	49695	35
28	38415	22
29	16311	6
30	19421	9
31	18201	8
32	29085	18
33	7683	7
34	17591	9
35	27530	18
36	23994	16
37	31707	21
38	41524	27
39	45091	36
40	37896	28
41	43537	32
42	38963	25

DENS2 - LATOKA
DENS2 - SANDST
DENS2 - CARB

If a half-quad has less than two wells it is not considered in the correlation analysis. Fourteen half-quads have two or more wells (Table 14).

A correlation coefficient (ρ) and significance probability level (α) were generated for each combination of the six parameters (Table 15). The null hypothesis states: "There is no correlation between linear density and well production." A correlation is assumed to be present if a relationship has a significance probability level greater than 95 percent ($\alpha \leq .05$) or a correlation coefficient greater than 0.5 ($\rho > 0.5$).

From Table 15, one significant correlationis found. Production values from the Carbonate Group (CARB) show a positive correlation ($\alpha = 0.0031$, $\rho = 0.72866$) with the number of linears per half-quad (DENS2). Most Carbonate Group production is from the relatively low porosity, impermeable Boone Formation (Van Den Heuval, 1979) and therefore may depend on the number of fractures.

A relationship is suggested ($\alpha = 0.0756$, $\rho = 0.51827$) between the Sandstone Group (SANDST) and the number of linears per half-quad (DENS2). Unlike the units in the Lower Atoka, the Sandstone Group includes more mature, calcareous sandstone. The calcareous cement of this sandstone could increase its responsiveness to natural fracturing.

Table 14. Data used for Pearson correlation coefficient for linear density.

OBS	QUAD	TOTAL	LATOKA	SANDST	CARB	DENS1	DENS2
1	8	0.0	0.0	0.0	0.0	43689	26
2	16	0.0	0.0	0.0	0.0	42226	23
3	17	0.0	0.0	0.0	0.0	43567	20
4	20	0.0	0.0	0.0	0.0	32805	22
5	21	21787.5	4567.0	9745.7	5557.8	26402	14
6	22	87511.0	3900.0	42100.0	39711.0	58079	47
7	23	20182.9	5961.9	2528.0	11693.0	44726	38
8	24	0.0	0.0	0.0	0.0	50732	29
9	29	730.0	730.0	0.0	0.0	16311	6
10	31	0.0	0.0	0.0	0.0	18201	8
11	33	0.0	0.0	0.0	0.0	7683	7
12	34	17130.0	8750.0	8300.0	80.0	17591	9
13	36	28262.0	11940.2	15703.0	618.0	23994	16
14	37	0.0	0.0	0.0	0.0	31707	21

Table 15. Pearson correlation coefficient - density.

CORRELATION COEFFICIENTS / PROB > |R| UNDER HO:RHO=0 / N = 14

	TOTAL	LATOKA	SANDST	CARB	DENS1	DENS2
TOTAL	1.00000 0.0000	0.49229 0.0737	0.98447 0.0001	0.93457 0.0001	0.39056 0.1674	0.59359 0.0253
LATOKA	0.49229 0.0737	1.00000 0.0000	0.47925 0.0829	0.20132 0.4901	-0.13951 0.6343	0.02562 0.9307
SANDST	0.98447 0.0001	0.47925 0.0829	1.00000 0.0000	0.88838 0.0001	0.34478 0.2273	0.51827 0.0576
CARB	0.93457 0.0001	0.20132 0.4901	0.88838 0.0001	1.00000 0.0000	0.53020 0.0511	0.72866 0.0031
DENS1	0.39056 0.1674	-0.13951 0.6343	0.34478 0.2273	0.53020 0.0511	1.00000 0.0000	0.91534 0.0001
DENS2	0.59359 0.0253	0.02562 0.9307	0.51827 0.0576	0.72866 0.0031	0.91534 0.0001	1.00000 0.0000

There is also a positive correlation (α = 0.0253, ρ = 0.59359) between total production (TOTAL) and total number of lineras per half-quad (DENS2). This finding is of questionable value because the Carbonate Group production makes up a large part of the total production. No other relationship of significance are found.

2. Proximity Analysis

For this analysis, two distance parameters are used. One is the distance from a given well to the nearest linear (DIST1) and the other is the distance from a given well to the nearest linear intersection (DIST2) (Table 16). Two linears are not considered intersecting if they are more than two line widths (0.5 mm) apart.

The definitions for both distances are based on the concept of an expanding circle with a given well as the center. As the circle expands it eventually meets a linear and a linear intersection. The distance is the radius of the circle at the point of contact with the linear and linear intersection.

By means of the Statistical Analysis System (SAS) (Barr et al., 1976) the Pearson correlation coefficient is used to test for a relationship between:

DIST1 - TOTAL
DIST1 - LATOKA
Dist1 - SANDST
DIST1 - CARB
DIST2 - TOTAL

Table 16. Data used for Pearson correlation coefficient for linear distance.

OBS	QUAD	WELL	TOTAL	LATOKA	SANDST	CARB	DIST1	DIST2
1	4	1	0.0	0.0	0.0	0.0	396	2347
2	7	1	0.0	.	.	.	1097	6309
3	8	1	0.0	0.0	0.0	0.0	610	823
4	8	2	0.0	.	.	.	91	823
5	12	1	0.0	0.0	0.0	0.0	975	3231
6	15	1	0.0	0.0	0.0	0.0	853	1768
7	16	1	0.0	0.0	0.0	.	213	3962
8	16	2	0.0	.	.	.	518	1494
9	17	1	0.0	0.0	0.0	.	670	2103
10	17	2	0.0	0.0	0.0	0.0	305	640
11	18	1	0.0	0.0	0.0	0.0	182	2012
12	19	1	500.0	.	500.0	.	579	5304
13	20	1	0.0	0.0	0.0	0.0	366	2530
14	20	2	0.0	0.0	0.0	0.0	1280	1707
15	21	1	8400.0	3500.0	2400.0	2500.0	610	670
16	21	2	1549.0	.	.	.	853	1067
17	21	3	1450.0	.	1082.0	.	457	1189
18	21	4	3009.0	1067.0	1942.0	.	61	1402
19	21	5	3168.0	.	2032.0	1136.0	182	1676
20	21	6	4211.5	.	2289.7	1921.8	91	305
21	22	1	4500.0	.	400.0	4100.0	213	823
22	22	2	36648.0	.	30773.0	5875.0	701	1311
23	22	3	14398.0	.	.	14398.0	488	610
24	22	4	13600.0	.	6000.0	7600.0	0	1311
25	22	5	500.0	.	500.0	.	579	792
26	22	6	3098.0	3000.0	.	98.0	335	1097
27	22	7	0.0	0.0	0.0	0.0	1006	1158
28	22	8	0.0	0.0	0.0	0.0	213	1737
29	22	9	0.0	0.0	0.0	0.0	182	701
30	22	10	6500.0	.	.	6500.0	31	1311
31	22	11	821.0	.	821.0	.	122	1097
32	22	12	2000.0	.	.	2000.0	549	2286
33	22	13	430.0	.	430.0	.	366	2347
34	22	14	2040.0	.	2000.0	40.0	610	2286

Table 16. Continued.

OBS	QUAD	WELL	TOTAL	LATOKA	SANDST	CARB	DIST1	DIST2
35	22	15	176.0	.	176.0	.	518	823
36	22	16	560.0	.	.	560.0	152	823
37	22	17	0.0	0.0	0.0	0.0	31	1158
38	22	18	0.0	0.0	0.0	0.0	488	1372
39	22	19	0.0	0.0	0.0	0.0	518	1737
40	22	20	2240.0	900.0	1000.0	340.0	457	1189
41	23	1	0.0	0.0	0.0	0.0	732	792
42	23	2	4899.0	.	.	4899.0	853	1067
43	23	3	3600.0	3000.0	.	600.0	182	305
44	23	4	6915.9	721.9	.	6194.0	1158	1280
45	23	5	2200.0	900.0	1300.0	.	549	2103
46	23	6	1000.0	.	1000.0	.	853	2073
47	23	7	0.0	0.0	0.0	0.0	396	579
48	23	8	0.0	0.0	0.0	0.0	274	518
49	23	9	228.0	.	228.0	.	549	1524
50	23	10	1340.0	1340.0	0.0	.	91	3505
51	24	1	0.0	0.0	0.0	0.0	427	2377
52	24	2	0.0	.	.	.	152	549
53	26	1	0.0	0.0	0.0	0.0	670	2743
54	29	1	0.0	0.0	0.0	0.0	670	5425
55	29	2	730.0	730.0	.	0.0	610	6279
56	30	1	0.0	0.0	0.0	0.0	670	762
57	31	1	0.0	0.0	0.0	0.0	2713	5608
58	31	2	0.0	0.0	0.0	0.0	182	549
59	33	1	0.0	0.0	0.0	0.0	701	7437
60	33	2	0.0	0.0	0.0	0.0	2530	7132
61	34	1	0.0	0.0	0.0	0.0	1737	7437
62	34	2	3500.0	3500.0	0.0	.	1615	14204
63	34	3	4430.0	1250.0	3100.0	80.0	2317	13167
64	34	4	2000.0	2000.0	0.0	.	1524	10485
65	34	5	0.0	0.0	0.0	0.0	213	4999
66	34	6	0.0	0.0	0.0	0.0	670	4572
67	34	7	0.0	0.0	0.0	0.0	1555	6675

Table 16. Continued.

OBS	QUAD	WELL	TOTAL	LATOKA	SANDST	CARB	DIST1	DIST2
68	34	8	0.0	0.0	0.0	0.0	244	13228
69	34	9	250.0	250.0	.	.	1341	5121
70	34	10	2600.0	.	2600.0	.	549	7529
71	34	11	1000.0	.	1000.0	0.0	793	1890
72	34	12	1750.0	1750.0	.	.	975	4511
73	34	13	1600.0	.	1600.0	0.0	427	6005
74	34	14	0.0	0.0	0.0	0.0	975	6675
75	34	15	0.0	0.0	0.0	0.0	1494	5639
76	35	1	1000.0	1000.0	.	.	762	1036
77	36	1	1900.0	1900.0	.	.	488	579
78	36	2	3600.0	.	3600.0	.	213	670
79	36	3	0.0	0.0	0.0	0.0	30	1890
80	36	4	0.0	0.0	0.0	0.0	1494	3322
81	36	5	6000.0	1000.0	5000.0	.	396	1250
82	36	6	4533.0	2502.0	2031.0	.	1128	3109
83	36	7	2750.0	250.0	2500.0	0.0	1524	3444
84	36	8	3175.0	2629.0	.	546.0	610	1829
85	36	9	1344.0	451.0	893.0	.	457	2469
86	36	10	140.0	.	140.0	.	122	2539
87	36	11	1751.2	212.2	1539.0	.	670	3231
88	36	12	72.0	.	.	72.0	823	2926
89	36	13	0.0	.	.	.	2591	4968
90	36	14	1373.0	1373.0	0.0	.	305	1554
91	36	15	0.0	0.0	0.0	0.0	213	1524
92	36	16	123.0	123.0	0.0	.	122	1646
93	36	17	500.0	500.0	0.0	.	427	1585
94	36	18	1000.0	1000.0	0.0	.	518	1798
95	36	19	0.0	0.0	0.0	0.0	1494	6279
96	37	1	0.0	0.0	0.0	0.0	549	1951
97	37	2	0.0	.	.	.	1585	2469
98	37	3	0.0	.	.	.	152	5029
99	37	4	0.0	0.0	0.0	0.0	670	1280
100	37	5	0.0	0.0	0.0	0.0	670	2377
101	38	1	0.0	0.0	0.0	0.0	1219	3901

DIST2 - LATOKA
DIST2 - SANDST
DIST2 - CARB

As before, a correlation coefficient (ρ) and significance probability level (α) are generated for each combination of the six parameters (Table 17). The null hypothesis states: "There is no correlation between distance to linear (and linear intersection) and well production." A correlation is assumed to be present if a relationship has a significance probability level greater than 95 percent ($\alpha \leq .05$) or a correlation coefficient greater than 0.5 ($\rho > 0.5$).

From Table 17 a negative correlation ($\alpha = 0.0450$, $\rho = -0.253$) is suggested between the Carbonate Group (CARB) productionand the distance to the nearest linear intersection (DIST2). In other words, the closer a well producing from the Carbonate Group is to a linear intersection, the greater its production rate. Most of the producing wells in the Carbonate Group are 305 to 2134 m from the nearest linear intersection and wells beyond 2134 m are dry holes. The fact that many dry holes are also between 305 and 2134 m from the nearest linear intersection explains the marginal correlation ($\alpha = 0.0450$, $\rho = -0.25348$).

The important relationship is between production from the Carbonate Group (CARB) and the number of linears per half-quad (DENS2). The marginal correlation of Table 17 reflects this relationship. As the number of linears per

Table 17. Pearson correlation coefficient - distance.

CORRELATION COEFFICIENTS / PROB > |R| UNDER HO:RHO=0 / N = 14

	TOTAL	LATOKA	SANDST	CARB	DIST1	DIST2
TOTAL	1.00000 0.0000 101	0.76376 0.0001 68	0.96595 0.0001 78	0.69623 0.0001 63	-0.05731 0.5692 101	-0.11265 0.2520 101
LATOKA	0.76376 0.0001 68	1.00000 0.0000 68	0.44851 0.0004 59	0.35209 0.0131 49	0.01675 0.8922 68	0.10257 0.4052 68
SANDST	0.96596 0.0001 78	0.44851 0.0004 59	1.00000 0.0000 78	0.66526 0.0001 52	-0.02385 0.8358 78	-0.08245 0.4730 78
CARB	0.69623 0.0001 63	0.35209 0.0131 49	0.66526 0.0001 52	1.00000 0.0000 63	-0.15686 0.2195 63	-0.25348 0.0450 63
DIST1	-0.05731 0.5692 101	0.01675 0.8922 68	-0.02385 0.8358 78	-0.15686 0.2195 63	1.00000 0.0000 101	0.53854 0.0001 101
DIST2	-0.11265 0.2620 101	0.10257 0.4052 68	-0.08245 0.4730 78	-0.25348 0.0450 63	0.53854 0.0001 101	1.00000 0.0000 101

half-quad increases, the frequency of intersecting linears also increases. In other words, if a producing well is in an area of high linear density, there is probably a linear intersection within 2134 m. This relationship has application for locating both exploration and development wells. In sandstone and carbonate strata, the distance to the nearest linear or linear intersection can be disregarded. A well is more likely to be productive if it is in an area of high linear density and if it penetrates structurally elevated carbonate strata.

C. Practical Application

Within the northern region, a relatively large number of producing gas wells are clustered in the vicinity of half-quads 34 and 22 (Fig. 16). Visual analysis of Figure 16 indicates a contrasting relationship for linears in these same quads. Whereas half-quad 34 (immediate vicinity of Rock Creek gas field) is characterized by few linears, half-quad 22 has a relatively large number of linears, especially in a north-south orientation. In an attempt to define the relationship between linears, subsurface structure, and gas production in these two contrasting areas, subsurface structure maps were constructed from mechanical well logs (induction electric, formation density, and gamma ray/neutron).

1. Batson Gas Field

Although a number of wells produce gas from sandstone units within the Atoka Formation, the Batson Field is the

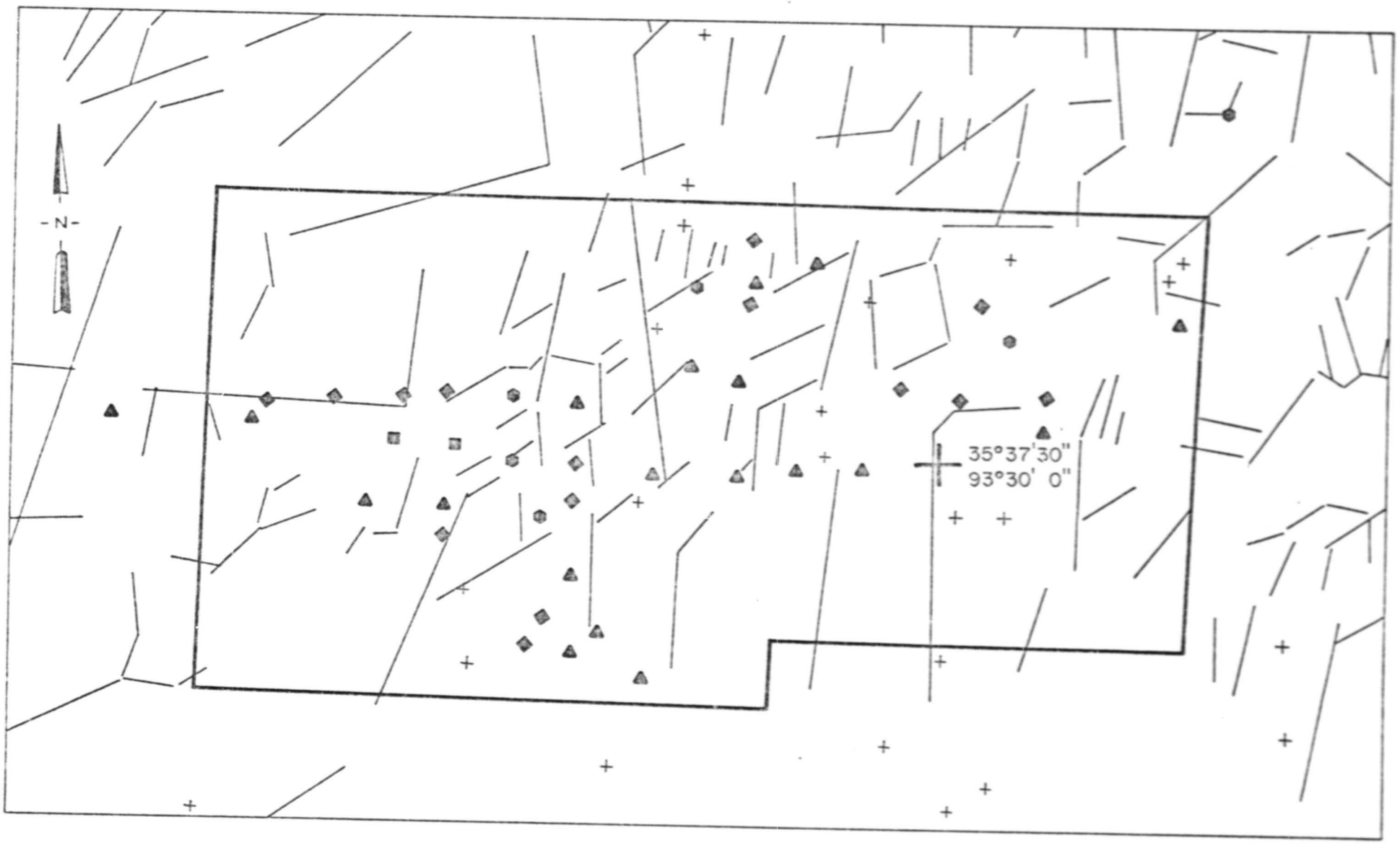

+ Non-producing well

▲ < 2 Million cubic feet

◆ 2 < 5 Million cubic feet

● 5 < 15 Million cubic feet

■ ≥ 15 Million cubic feet

0 1 2 3 4 5

Kilometers

Figure 17. Linears detected from Landsat analysis, well locations with initial production, Batson field.

only area of significant Boone Formation production in the entire Arkoma basin. Figure 17 is an enlarged plot of linears and gas-producing wells in all rock units in the Batson field area.

Wells producing gas from the Boone Formation are on structural highs in the Batson field, and wells not on structural highs have produced water. From Figure 18, the -900 foot (below sea level) contour was chosen to distinguish wells that are structurally high from those that are structurally low. There is a positive correlation between production from the Boone Formation and well location with respect to structure, with two exceptions. The well in SW 1/4 of Sec. 32, T. 12 N., R. 24 W. (Fig. 18) is a dry hole in the Boone Formation in spite of its structurally high position. Examination of subsurface cross-sections constructed from mechanical well logs indicates that the well intercepts a fault, which appears to eliminate any production possibility. The well in Sec. 29, T. 11 N., R. 24 W. (Fig. 18) is a producing well but is in a structurally low area of the Boone Formation. The well is outside the area where the contours can be drawn with confidence (limited control points). Moreover, production records show this particular well to be a very low producer (72.4 MCFGPD).

2. Rock Creek Field

Figure 19 is an enlarged plot of linears and gas-producing wells in the Rock Creek field. A structure contour map was

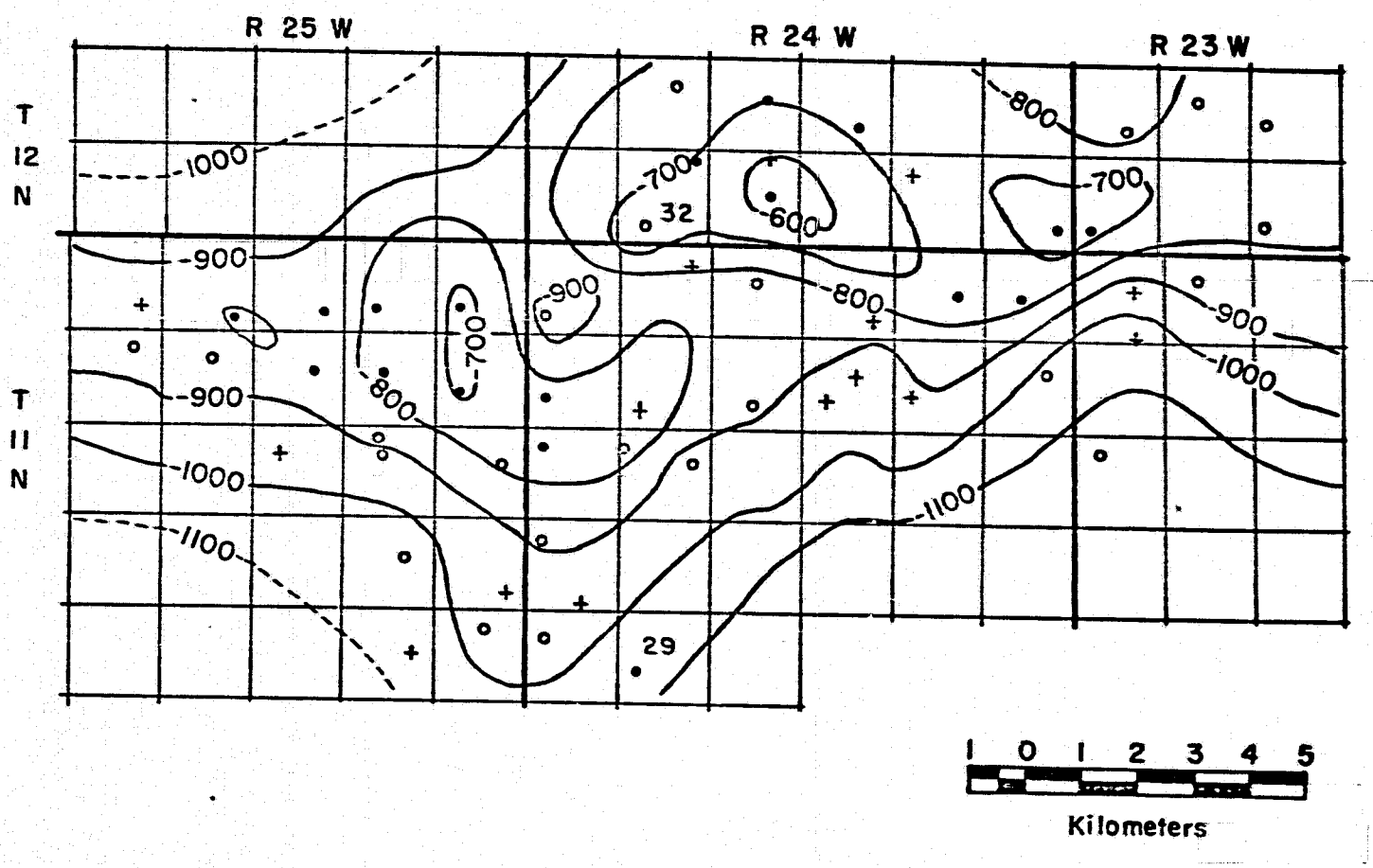

- Well producing from Boone Formation
- Dry hole in Boone Formation
+ Well penetrating upper Boone Formation only

Figure 18. Structure contour map for the top of the Boone Formation, Batson field.

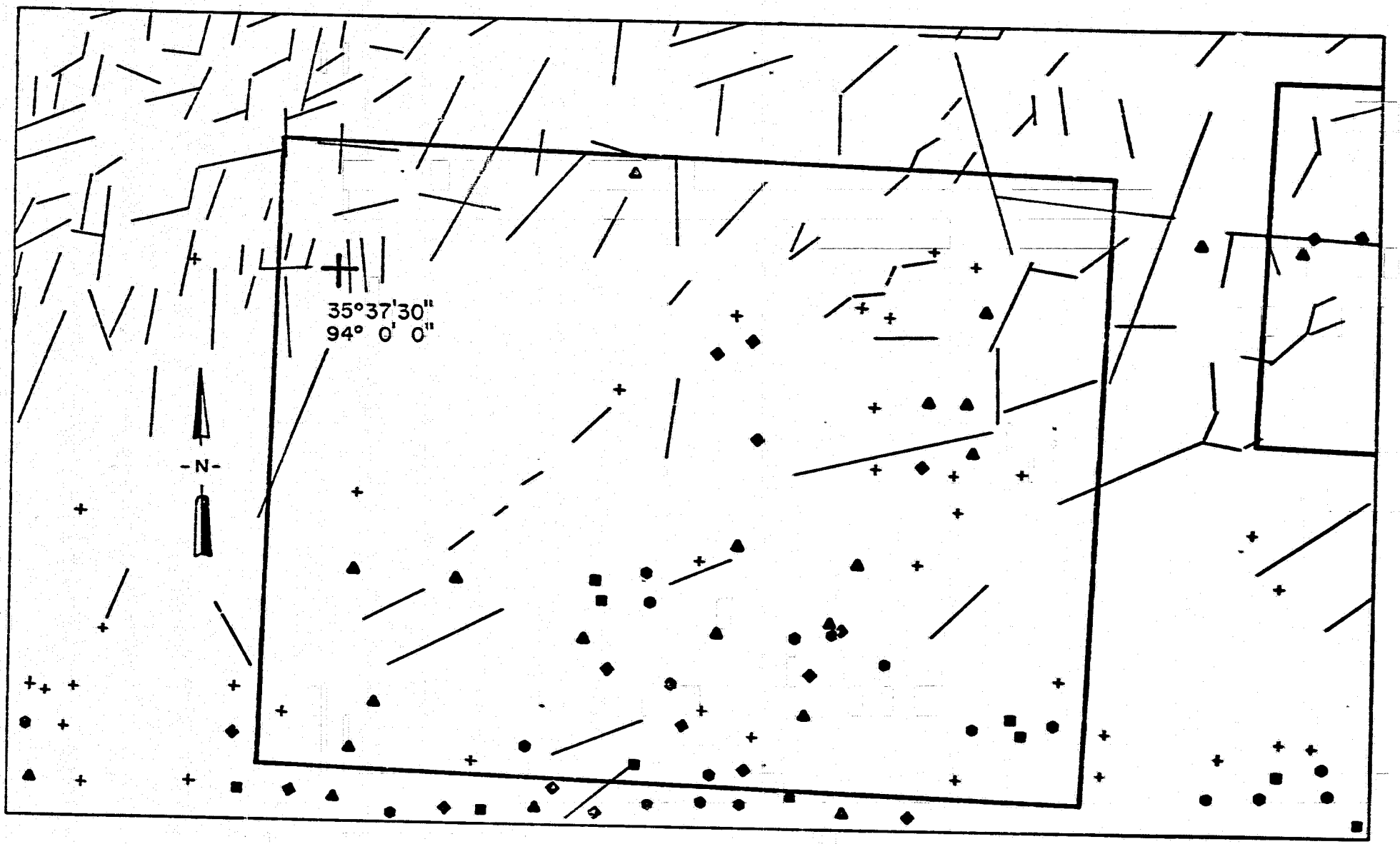

+ Non-producing well

▲ < 2 Million cubic feet

◆ 2 < 5 Million cubic feet

● 5 < 15 Million cubic feet

■ ≥ 15 Million cubic feet

0 2 4 6 8 10

Kilometers

Figure 19. Linears detected from Landsat analysis, well locations with initial production, Rock Creek field.

constructed for the top of the Boone Formation (Fig. 20). Several structural highs are present but, unlike wells in the Batson field, wells on these highs do not produce from the Boone Formation. In the entire area only two wells produce from the Boone Formation (Fig. 20) and both are relatively low producers. Inspection of the samples from the productive horizon of the well in Sec. 24, T. 11 N, R. 28 W. (Fig. 20) shows minor fracture porosity. For the producing well in Sec. 22, T. 11 N., R. 27 W. (Fig. 20), fracture porosity is not found but production records show the well to be a very low producer (80 MCFGPD).

3. Data Analysis

The Boone Formation (up to 60-70 percent chert) yields gas in the Batson field which is situated on a structural high coincident with high linear density. However, in the Rock Creek field, the Boone Formation is on a structural high in an area of low linear density and is essentially nonproductive. A study of mechanical logs from both fields indicates that the Boone interval is generally lithologically consistent throughout.

The Pearson correlation coefficient indicates a positive correlation between the number of liners in a given area (linear density) and production from the Boone Formation; however, there is no significant correlation between production and the distance to the nearest linear. Because the Boone

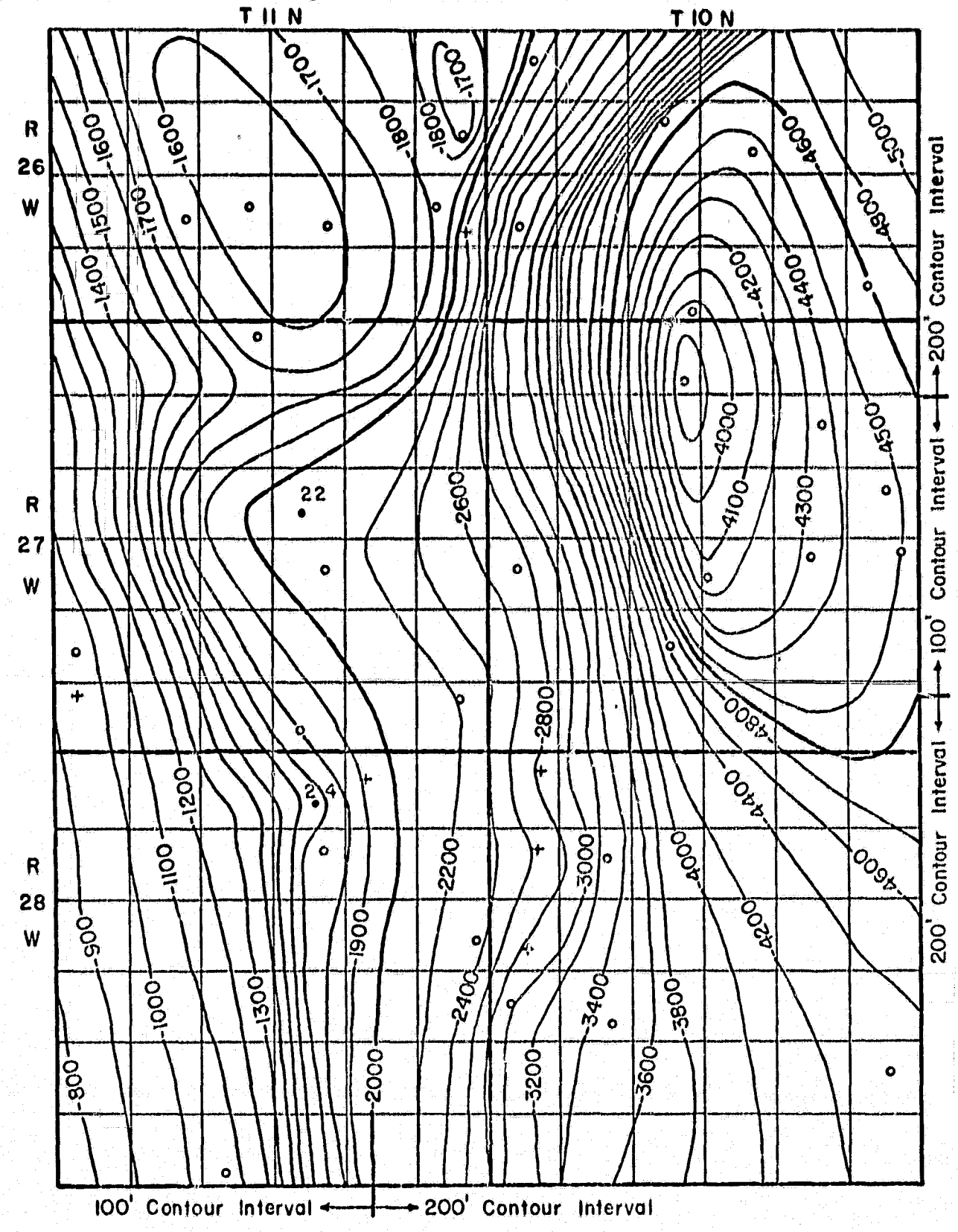

Figure 20. Structure contour map for the top of the Boone Formation, Rock Creek field.

ORIGINAL PAGE IS
OF POOR QUALITY

Formation is a brittle, high-chert-content limestone with very low porosity and permeability (Van Den Heuval, 1979), it is reasonable that the high surface linear density is a reflection of fracture porosity/permeability in the subsurface.

Previous studies in other areas (Harris et al., 1960; Stearns and Friedman, 1972; Gorham et al., 1979) indicate that the strongest surface fracturing is on the flanks of folds where curvature is at a maximum. In addition, Gorham et al. (1979) suggest that open fractures had to develop where tensional joints form at places of maximum curvature of beds (i.e., where there is greatest rate of change of dip, not necessarily where the dips are steepest). The Batson field is on the hinge line of a regional east-west-trending monocline resulting from the transition from essentially horizontal strata of the northern Arkansas structural platform to the southward-dipping strata of the Arkoma basin. Open fractures are believed to develop where tensional joints form at places of maximum curvature (hinge line) of the beds (Gorham et al., 1979). Figure 17 does not indicate a prominent east-west-trending linear pattern. However, if the fracture-development hypothesis is correct and such an east-west-trending pattern is present in the subsurface rocks, the prominent north to northeasterly linear pattern defined from Figure 17 would be superimposed upon it. The somewhat orthogonal nature of such a pattern appears to be supported by field work, as a general north-south and

C-2

east-west pattern of surface joint data has been recorded (Figure 4).

As discussed in Section IV, the east-west-trending non-systematic surface joints are probably not characteristically indicative of tensional stress conditions; however, because of the structural position of the Batson field, relatively tight fractures may have been changed to open fractures. The structural position of the Batson field on a regional monocline, coincident with a local structural high with increased linear density, provides empirical support for an interrelationship between remote sensor-derived linears and fracture production. The Rock Creek field, although on a local structural high, is off the hinge line of the monocline in an area of low linear density, and has minimal evidence of fracture production. These findings have direct application to exploration and development of the Boone Formation in the northern Arkoma basin. More important, the findings agree with those of Gorham et al. (1979) that exploration efforts for traps with fractured reservoirs should focus on areas of maximum curvature of folds, especially monoclines.

VII. GEOPHYSICAL STUDIES

A. Gravity and Magnetic Surveys

Gravity and magnetic surveys were completed along the southern extension of three prominent northeast-trending lineaments (Drakes Creek, Ponca and Lurton) which appear to

transect several structural domains (Fig. 21). These lineaments appear to extend from the northern Arkansas structural platform southward into the Arkansas part of the Arkoma basin. North of the Arkoma basin parts of these lineaments have been mapped as normal faults that are downthrown on the southeast. Although there is no identifiable surface evidence of faulting for these lineaments in the Arkoma basin, geophysical studies were conducted in an attempt to establish their southward extension into the gas-bearing strata of the Arkoma basin.

1. Location and Data Collection

Survey patterns were established in two separate areas (Areas I and II, Fig. 21) for collecting gravity and magnetic data. Gravity data were obtained with a Worden gravimeter and standard error corrections were applied before values were plotted on base maps. Magnetic data were obtained with a Varian proton procession magnetometer. Short-term variations in the earth's magnetic field were established approximately every two hours to increase the accuracy of readings at individual stations. In addition to contouring data, gravity and magnetic maps were evaluated with the aid of a Fortran IV-Henderson-2 program (Henderson, 1960). This program generates both first and second derivative maps and upward and downward continuation maps.

ORIGINAL PAGE IS
OF POOR QUALITY

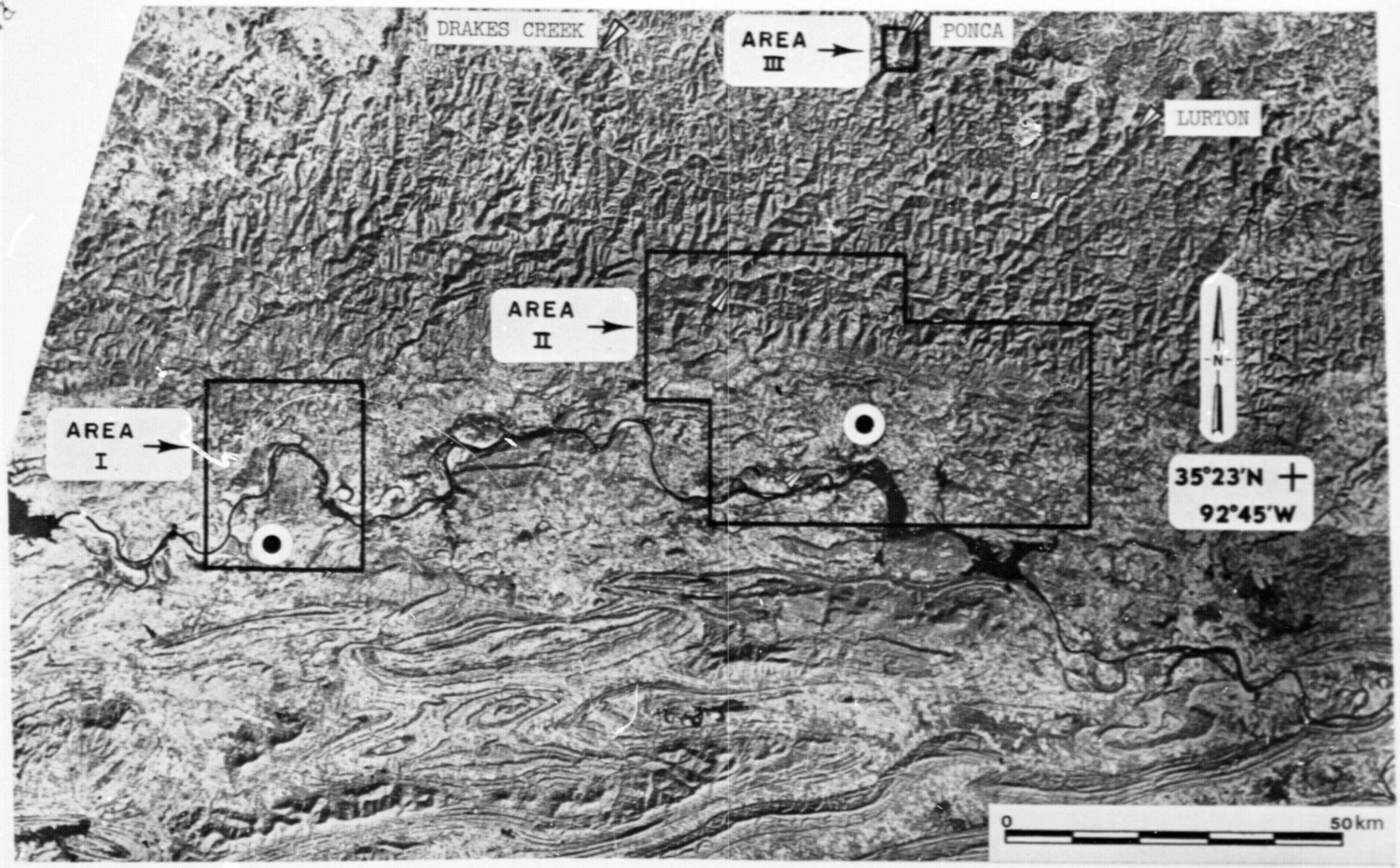

Figure 21. Geophysical survey site locations, Landsat mosaic, winter scene.

2. Data Analysis

In the northern part of Area I, a small gravity trough with a maximum magnitude of 3 mgals was delineated more or less on trend with the Drakes Creek lineament. Associated with this feature is a fairly uniform decrease in magnetic intensity, sloping to the southeast. It is possibly indicative of displacement of basement downward on the southeast along the Drakes Creek lineament. In the southern central part of Area I is a roughly circular magnetic anomaly of at least 100 gammas magnitude (circle in Area I, Fig. 21). This anomaly is adjacent to the possible southwest extension of the Drakes Creek lineament. Modeling led to the conclusion that the source of this anomaly is either an erosional remnant or possibly a rhyolitic extrusive pile on basement (Watkins, 1978; Schumacher, 1979).

Magnetic profile data across the southwestern extension of the Ponca lineament in Area II are somewhat similar to profile data obtained by Smith (1977) along the Ponca lineament's northeasternmost extension (Area III, Fig. 21). Smith (1977) noted that the Ponca lineament (Area III) coincides with the linear arrangement of lead-zinc mines in the Ponca-Boxley district. On the basis of gravity and magnetic data analysis, Smith suggested that the northern part of the Ponca lineament is probably a first-order fracture and/or shear zone that penetrates both Paleozoic and Precambrian rock. By inference, then, the Ponca lineament may

provide a continuous shear zone from Area III through Area II.

A large, nearly circular magnetic high is centered about 1.6 km north of Clarksville, Arkansas, intersecting the trend of the Lurton lineament (circle in Area II, Fig. 21). This anomaly covers nearly three townships and has a magnitude of approximately 450 gammas above the regional field (McBride, 1980). Preliminary modeling suggests that an intrusive body with relatively high magnetic susceptibility is present in the Precambrian basement. Because of the masking effect of this large anomaly, the subsurface extent or presence of the southwestern extension of the Lurton lineament cannot be determined.

B. Results

Gravity and magnetic data analysis provides evidence to support the southwestward continuation of the Drakes Creek lineament into the gas-bearing strata of the Arkoma basin (Area I). The extension of the Ponca lineament (Area II) may coincide with inferred magnetic gradients related to basement shear zones, but similar evidence is lacking to support the presence of the Lurton lineament. It should be noted, however, that parallelism between northeast-southwest-trending lineaments and magnetic gradient anomalies has been reported in the next physiographic province on the east, the northern Mississippi embayment (O'Leary and Simpson, 1977). In addition, recent analysis of gravity and

aeromagnetic data from the northern part of the Mississippi embayment suggests that basement tectonics are largely responsible for the close association between geophysical anomalies and intrusions of basic and ultrabasic rocks (Braile et al., 1979; Hendricks, 1979; Hildenbrand et al., 1979).

The relationship between lineament extension, gas production, and reservoir characteristics is not apparent. There is no correlation between gas production and proximity to the three lineaments extended into the Arkoma basin.

VIII. SEASAT IMAGERY

Seasat swath Rev 795 provided a 100-km swath of SAR imagery across southern and western Arkansas. Unfortunately, the digitally processed SAR covers only the northwesternmost corner of the test site area. No comparison with linear data sets could be accomplished.

IX. SUMMARY AND CONCLUSIONS

Surface joints in the Arkoma basin consist of two orhtogonally oriented sets. One set (systematic), trending N10°W, consists of straight, planar, through-going joints. Plumose structures on many of these joints suggest a tensional origin. The other set of joints (non-systematic) has an average orientation of N86°E and consists of short and often curved joints which cut the rock between the systematic joints. Along the northern flank of the Arkoma basin, where gas

production appears to be from a fractured reservoir, the north-south-trending joint set is somewhat coincident with a prominent north-south linear trend. In general, the influence of surface jointing on linears throughout the Arkoma basin is not obvious.

Of Landsat bands, band 7 detects the greatest number of topographic linears. However, the variation among the three operators is least with band 6. The winter Landsat scene consistently provides for the detection of more linears than the summer Landsat scene because of the lower solar elevation during the winter. The uniform distribution stretch enables interpreters to detect more linears than the Gaussian stretch. The Gaussian stretch enhancement decreases contrast in the middle-gray range, thereby suppressing linear expression. In summary, the best Landsat combination is the winter scene, band 7, uniform distribution stretch.

Of the SAR data products, the VH SAR radar mosaic provided for detection of the most linears; however, none of the SAR enhancement products is significantly better than the others. Two of three operators detected fewer linears from the radar/Landsat merge than from the Landsat data set alone; however, because of operator variability, the results are inconclusive. A black and white band 7 winter Landsat scene merged with radar mosaic (VH), having a look-direction orthogonal to the Landsat solar azimuth, is suggested as a complementary image merge. Both of these data sets alone allowed for the detection of most linears.

Radar look-direction and Landsat solar azimuth illumination direction tend to suppress topographic linears more parallel with illumination direction and to accentuate those having a more perpendicular relationship.

The operator variability studies determined that generally the frequency, average length, and coincidence of linears differ greatly among operators, although major linear orientation trends show some degree of similarity. This observation has also been made by Podwysocki (1975) and Siegal (1977). In general, linear analyses tend to be subjective and highly variable. Even when the operator variables are minimized, variations between remote sensor data sets may produce significant differences in interpretations. No single technique of interpretation or single type of imagery seems to be universally best for minimizing operator variability. However, maps derived from linear density analysis tend to be somewhat less influenced by operator variability. Generally, conservative linear "mappers" tend to infer fewer linears per unit area, but relative concentrations are sometimes agreed upon among operators.

Gravity and magnetic data analysis provides evidence to support the southward continuation of two of three major lineaments into the gas-bearing strata of the Arkoma basin. The relationship between lineament extension, gas production, and reservoir characteristics is not apparent. No correlation is found between gas production and proximity to the three lineaments extended into the Arkoma basin.

The southern region of the Arkansas Arkoma basin proper is characterized by high well density but few linears. Little relationship is discernible between surface structure and gas production, and no correlation is found between gas productivity and linear proximity or linear density as determined from remote sensor data. Stratigraphic gas entrapment is most probably related to depositional environment, and is the main factor influencing porosity and permeability in the predominantly sandstone reservoirs.

In the northern Arkoma basin a positive correlation is found between the number of linears in a given area and production from cherty carbonate strata. Most such production is from the Boone Formation. The high chert content of the Boone Formation makes it particularly susceptible to fracturing and the development of fracture permeability. No correlation is evident between linear density and any of the other gas-bearing units. These other gas-bearing units are predominantly sandstone, and are somewhat similar lithologically to the sandstone reservoirs in the southern Arkoma basin.

Linear density analysis should not be the single basis for petroleum exploration on the northern flank of the Arkoma basin. Regional and local structural position and surface joint orientation are equally important data sets to be evaluated in an exploration program. However, the probability of economic savings in the exploration for fractured reservoirs (similar to the Boone Formation) in other parts of the world

can be considerable if linear density maps derived from radar/Landsat merges, are used to target prospects for further geological and geophysical investigations.

X. RECOMMENDATIONS

The following recommendations are based on the experience gained in the performance of this contract.

1. Simultaneous multifrequency-multipolarization radar imagery should be obtained in an area where linears are numerous, but where operator variability can be held to a minimum. The test site should be flown in such a fashion to provide four orthogonal look-directions, and at least three contrasting depression angles (20°, 45°, 70°). This data set would provide sufficient imagery to allow quantitative analysis.

2. Individual interpretations of identical imagery are highly variable and tend to be subjective. The applicability of using machine processing needs to be determined.

3. The optimum Landsat data set (winter scene band-7) and L-band SAR imagery should be merged and evaluated with respect to the radar/Landsat combinations reported on in this study.

4. Space Shuttle radar imagery (with a look-direction different from Landsat solar azimuth preferably orthogonal) should be viewed in a complementary role for topographic linear analysis where Landsat imagery is available.

ORIGINAL PAGE IS
OF POOR QUALITY
FOLDOUT FRAME

5. Linear density rather than linear proximity should be emphasized in the search for fractured reservoirs; however, linear analysis should be used in concert with other geologic and geophysical information.

REFERENCES

Alpay, O.A., 1973, Application of aerial photographic interpretation to the study of reservoir natural fracture systems: Jour. Petroleum Technology, Jan. 1973, p. 37-45.

Arkansas Annual Oil and Gas Report, 1978, Arkansas Oil and Gas Commission, El Dorado, Arkansas, 31 p.

Barr, A.J., J.H. Goodnight, J.P. Sall, and J.T. Hellwig, 1976, A user's guide to SAS 76, Sparks Press, Raleigh, North Carolina, July 1976, 326 p.

Beebe, R.R., and H.W. Rauch, 1978, Lineaments and water wells as exploration tools in Midway-Extra gas field, West Virginia: Am. Assoc. Petroleum Geologists Bull. v. 63, no. 9, p. 1575.

Bench, B.M., W.P. Diamond, and C.M. McCulloch, 1977, Methods of determining the orientations of bedrock fracture systems in southwestern Pennsylvania and northern West Virginia: U.S. Bureau of Mines Report of Investigation No. 8217, 35 p.

Blanchet, P.H., 1957, Development of fracture analysis as an exploration method: Am. Assoc. Petroleum Geologists Bull., v. 41, no. 8, p. 1748-1759.

Braile, L.W., W.J. Hinze, G.R. Keller, and E.G. Lidiak, 1979, What is the northeastern extent of the New Madrid fault zone?: Geol. Soc. America Abstracts with Programs, v. 11, no. 2, p. 145.

Branan, C.B., Jr., 1968, Natural gas in Arkoma basin of Oklahoma and Arkansas: in Natural gases of North America: Am. Assoc. Petroleum Geologists Mem. 9, v. 2, p. 1616-1635.

Diggs, W.E., 1961, Structural framework of the Arkoma basin: Field Conference, Tulsa Geol. Soc.--Fort Smith Geol. Soc. Field Guide Book, April 14-15, p. 62-65.

Gelnett, R.H., 1977, The importance of look-direction and depression angle in geologic applications of SLAR: in Proc. Microwave Remote Sensing Symp., NASA/JSC, Houston, TExas, Dec. 1977, p. 142-154.

Gorham, F.D., Jr., L.A. Woodward, J.R. Callender, and A.R. Greer, 1979, Fractures in Cretaceous rocks from selected areas of San Juan basin, New Mexico--exploration implications: Am. Assoc. Petroleum Geologists Bull., v. 63, no. 4, p. 598-607.

Gramberg, J., 1966, A theory on the occurrence of various types of vertical and sub-vertical joints in the earth's crust: in Proc. First Congress of the International Society of Rock Mechanics, v. 1, p. 443-450.

Haman, P.J., 1961, Lineament analysis on aerial photographs--exemplified in the north Sturgeon Lake area, Alberta: West Canadian Research Pub., series 2, no. 1, 22 p.

Haman, P.J., 1972, A regimatic lineament pattern--Innisfail area, Alberta: West Canadian Research Pub., series 2, no. 3, 31 p.

Harris, J.F., G.L. Taylor, and J.L. Walper, 1960, Relation of deformation fractures in sedimentary rocks to regional and local structure: Am. Assoc. Petroleum Geologists Bull., v. 44, no. 12, p. 1853-1973.

Henderson, R.G., 1960, A comprehensive system of automatic computation in magnetic and gravity interpretation: Geophysics, v. 12, no. 1, p. 428-436.

Hendricks, J.D., 1979, Bouger gravity of eastern Arkansas: Geol. Soc. America Abstracts with Programs, v. 11, no. 2, p. 149.

Hildenbrand, T.G., M.F. Kane, and J.D. Hendricks, 1979, Structural control of upper Mississippi embayment seismicity inferred from analyses of aeromagnetic and gravity data: Geol. Soc. America Abstracts with Programs, v. 11, no. 2, p. 149.

Hobbs, W.H., 1911, Repeating patterns in the relief and in the structure of the land: Geol. Soc. America Bull., v. 22, p. 123-176.

Hodgson, R.H., 1961a, Regional study of jointing in the Comb Ridge--Navajo Mountain area, Arizona and Utah: Am. Assoc. Petroleum Geologists Bull., v. 45, no. 1, p. 1-38.

Hodgson, R.A., 1961b, Classification of structures on joint surfaces: Am. Jour. Science, v. 259, p. 493-502.

Hodgson, R.E., Ed., 1976, Proceedings of First International Conference on the New Basement Tectonics, Utah Geol. Assoc. Publ. 5, 636 p.

Hoppin, R.A., 1974, Lineaments: their role in tectonics of central Rocky Mountains: Am. Assoc. Petroleum Geologists Bull., v. 58, no. 11, p. 2260-2273.

Huntington, J.R., and A.P. Raiche, 1978, A multi-attribute method for comparing geological lineament interpretations: Remote Sensing of Environment, v. 7, p. 145-161.

Jackson, P.L., H.L. Wagner, and R.A. Shuchman, 1979, Investigation of remote sensing for geologic reconnaissance over the Cottageville, West Virginia, eastern shale gas field: Final Report, Contract DE-AC05-77ET12137, USDOE, Morgantown Energy Research Center, Morgantown, West Virginia, 90 p.

Johnson, A.C., Jr., 1974, Lineament Analysis: an exploration method for the delineation of structural and stratigraphic anomalies: in Proc. First International Conference on the New Basement Tectonics, p. 449-452.

Jones, D.S., and H.W. Rauch, 1978, Lineaments and groundwater quality as exploration tools for groundwater in the Cottageville area of western West Virginia: in Second Eastern Gas Shales Symp., USDOE, Morgantown Energy Technology Center, Morgantown, West Virginia, p. 196-205.

Knoring, L.D., 1965, The density of joints as a measure of stress: Doklady Akademii Nauk SSSR, v. 164, no. 1, p. 164-167.

Kowalik, W.S., and D.P. Gold., 1975, The use of Landsat-1 imagery in mapping lineaments in Pennsylvania: in First International Conference on the New Basement TEctonics, p. 236-249.

Lattman, L.H., 1958, Technique of mapping geologic fracture traces and lineaments on aerial photographs: Photogrammetric Engineering, v. 24, p. 568-576.

Lattman, L.H., and R.H. Matzke, 1961, Geological significance of fracture traces: Photogrammetric Engineering, v. 27, no. 3, p. 435-438.

Lattman, L.H., and R.R. Parizek, 1964, Relationship between fracture traces and the occurrence of groundwater in carbonate rocks: Jour. Hydrology, v. 2, p. 73-91.

MacDonald, H.C., J.N. Kirk, L.F. Dellwig, and A.J. Lewis, 1969, The influence of radar look-direction on the detection of selected geologic features: in Proc. Sixth International Symp. on Remote Sensing of Environment, University of Michigan, Ann Arbor, p. 637-650.

McBride, J.H., 1980, Ground magnetic and gravity study of the central portion of the Arkoma basin, Arkansas: unpublished M.S. thesis, University of Arkansas, in preparation.

McQuillan, H., 1973, Small-scale fracture density in Asmari Formation of southwest Iran and its relation to bed thickness and structural setting: Am. Assoc. Petroleum Geologists Bull., v. 57, no. 12, p. 2367-2385.

Mollard, J.D., 1957, Aerial mosaics reveal fracture patterns on surface materials in southern Saskatchewan and Manitoba: Oil in Canada, August 5, 1957, p. 26-50.

Moore, G.K., 1976, Lineaments on Skylab photographs--detection, mapping, and hydrologic significance in central Tennessee: USGS open file report 76-196, 76 p.

Ogden, A.E., 1976, The hydrology of the central Monroe County karst, West Virginia: unpublished Ph.D. dissertation, West Virginia University.

O'Leary, D.W., J.D. Friedman, and H.A. Pohn, 1976, Lineament and linear, a termonolgoical reappraisal: in Proc. Second International Conference on Basement Tectonics, Basement Tectonics Comm. Inc., Denver, Colorado, p. 571-577.

O'Leary, D.W., and S.L. Simpson, 1977, Remote sensor applications to tectonism and seismicity in the northern part of the Mississippi embayment: Geophysics, v. 42, no. 3, p. 542-548.

Overbey, W.K., Jr., and R.L. Rough, 1971, Prediction of oil- and gas-bearing rock fractures from surface structural features: U.S. Bureau of Mines Report of Investigation No. 7500, 14 p.

Overbey, W.K., W.K. Sawyer, and B.R. Henniger, 1974, Relationships of earth fracture systems to productivity of a gas storage reservoir: U.S. Bureau of Mines Report of Investigation No. 7952, 133 p.

Podwysocki, M.H., J.G. Moik, and W.C. Shoup, 1975, Quantification of geologic lineaments by manual and machine processing techniques: in NASA Earth Resources Survey Symp., Houston, Texas, v. 1-B, p. 885-904.

Podwysocki, M.H., and J.L. Earle, Eds., 1976, Proc. Second International Conference on Basement Tectonics, Basement Tectonics Comm. Inc., Denver, Colorado, 595 p.

Podwysocki, M.H., and D.P. Gold, 1976, Some possible surface expressions of a regular fracture grid deformed by subsurface structures: in Proc. Second International Conference on Basement Tectonics, Basement Tectonics Comm. Inc., Denver, Colorado, p. 542-559.

Pohn, H.A., 1970. Remote sensor application studies progress report, July 1, 1968 to June 30, 1969: Analysis of images and photographs by Ronchi grating: USGS open file report, available: NTIS, Springfield, Virginia, PB 197-101, 9 p.

Price, N.J., 1959, Mechanics of jointing in rocks: Geology Magazine, v. 96, p. 149-167.

Rumsey, I.A.P., 1971, Relationship of fractures in unconsolidated superficial deposites to those in the underlying bedrock: Modern Geology, v. 3, p. 25-41.

Rumsey, I.A.P., and R.H. Gelnett, 1976, Airborne radar finds deep fracture controlled pools: World Oil, v. 182, no. 1, p. 115-118.

Ryan, W.M., 1976, Remote sensing fracture study--western Virginia and southern Kentucky: USERDA, Morgantown Energy Research Center, Morgantown, West Virginia, Report SP-76/2, p. 94-97.

Saunders, D.F., and D.E. Hicks, 1976, Regional geomorphic lineaments on satellite imagery--their origin and applications: in Proc. Second International Conference on Basement Tectonics, Basement Tectonics Comm. Inc., Denver, Colorado, p. 326-352.

Schumacher, A.L., 1979, Gravity survey and subsurface investigation of the Van Buren quadrangle, Arkansas and Oklahoma: unpublished M.S. thesis, University of Arkansas, 86 p.

Setzer, J.L., 1966, Hydraulic significance of tectonic fractures detectable on air photos: Groundwater, v. 4, no. 4, p. 23-27.

Siddiqui, S.H., and R.R. Parizek, 1971, Hydrologic factors influencing well yields and aquifer hydraulic properties of folded and faulted carbonate rocks in central Pennsylvania: Water Resources Research, v. 7, no. 5, p. 1295-1312.

Siegal, B.S., 1977, Significance of operator variation and the angle of illumination in lineament analysis on synoptic images: Modern Geology, v. 6, p. 75-85.

Smith, D.A., 1977, Lead-zinc mineralization in the Ponca-Boxley area, Arkansas: unpublished M.S. thesis, University of Arkansas, 188 p.

Sonderegger, J.L., 1970, Hydrology of limestone terrains: Alabama Geological Survey Division of Water Resources Bull. 94, part C, p. 1-27.

Stearns, D.W., and M. Friedman, 1972, Reservoirs in fractured rock: in Stratigraphic oil and gas fields: Am. Assoc. Petroleum Geologists Mem. 16, p. 82-106.

Van Den Heuval, P., 1979, Petrography of the Boone Formation, northwest Arkansas: unpublished M.S. thesis, University of Arkansas, 75 p.

Watkins, J.P., 1978, A ground magnetic and subsurface investigation of the Van Buren quadrangle, Arkansas and Oklahoma: unpublished M.S. thesis, University of Arkansas, 84 p.

Werner, E., 1976, Photolineament mapping in the Appalachian plateau and continental interior geological provinces--a case study: Remote Sensing of Earth Resources, v. 5, p. 403-416.

Werner, E., 1978, Interrelationships of photolineaments, geological structures, and fracture production of natural gas in the Appalachian plateau of West Virginia: in First Eastern Gas Shales Symp., Morgantown Energy Research Center, Morgantown, West Virginia, p. 474-483.

Whitesides, D.V., 1971, Yield and specific capacities of bedrock wells in Kentucky: USGS Bull., Series 10, Info. Circ. 21, 18 p.

Wise, D.U., 1968, Regional and sub-continental sized fracture systems detectable by topographic shadow techniques: in Conference on Research in Tectonics, A.J. Baer and D.K. Norris, eds., Geol. Survey Canada Paper 68-52, p. 175-199.

Wise, D.U., 1969, Pseudo-radar topographic shadowing for detection of sub-continental sized fracture systems: in Proc. Sixth International Symp. on Remote Sensing of Environment, University of Michigan, Ann Arbor, p. 603-615.

Wobber, F.J., 1967, Fracture traces in Illinois: Photogrammetric Engineering, v. 33, no. 5, p. 499-506.

Zirk, W.E., and S.J. Lahoda, 1978, A relationship between productivity of gas wells and their locations with respect to lineaments; a statistical analysis: USDOE, Morgantown Energy Technology Center, Morgantown, West Virginia, Rept. No. METC/CT-78/14, 36 p.

APPENDIX

Index to Linear Histograms

Histogram Number

Landsat Winter, Gaussian Stretch

1. Band 4
2. Band 5
3. Band 6
4. Band 7

Landsat Winter, Uniform Distribution Stretch

5. Band 4
6. Band 5
7. Band 6
8. Band 7

Landsat Summer, Gaussian Stretch

9. Band 4
10. Band 5
11. Band 6
12. Band 7

Landsat Summer, Uniform Distribution Stretch

13. Band 4
14. Band 5
15. Band 6
16. Band 7

17. Landsat Winter, Enhanced Color
18. Landsat Winter, Standard Color
19. Landsat Summer, Enhanced Color
20. Landsat Summer, Standard Color

SAR, L-Band Imagery--May 1977

21. Uncontrolled Mosaic (HH)
22. Uncontrolled Mosaic (HV)

SAR, L-Band Imagery--April, 1978 HH Mosaic

23. Response Range Dependence Removed
24. Uniform Distribution
25. High Pass Filter
26. High Pass, 20% Added Back

SAR, L-Band Imagery--April, 1978 VH Mosaic

27. Response Range Dependence Removed

SAR Radar/Landsat Composite

28. SAR-HH and Landsat Winter, Enhanced Color
29. SAR-HH and Landsat Summer, Enhanced Color

Modified Area Histogram Coverage

30. Landsat Summer, Enhanced Color
31. Landsat Winter, Enhanced Color
32. HH Mosaic

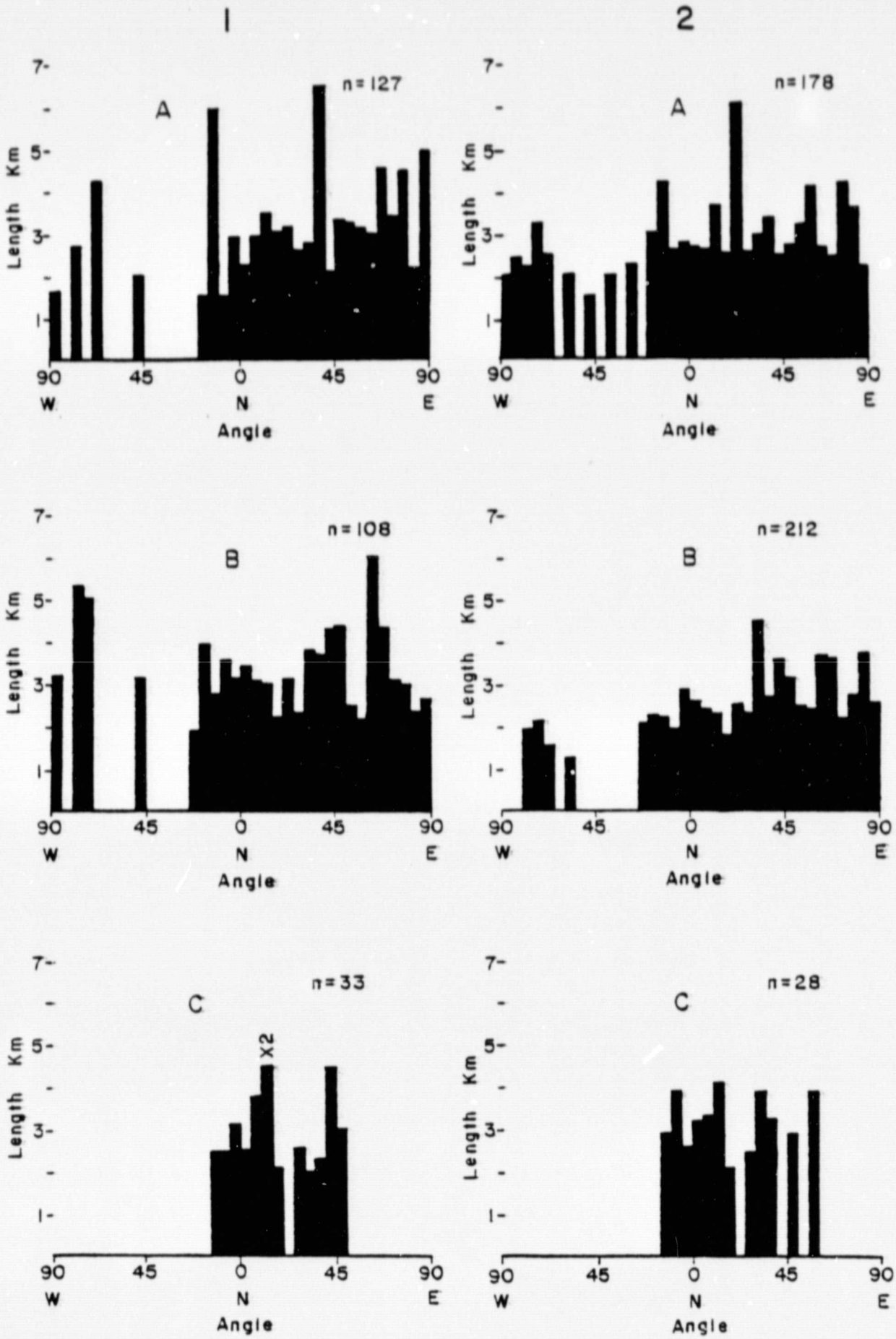
1
2
A
n=127
n=178
B
n=108
n=212
C
n=33
n=28
X2
Length Km
7
5
3
1
90
45
0
W
N
E
Angle

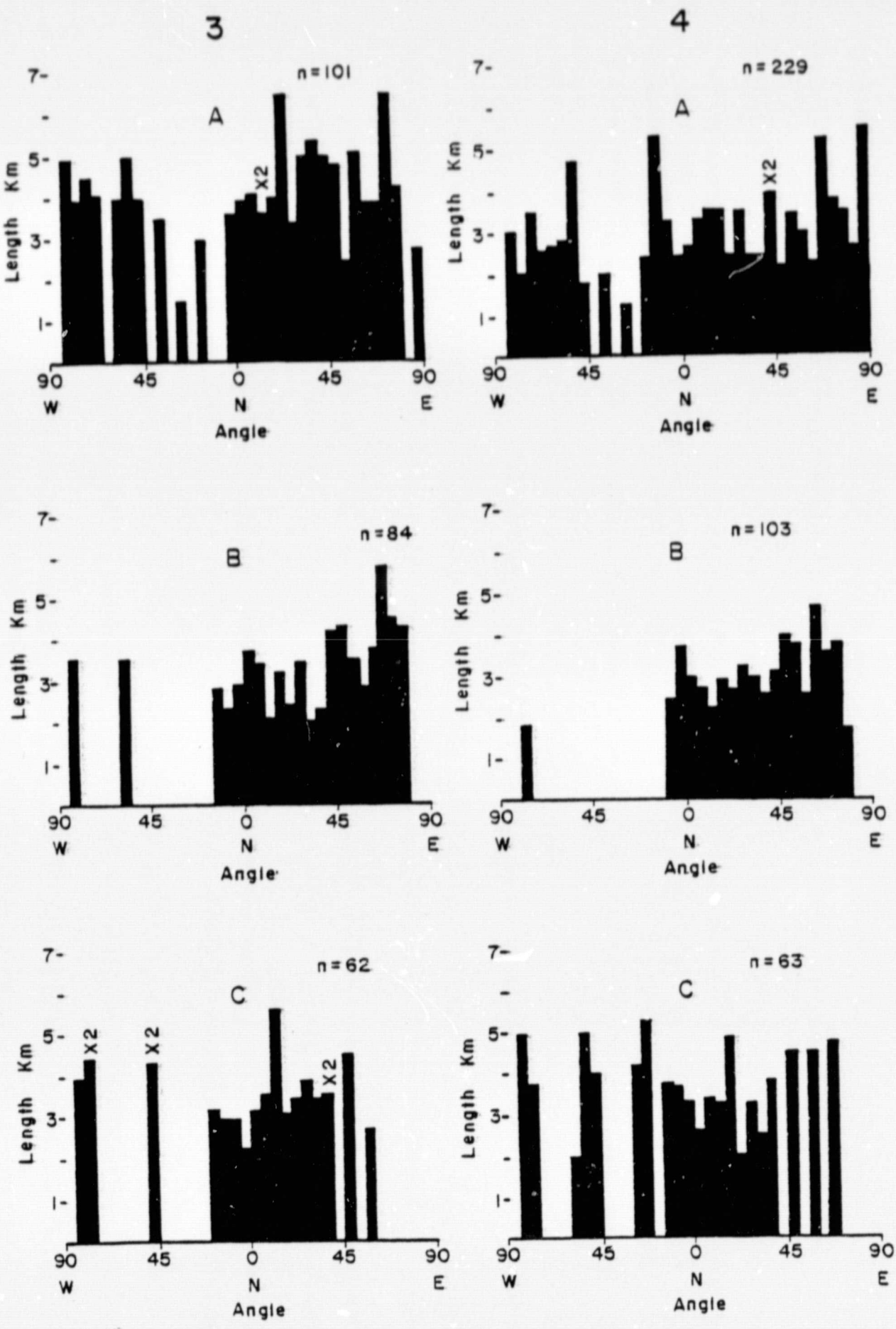

ORIGINAL PAGE IS
OF POOR QUALITY

5

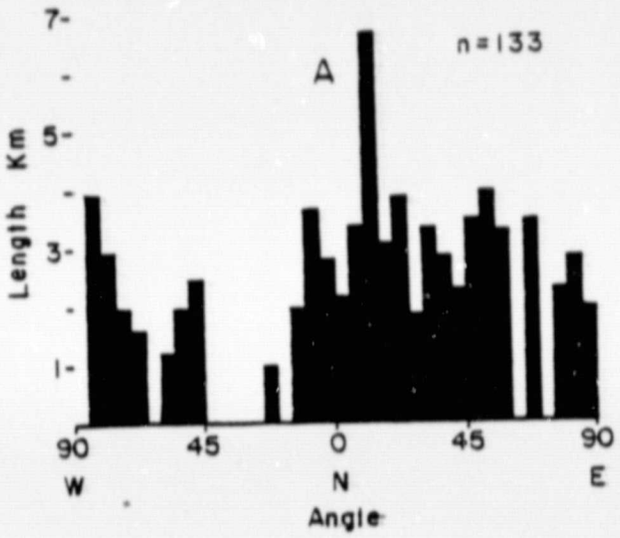
A
n=133
Length Km
7
5
3
1
90
W
45
0
N
45
90
E
Angle

6

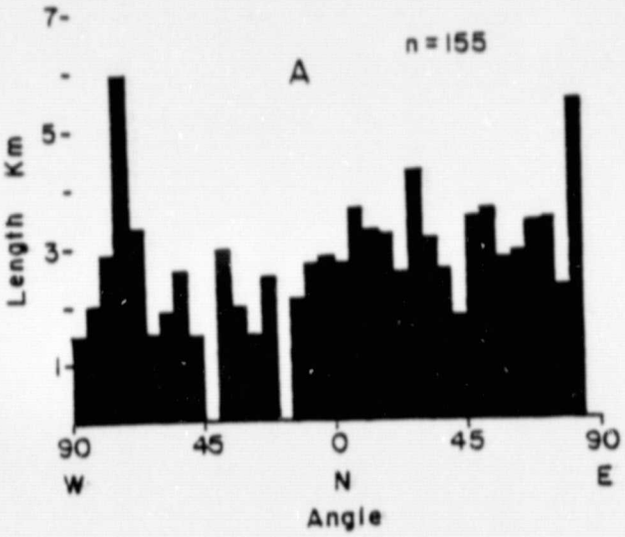
A
n=155
Length Km
7
5
3
1
90
W
45
0
N
45
90
E
Angle

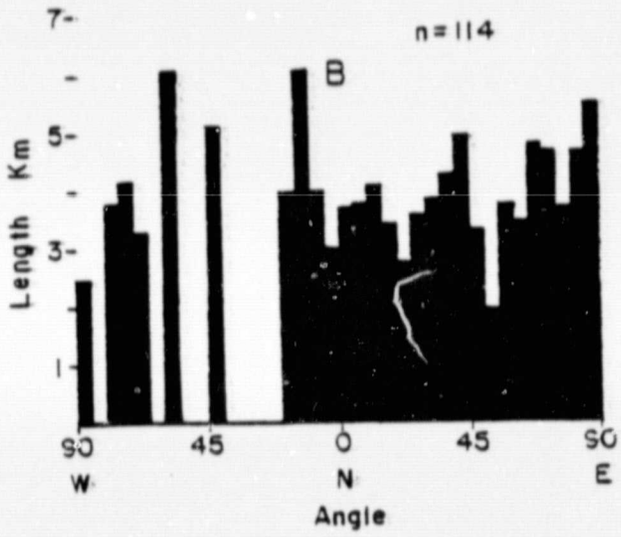
B
n=114
Length Km
7
5
3
1
90
W
45
0
N
45
90
E
Angle

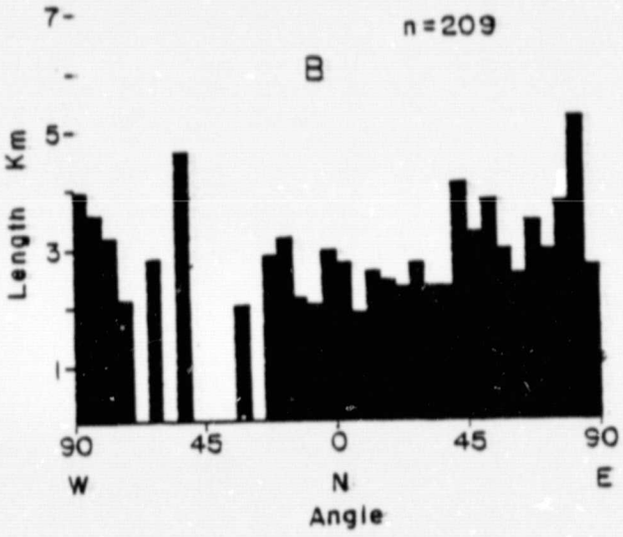
B
n=209
Length Km
7
5
3
1
90
W
45
0
N
45
90
E
Angle

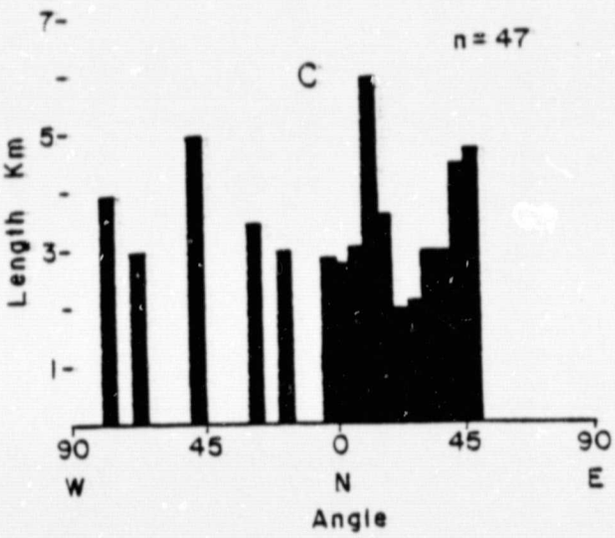
C
n=47
Length Km
7
5
3
1
90
W
45
0
N
45
90
E
Angle

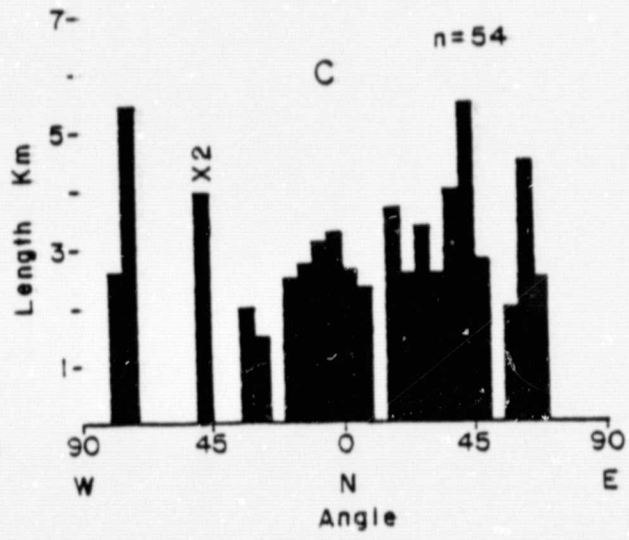
C
n=54
X2
Length Km
7
5
3
1
90
W
45
0
N
45
90
E
Angle

7

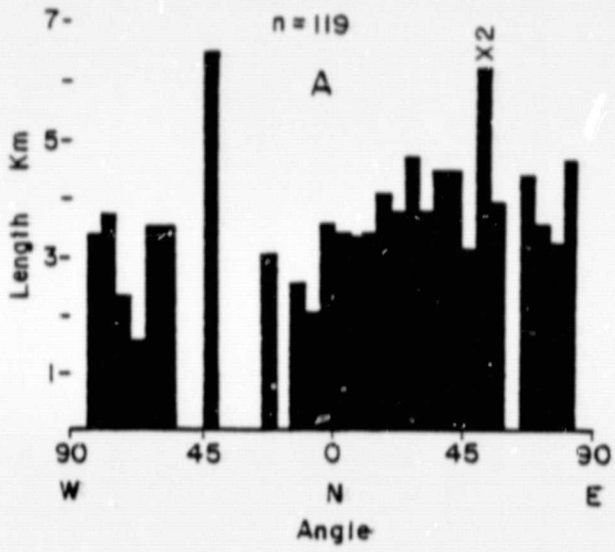
n = 119
A
X2
Length Km
7
5
3
1
90
45
0
45
90
W
N
E
Angle

8

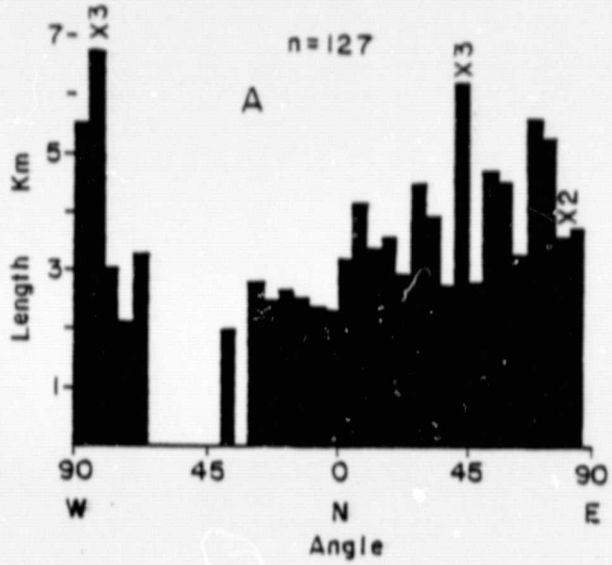
n = 127
A
X3
X3
X2
Length Km
7
5
3
1
90
45
0
45
90
W
N
E
Angle

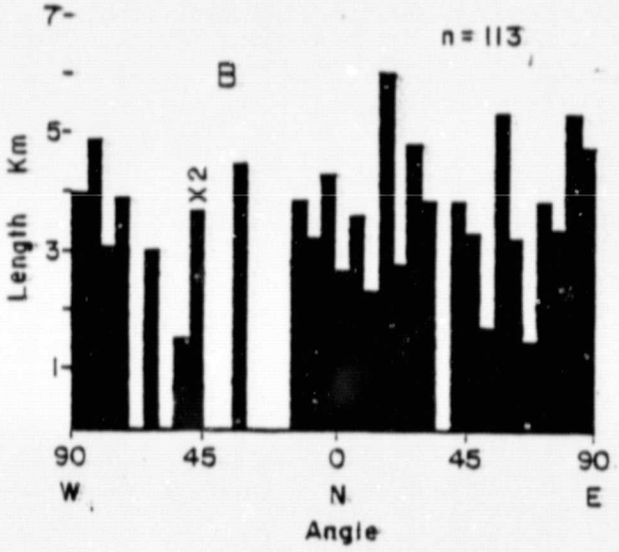
n = 113
B
X2
Length Km
7
5
3
1
90
45
0
45
90
W
N
E
Angle

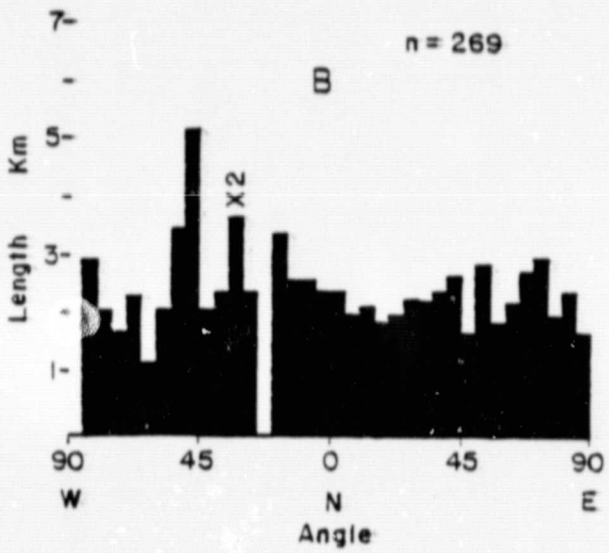
n = 269
B
X2
Length Km
7
5
3
1
90
45
0
45
90
W
N
E
Angle

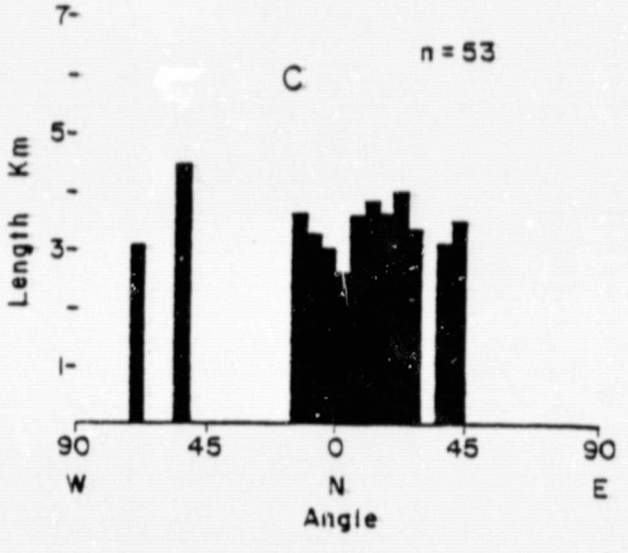
n = 53
C
Length Km
7
5
3
1
90
45
0
45
90
W
N
E
Angle

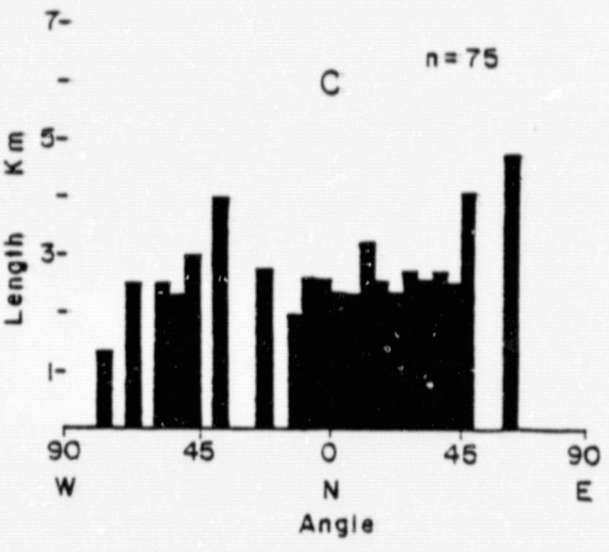
n = 75
C
Length Km
7
5
3
1
90
45
0
45
90
W
N
E
Angle

9

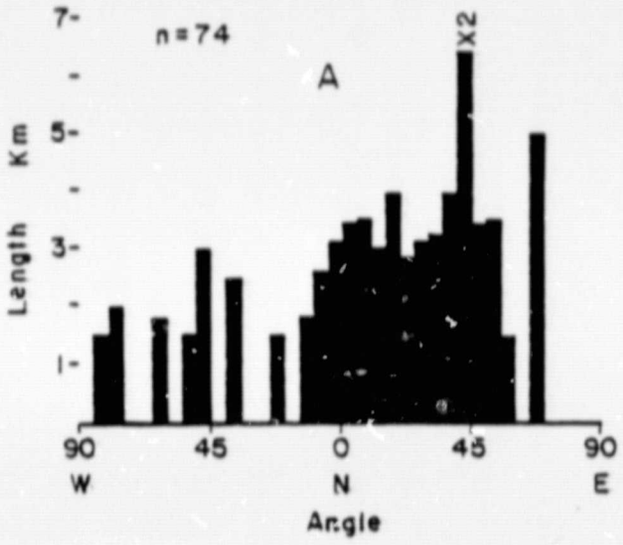
n=74
A
X2
Length Km
7
5
3
1
90
45
0
45
90
W
N
E
Angle

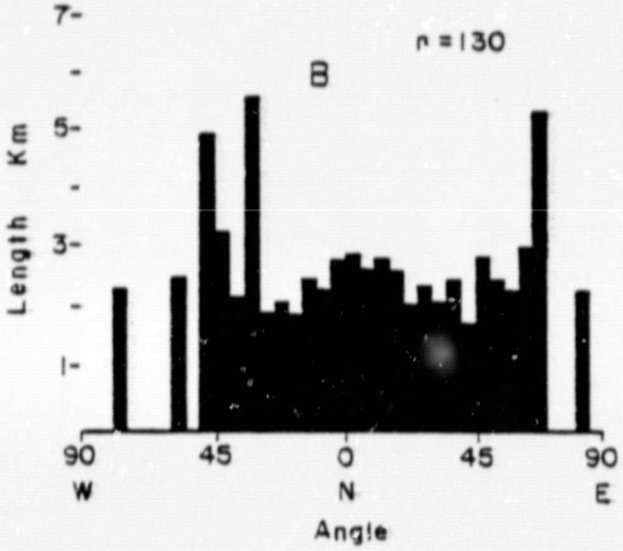
n=130
B
Length Km
7
5
3
1
90
45
0
45
90
W
N
E
Angle

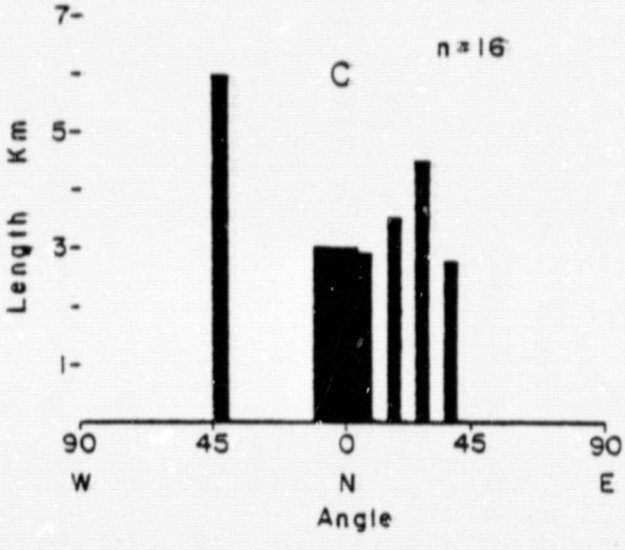
n=16
C
Length Km
7
5
3
1
90
45
0
45
90
W
N
E
Angle

10

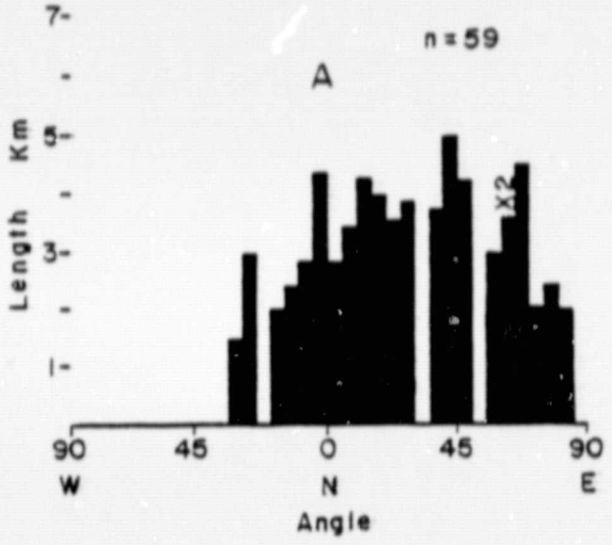
n=59
A
X2
Length Km
7
5
3
1
90
45
0
45
90
W
N
E
Angle

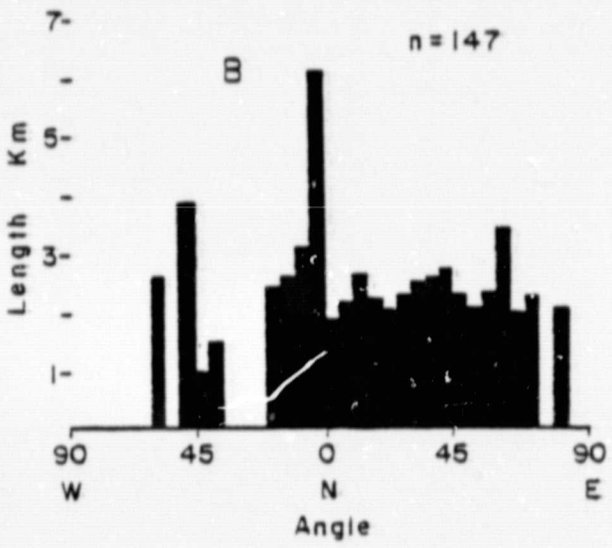
n=147
B
Length Km
7
5
3
1
90
45
0
45
90
W
N
E
Angle

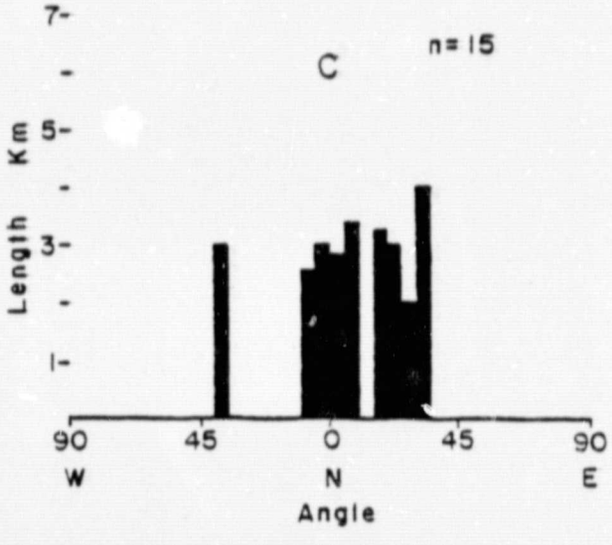
n=15
C
Length Km
7
5
3
1
90
45
0
45
90
W
N
E
Angle

11

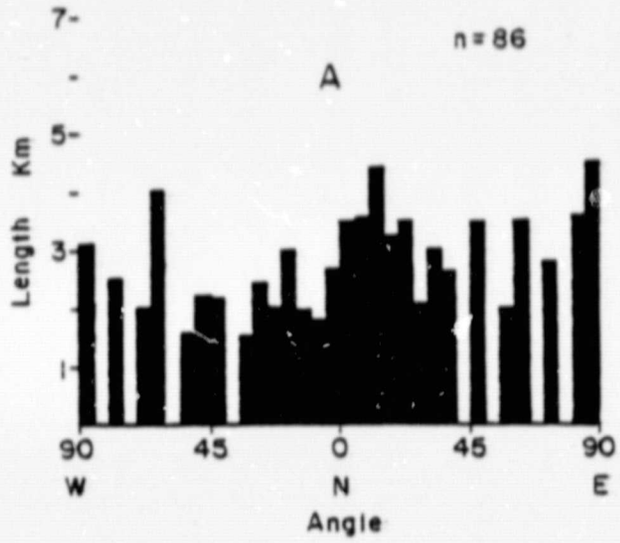
n=86
A
Length Km
7
5
3
1
90
45
0
45
90
W
N
E
Angle

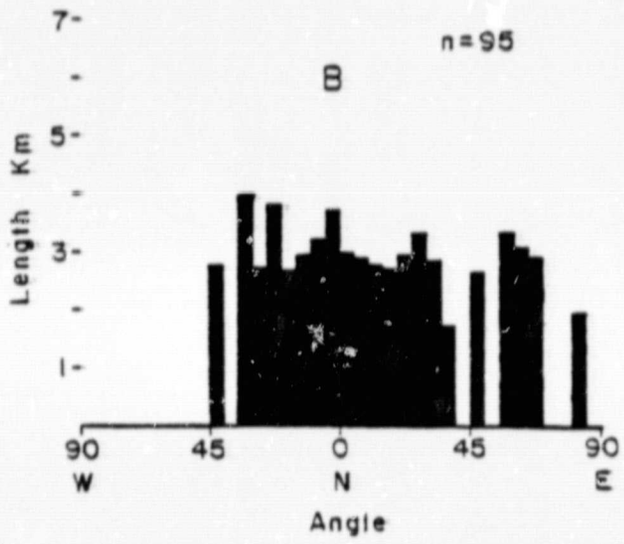
n=95
B
Length Km
7
5
3
1
90
45
0
45
90
W
N
E
Angle

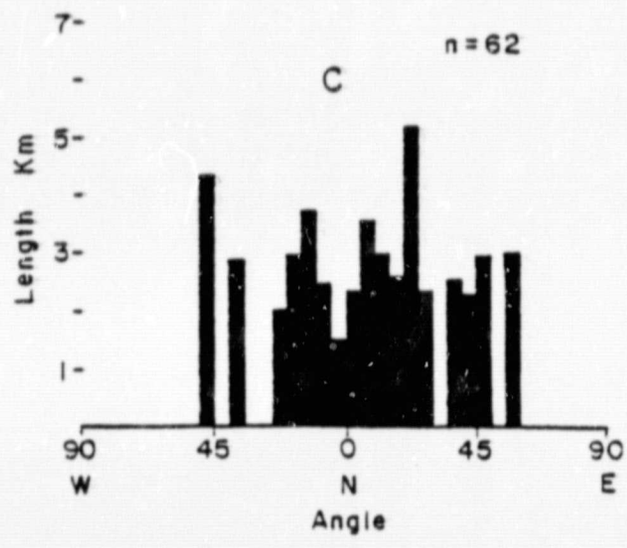
n=62
C
Length Km
7
5
3
1
90
45
0
45
90
W
N
E
Angle

12

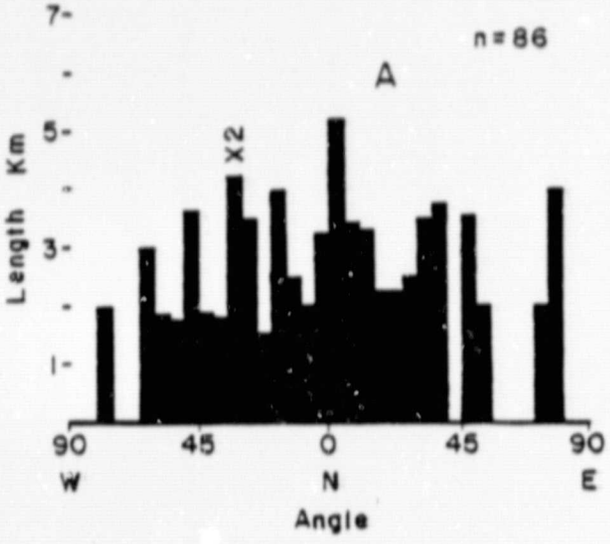
n=86
A
X2
Length Km
7
5
3
1
90
45
0
45
90
W
N
E
Angle

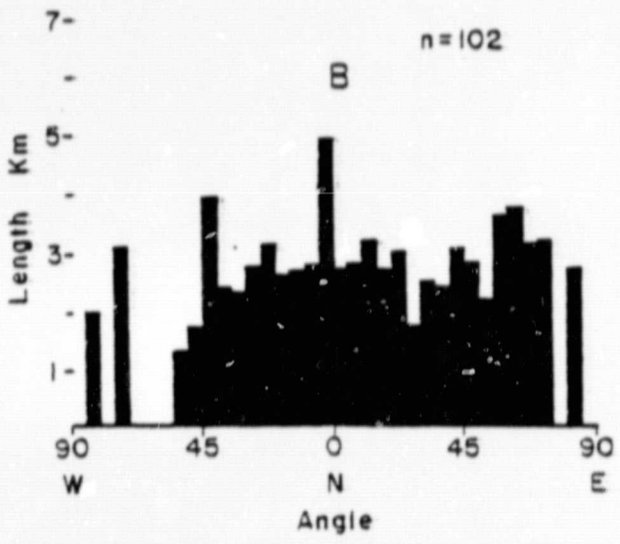
n=102
B
Length Km
7
5
3
1
90
45
0
45
90
W
N
E
Angle

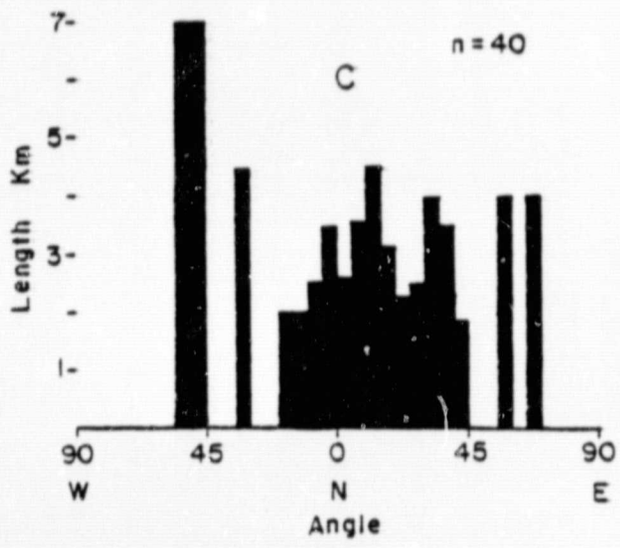
n=40
C
Length Km
7
5
3
1
90
45
0
45
90
W
N
E
Angle

13

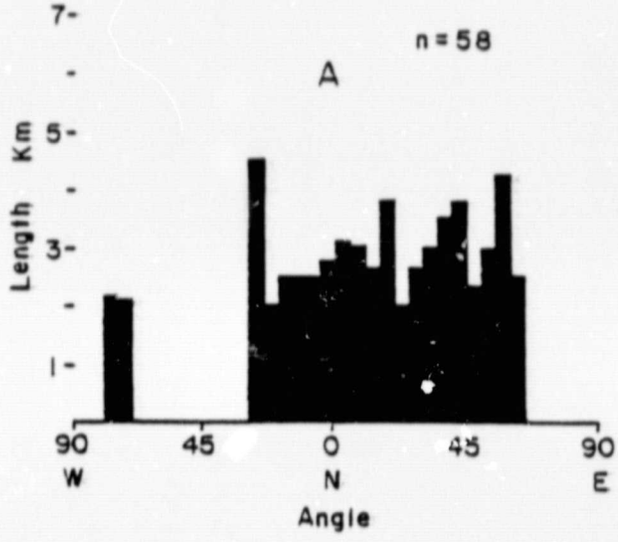
n=58
A
Length Km
7
5
3
1
90
W
45
0
N
45
90
E
Angle

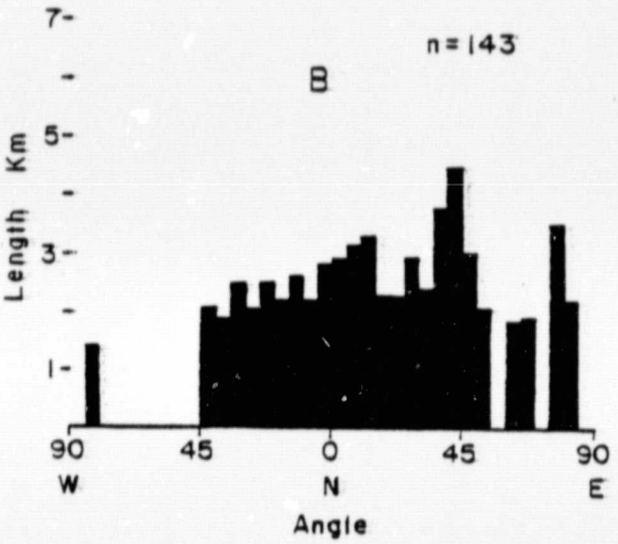
n=143
B
Length Km
7
5
3
1
90
W
45
0
N
45
90
E
Angle

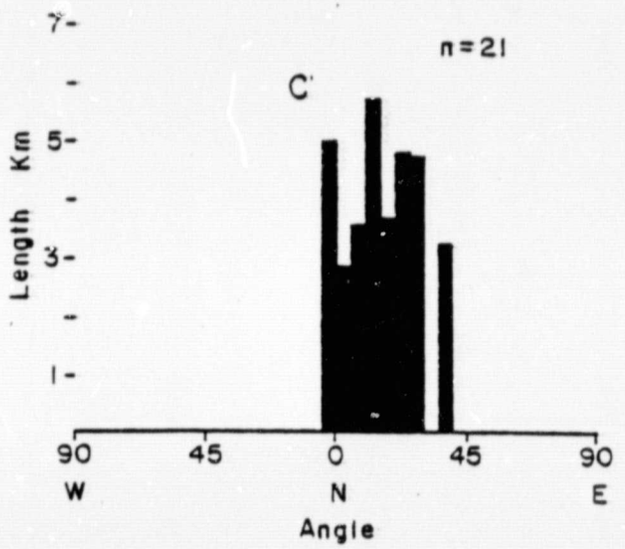
n=21
C
Length Km
7
5
3
1
90
W
45
0
N
45
90
E
Angle

14

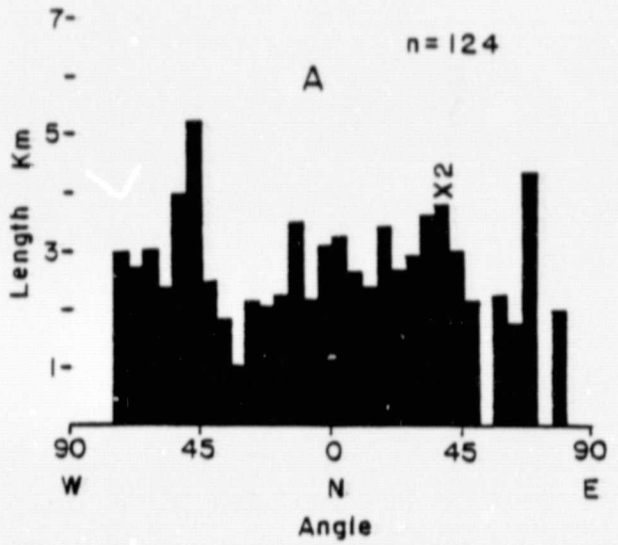
n=124
A
X2
Length Km
7
5
3
1
90
W
45
0
N
45
90
E
Angle

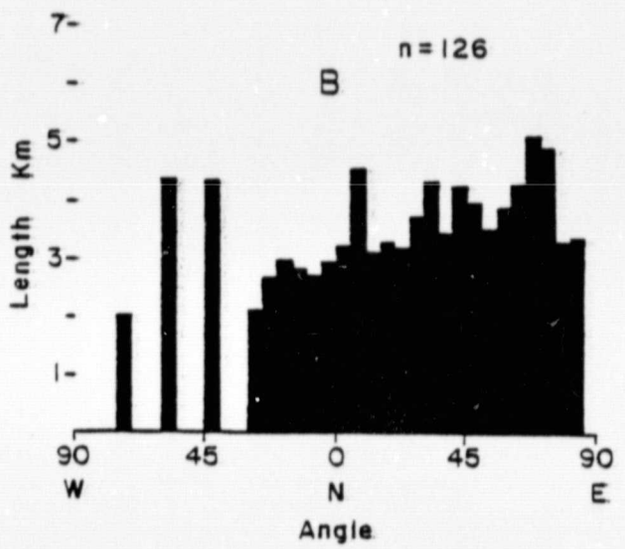
n=126
B
Length Km
7
5
3
1
90
W
45
0
N
45
90
E
Angle

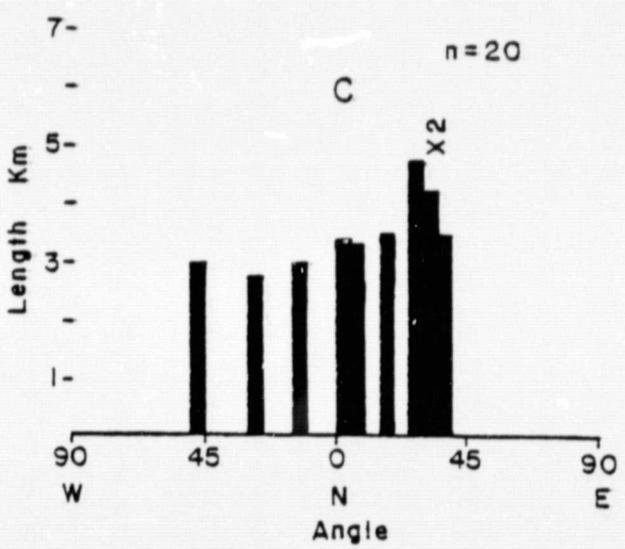
n=20
C
X2
Length Km
7
5
3
1
90
W
45
0
N
45
90
E
Angle

15

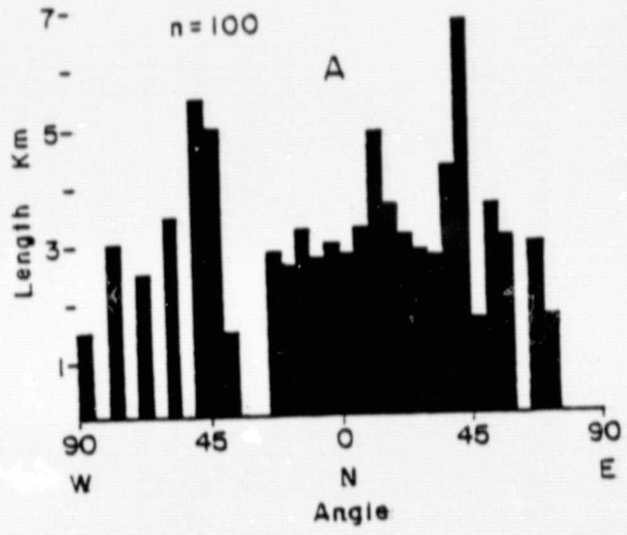

16

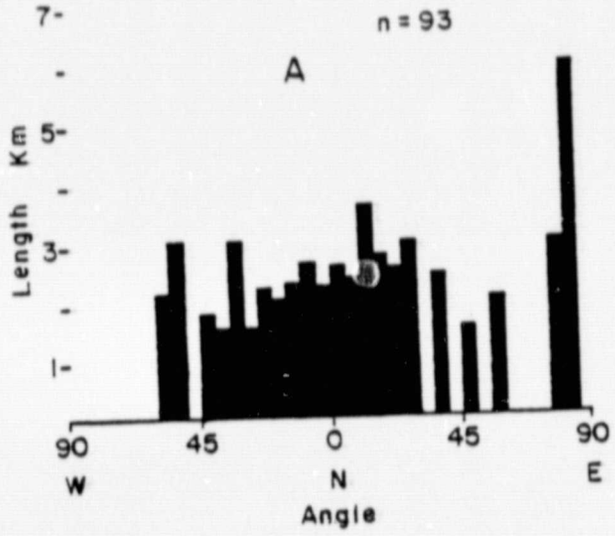

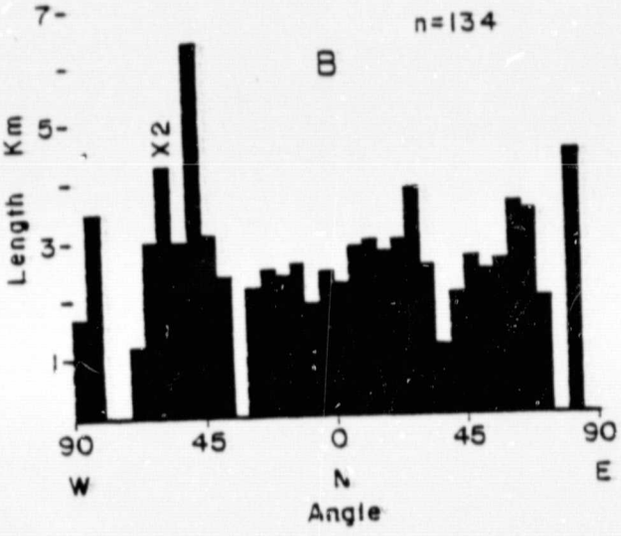

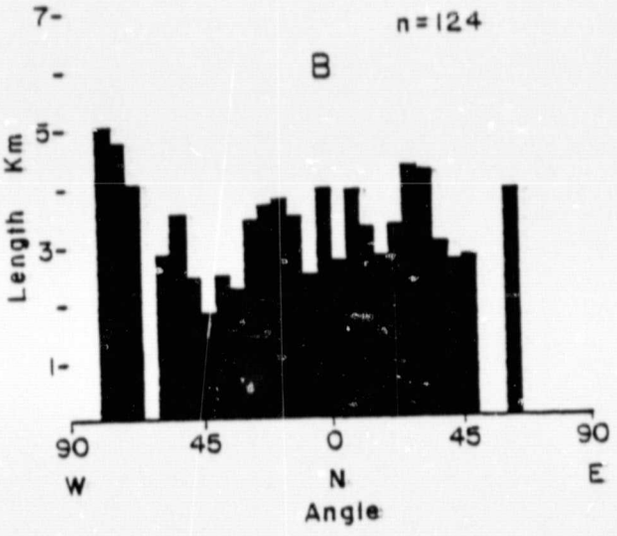

ORIGINAL PAGE IS
OF POOR QUALITY

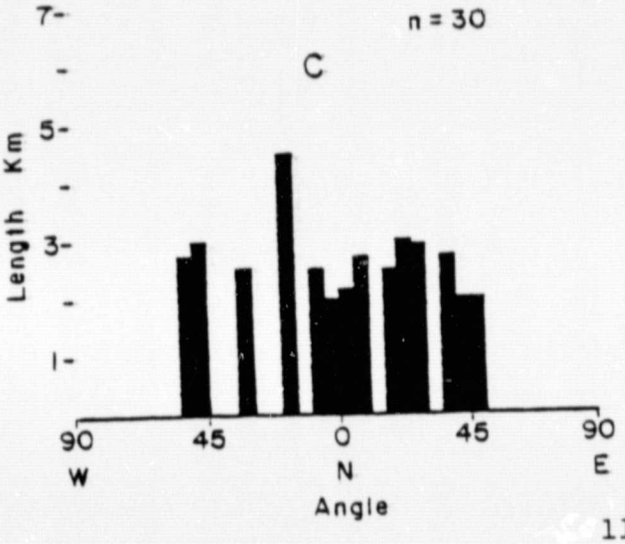

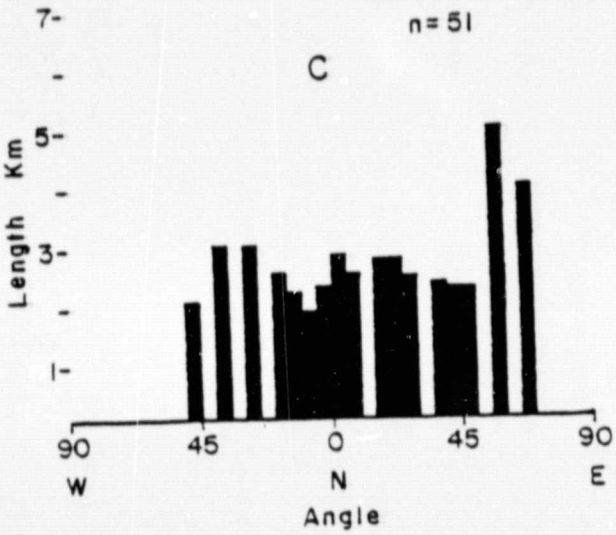

17

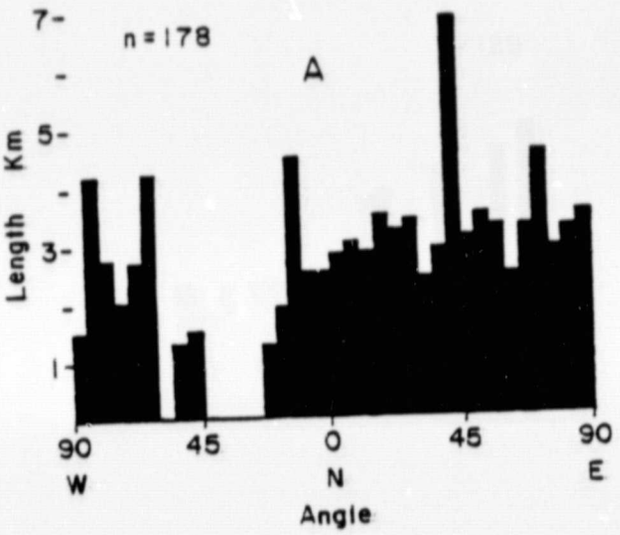
n=178
A
Length Km
7
5
3
1
90
W
45
0
N
45
90
E
Angle

18

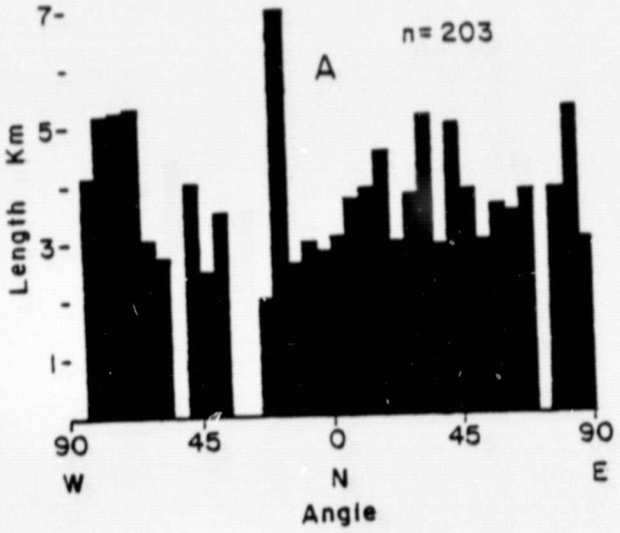
n=203
A
Length Km
7
5
3
1
90
W
45
0
N
45
90
E
Angle

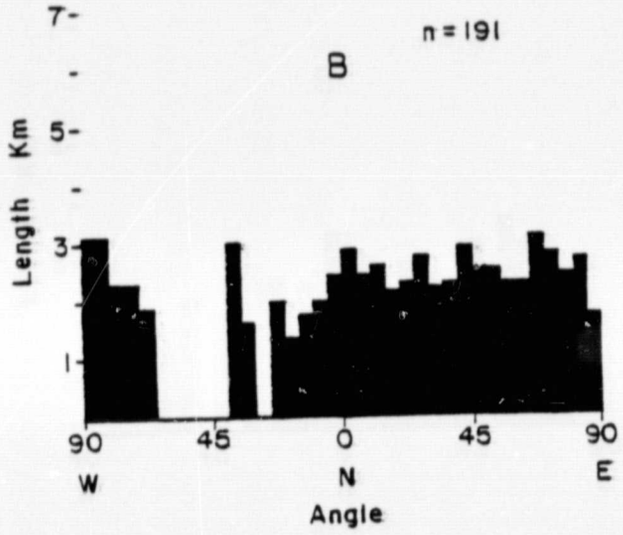
n=191
B
Length Km
7
5
3
1
90
W
45
0
N
45
90
E
Angle

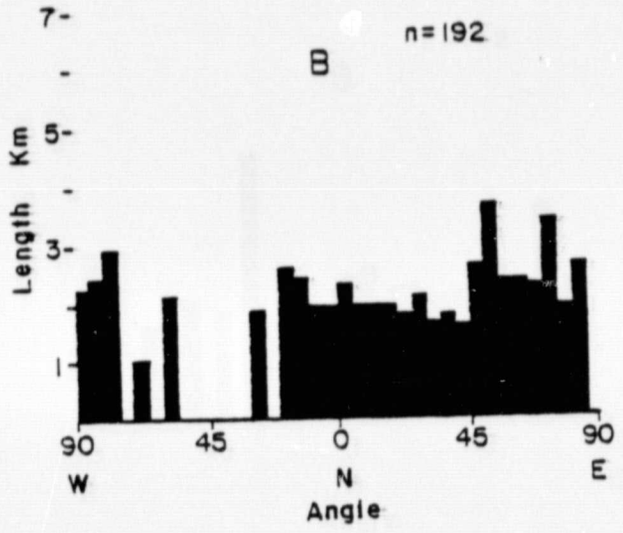
n=192
B
Length Km
7
5
3
1
90
W
45
0
N
45
90
E
Angle

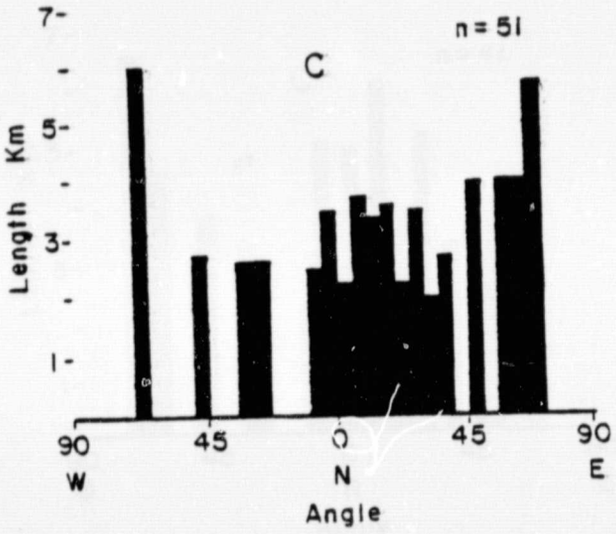
n=51
C
Length Km
7
5
3
1
90
W
45
0
N
45
90
E
Angle

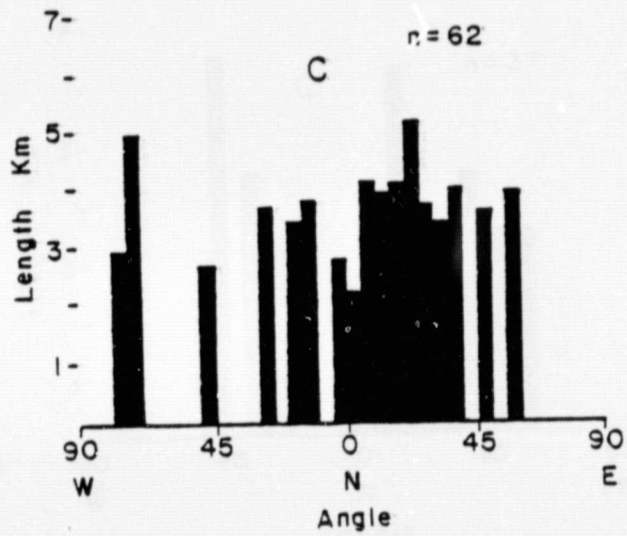
n=62
C
Length Km
7
5
3
1
90
W
45
0
N
45
90
E
Angle

19

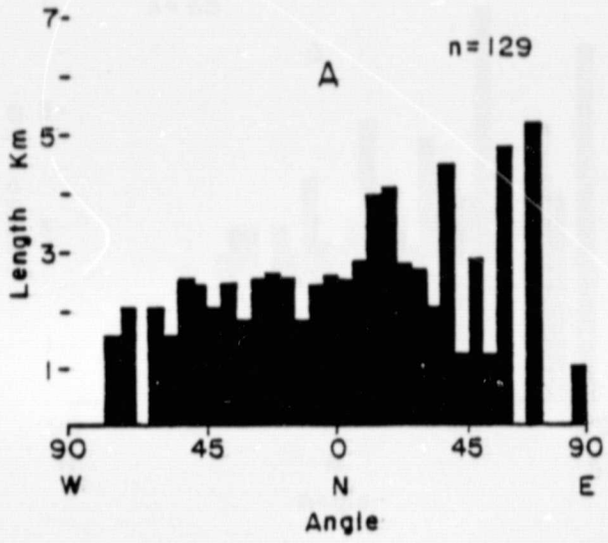
A
n=129
Length Km
7
5
3
1
90
45
0
45
90
W
N
E
Angle

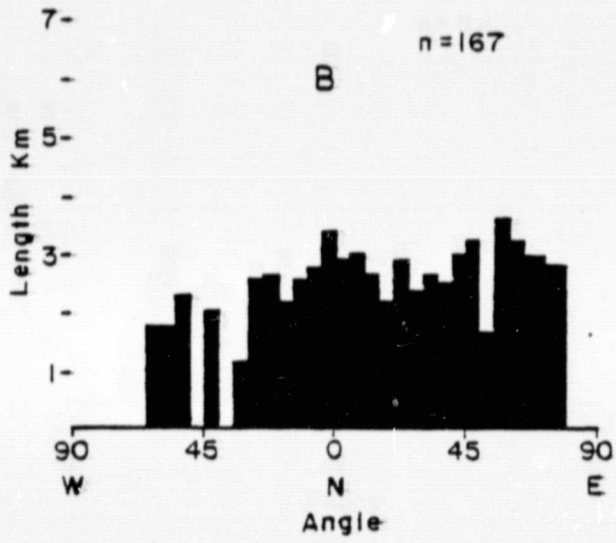
B
n=167
Length Km
7
5
3
1
90
45
0
45
90
W
N
E
Angle

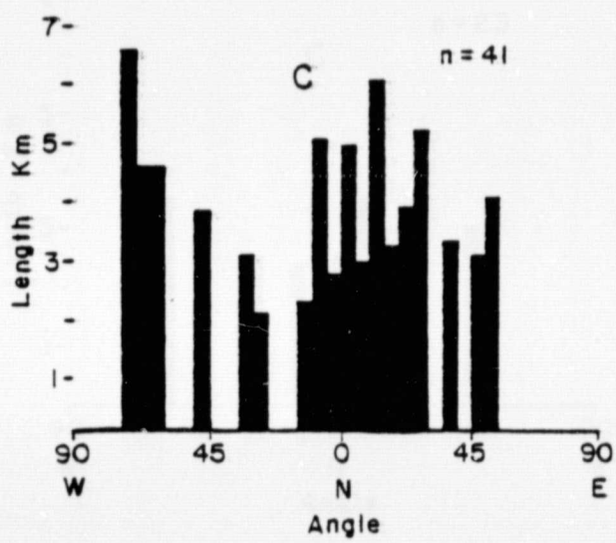
C
n=41
Length Km
7
5
3
1
90
45
0
45
90
W
N
E
Angle

20

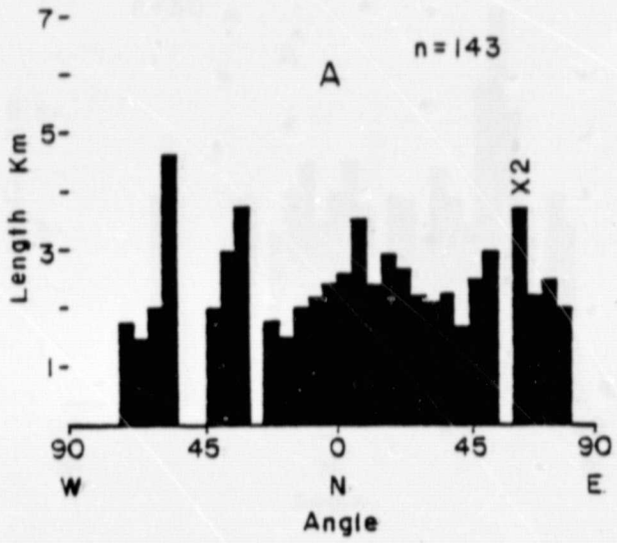
A
n=143
X2
Length Km
7
5
3
1
90
45
0
45
90
W
N
E
Angle

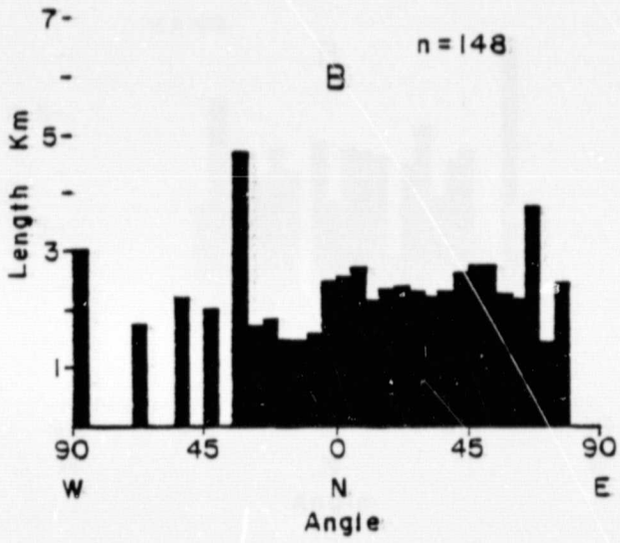
B
n=148
Length Km
7
5
3
1
90
45
0
45
90
W
N
E
Angle

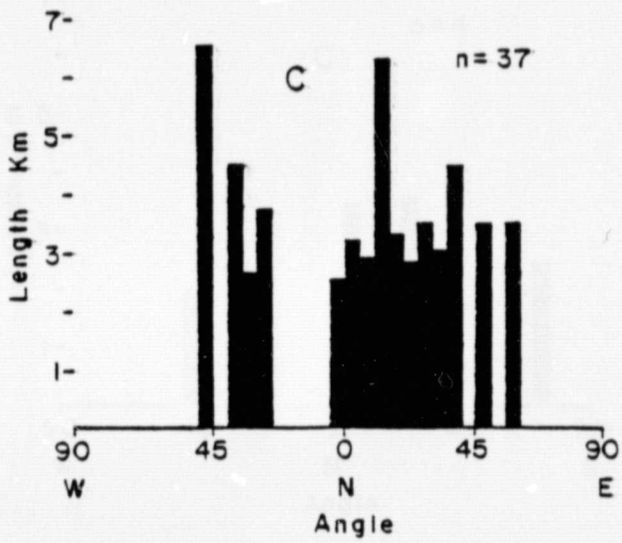
C
n=37
Length Km
7
5
3
1
90
45
0
45
90
W
N
E
Angle

21

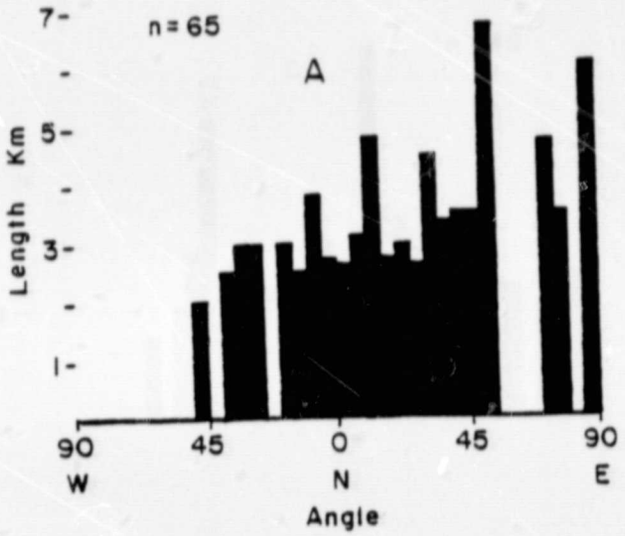

22

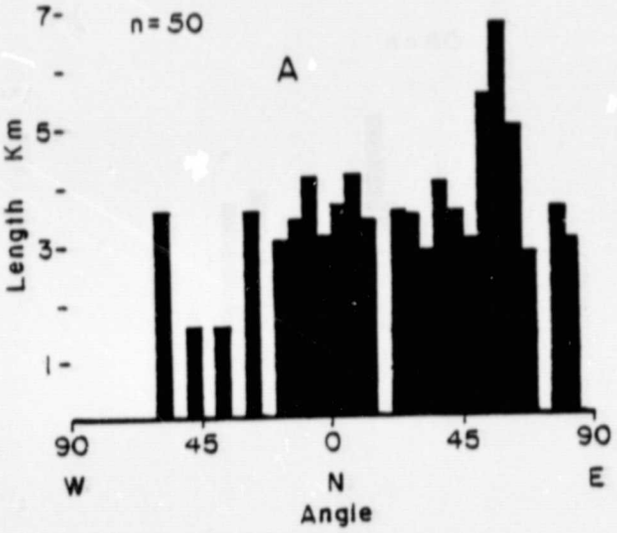

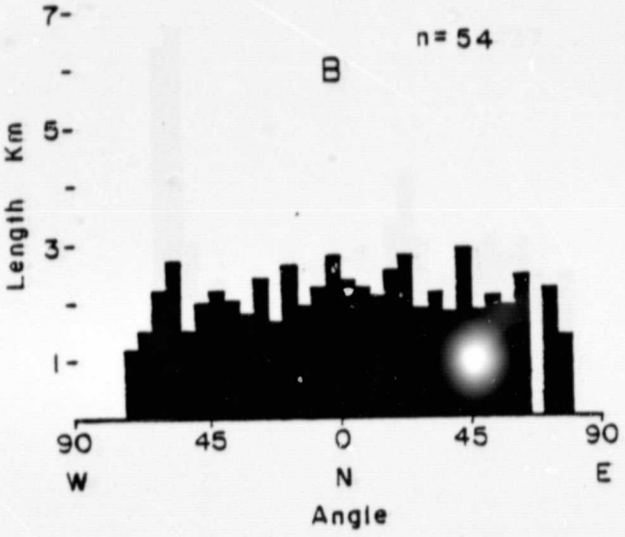

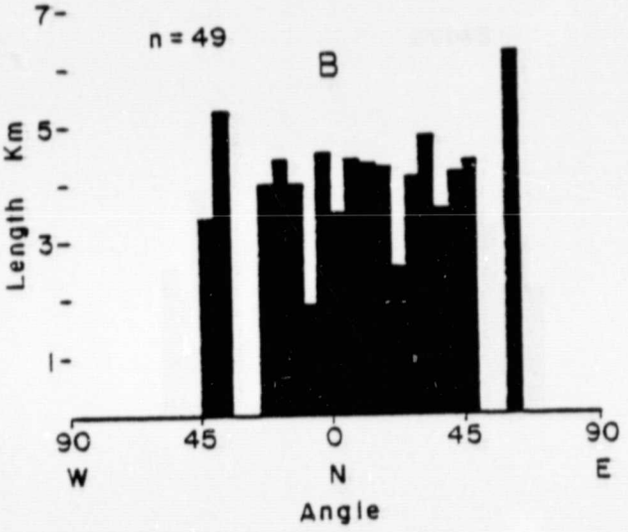

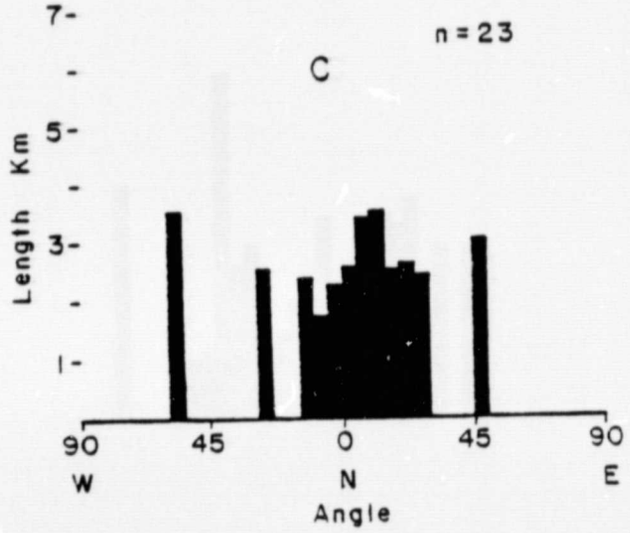

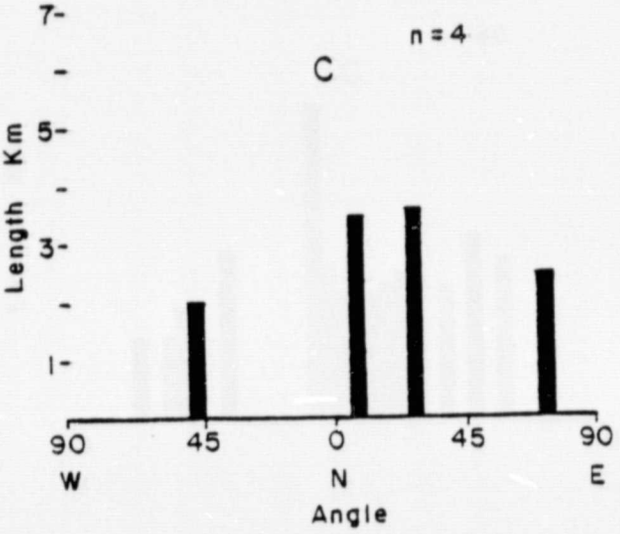

ORIGINAL PAGE IS
OF POOR QUALITY

23

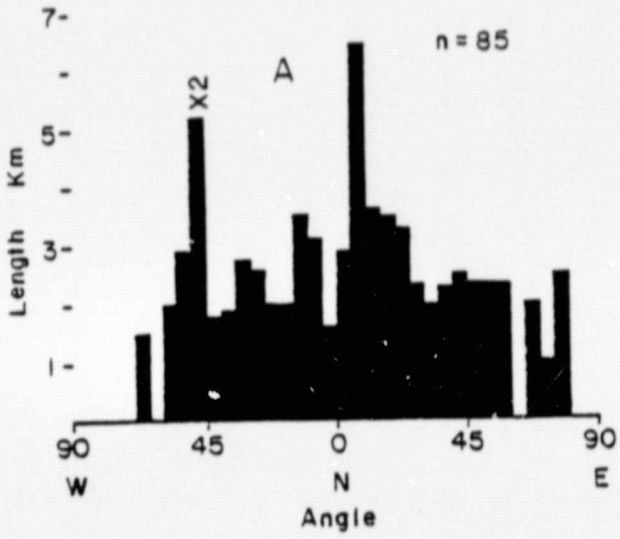
A
n = 85
X2
Length Km
7
5
3
1
90
45
0
45
90
W
N
E
Angle

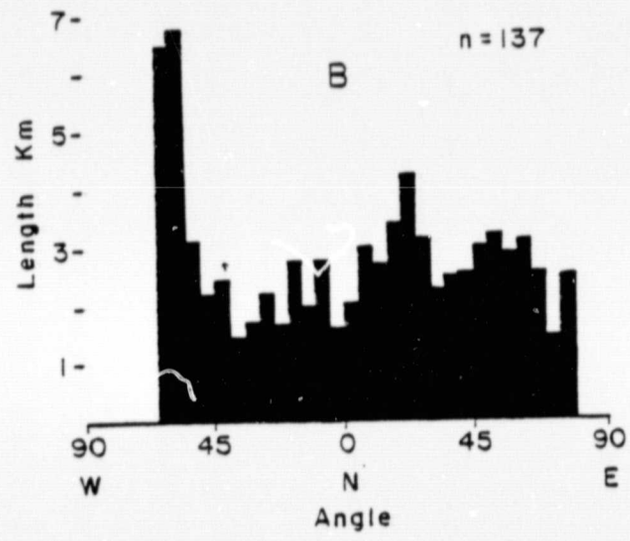
B
n = 137
Length Km
7
5
3
1
90
45
0
45
90
W
N
E
Angle

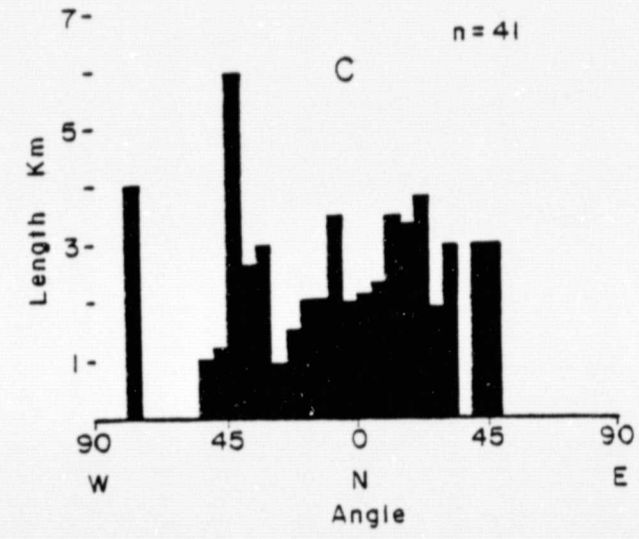
C
n = 41
Length Km
7
5
3
1
90
45
0
45
90
W
N
E
Angle

24

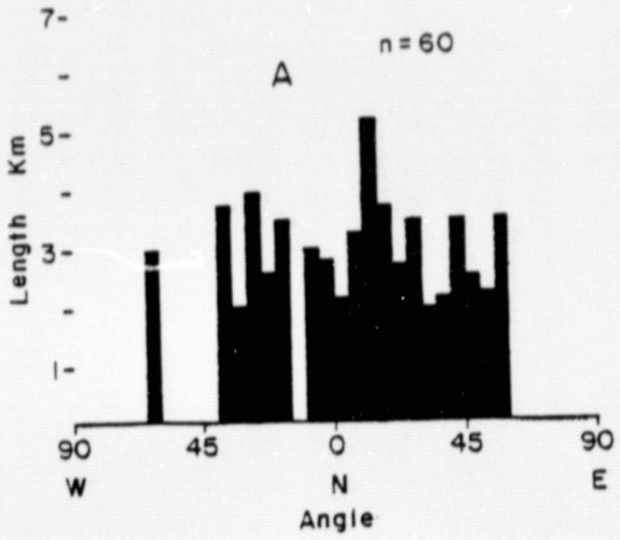
A
n = 60
Length Km
7
5
3
1
90
45
0
45
90
W
N
E
Angle

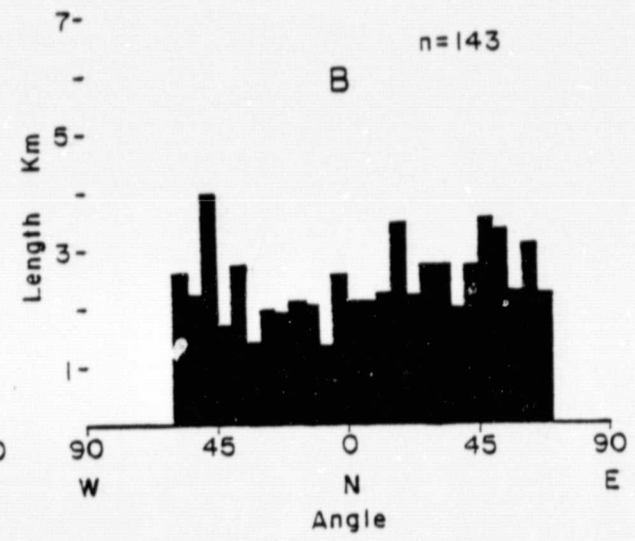
B
n = 143
Length Km
7
5
3
1
90
45
0
45
90
W
N
E
Angle

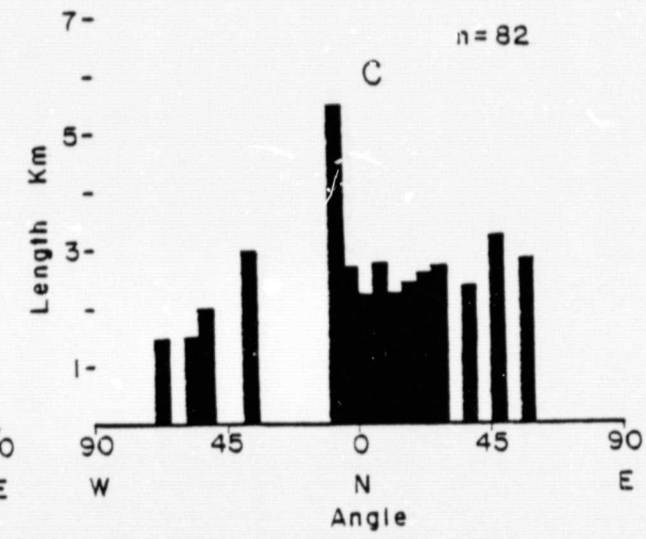
C
n = 82
Length Km
7
5
3
1
90
45
0
45
90
W
N
E
Angle

25

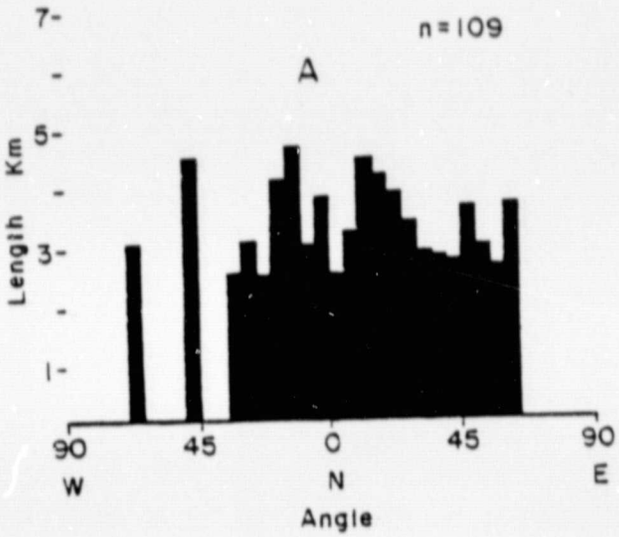
n=109
A
Length Km
7
5
3
1
90
W
45
0
N
45
90
E
Angle

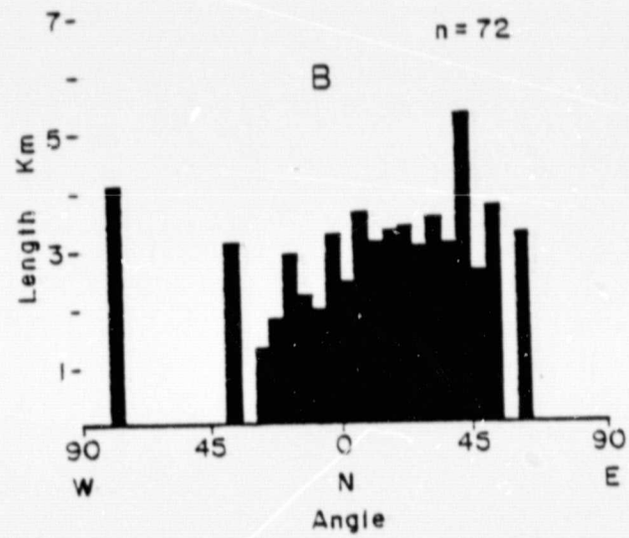
n=72
B
Length Km
7
5
3
1
90
W
45
0
N
45
90
E
Angle

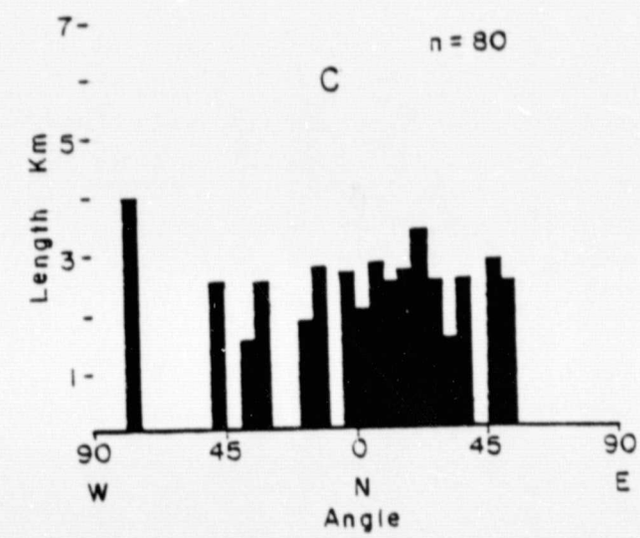
n=80
C
Length Km
7
5
3
1
90
W
45
0
N
45
90
E
Angle

26

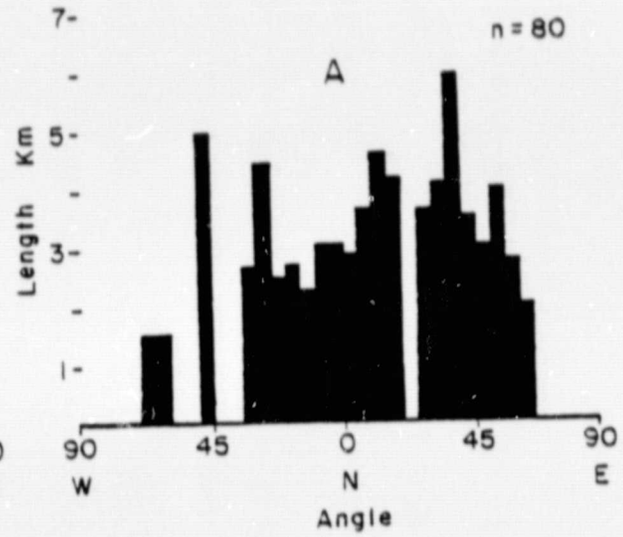
n=80
A
Length Km
7
5
3
1
90
W
45
0
N
45
90
E
Angle

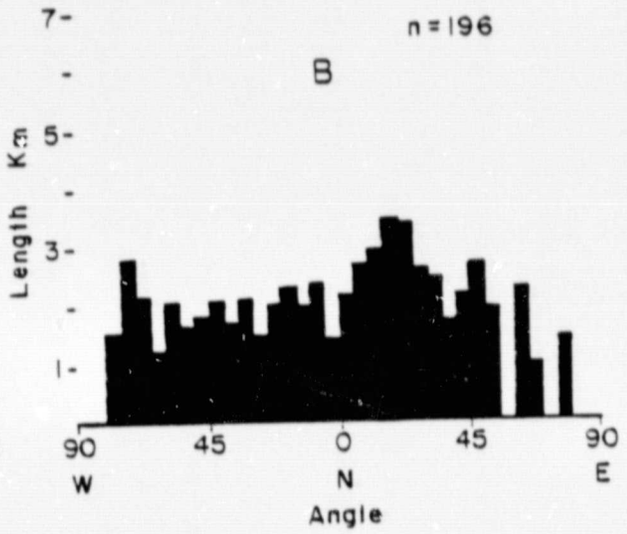
n=196
B
Length Km
7
5
3
1
90
W
45
0
N
45
90
E
Angle

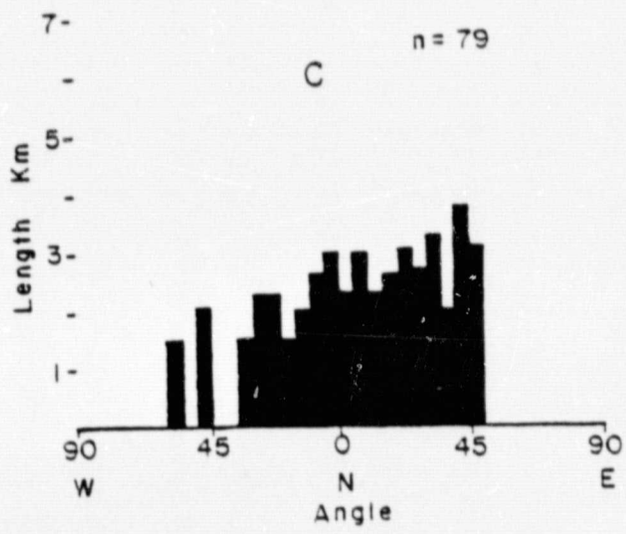
n=79
C
Length Km
7
5
3
1
90
W
45
0
N
45
90
E
Angle

27

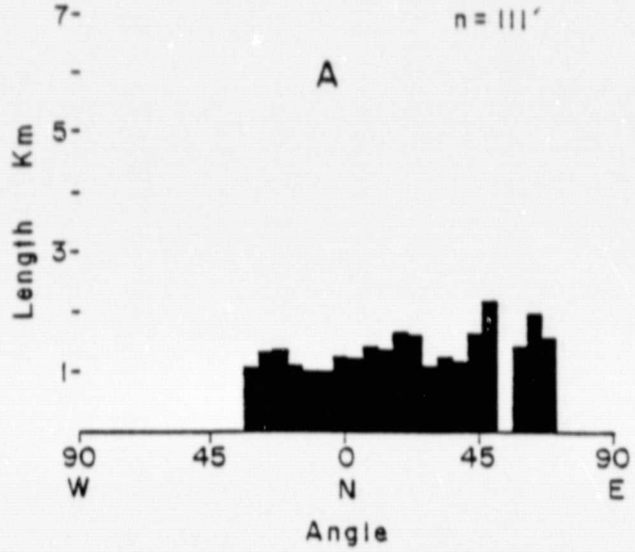
n = 111
A
Length Km
7
5
3
1
90 W
45
0 N
45
90 E
Angle

28

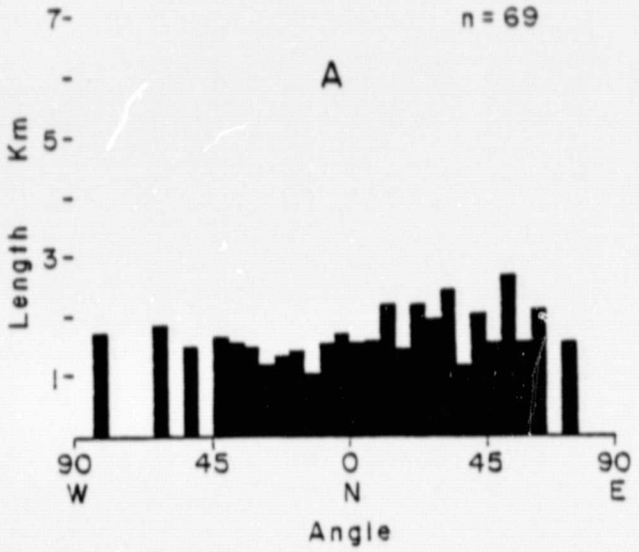
n = 69
A
Length Km
7
5
3
1
90 W
45
0 N
45
90 E
Angle

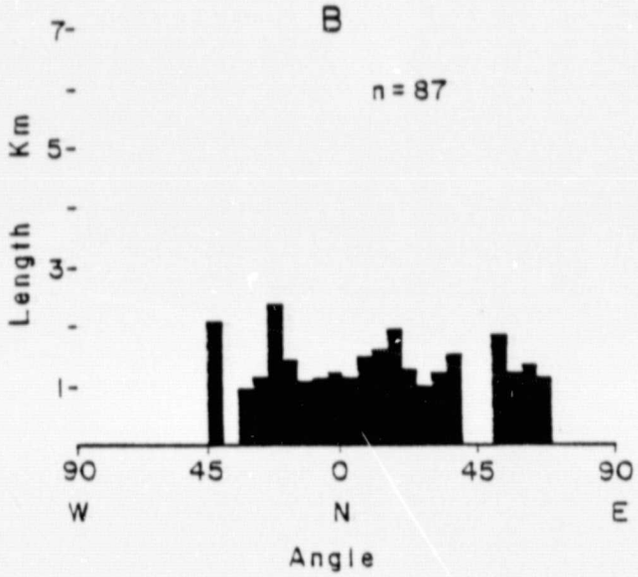
B
n = 87
Length Km
7
5
3
1
90 W
45
0 N
45
90 E
Angle

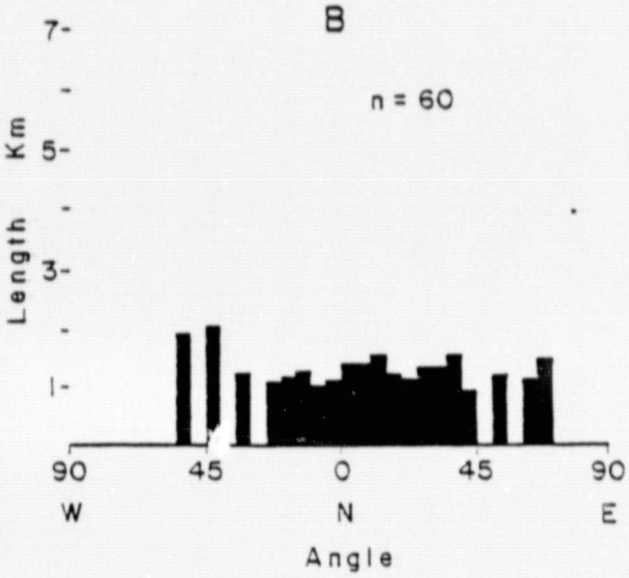
B
n = 60
Length Km
7
5
3
1
90 W
45
0 N
45
90 E
Angle

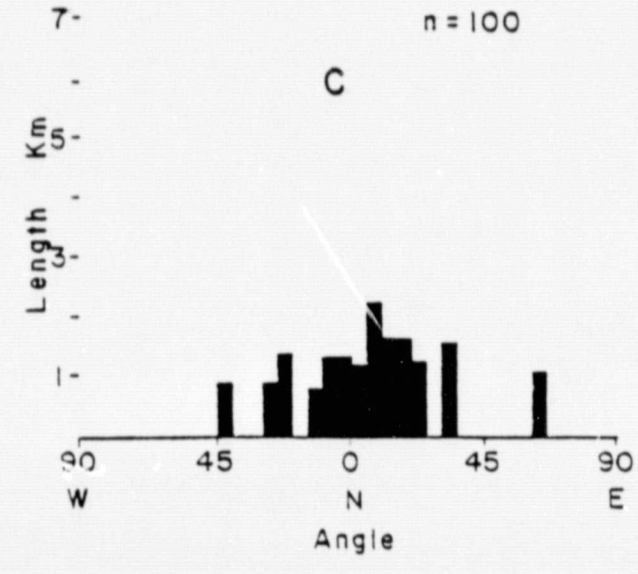
n = 100
C
Length Km
7
5
3
1
90 W
45
0 N
45
90 E
Angle

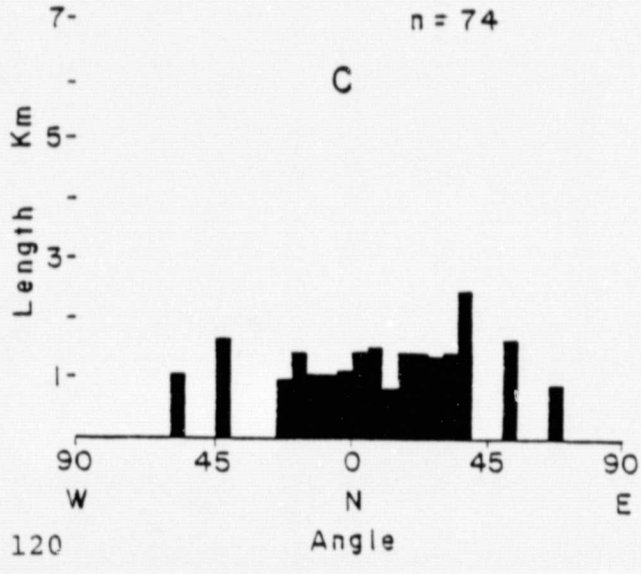
n = 74
C
Length Km
7
5
3
1
90 W
45
0 N
45
90 E
Angle

29

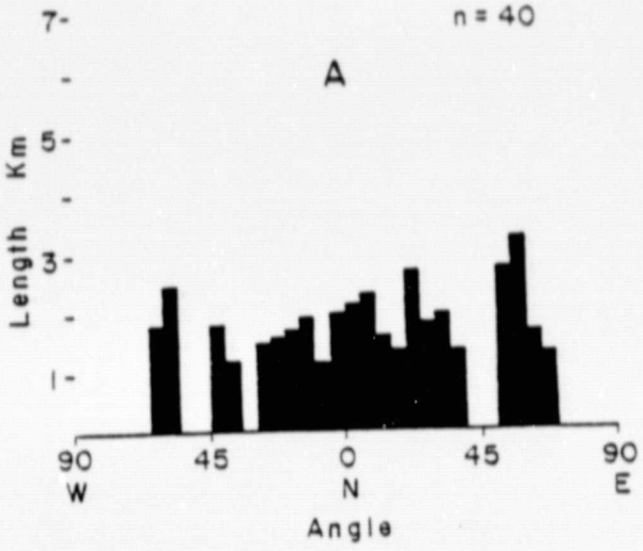
n = 40
A
Length Km
7
5
3
1
90 W
45
0 N
45
90 E
Angle

30

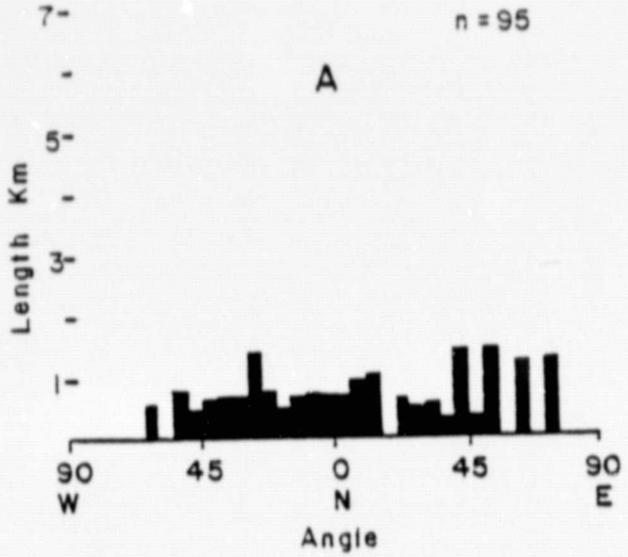
n = 95
A
Length Km
7
5
3
1
90 W
45
0 N
45
90 E
Angle

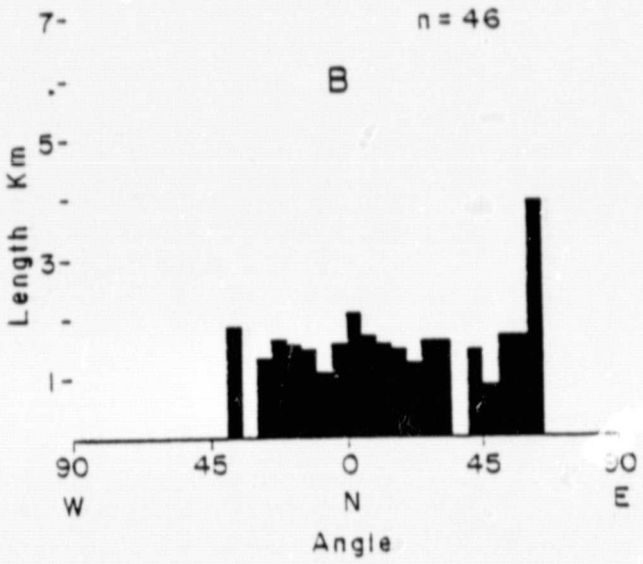
n = 46
B
Length Km
7
5
3
1
90 W
45
0 N
45
90 E
Angle

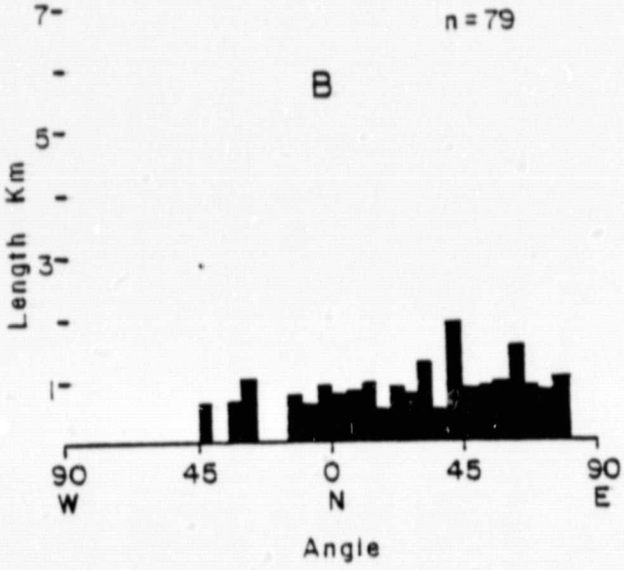
n = 79
B
Length Km
7
5
3
1
90 W
45
0 N
45
90 E
Angle

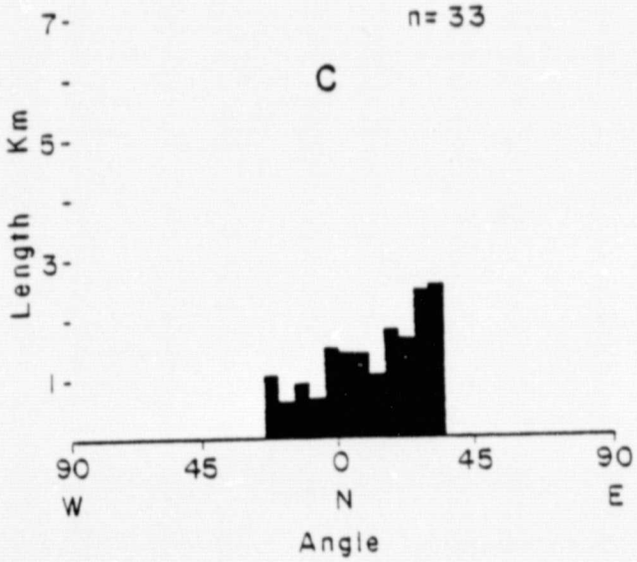
n = 33
C
Length Km
7
5
3
1
90 W
45
0 N
45
90 E
Angle

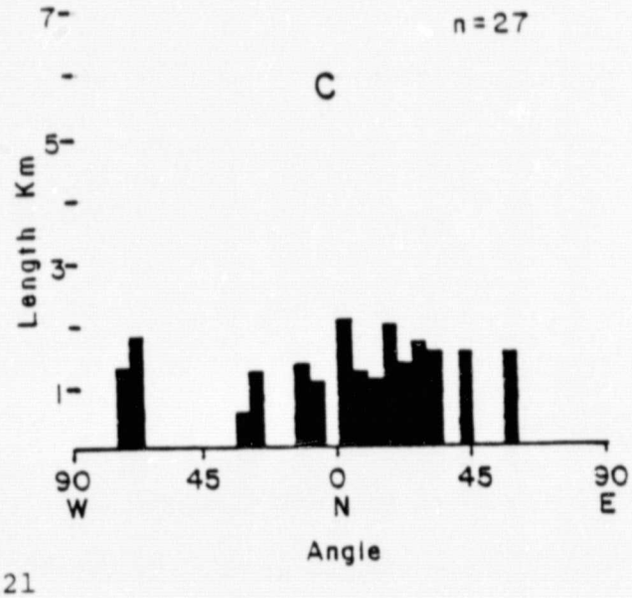
n = 27
C
Length Km
7
5
3
1
90 W
45
0 N
45
90 E
Angle

31

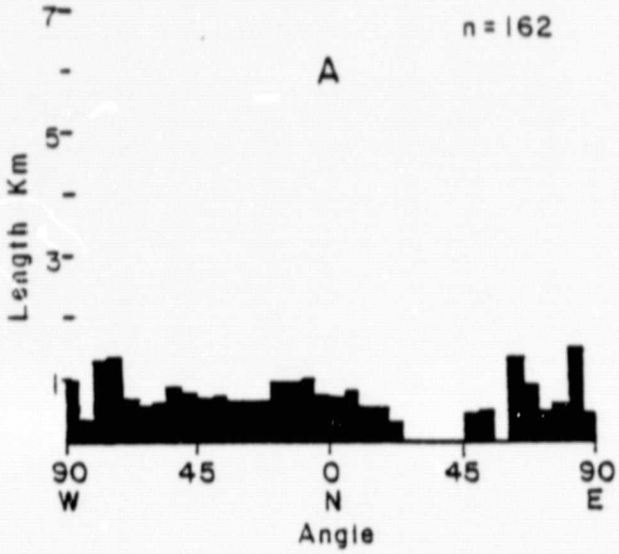
n = 162
A
Length Km
7
5
3
1
90 W
45
0 N
45
90 E
Angle

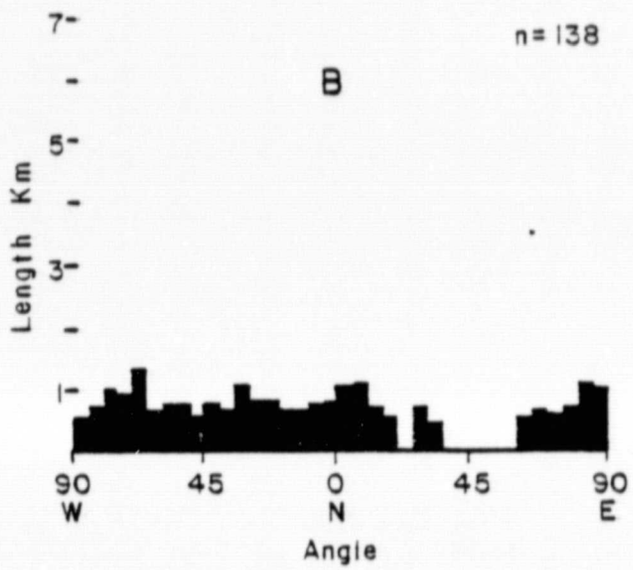
n = 138
B
Length Km
7
5
3
1
90 W
45
0 N
45
90 E
Angle

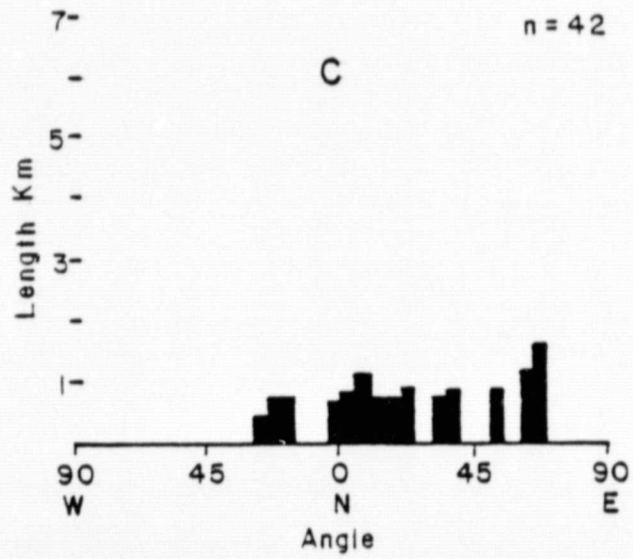
n = 42
C
Length Km
7
5
3
1
90 W
45
0 N
45
90 E
Angle

32

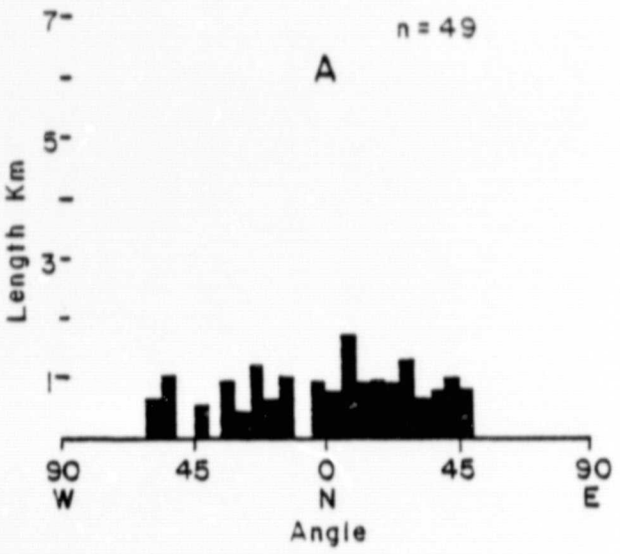
n = 49
A
Length Km
7
5
3
1
90 W
45
0 N
45
90 E
Angle

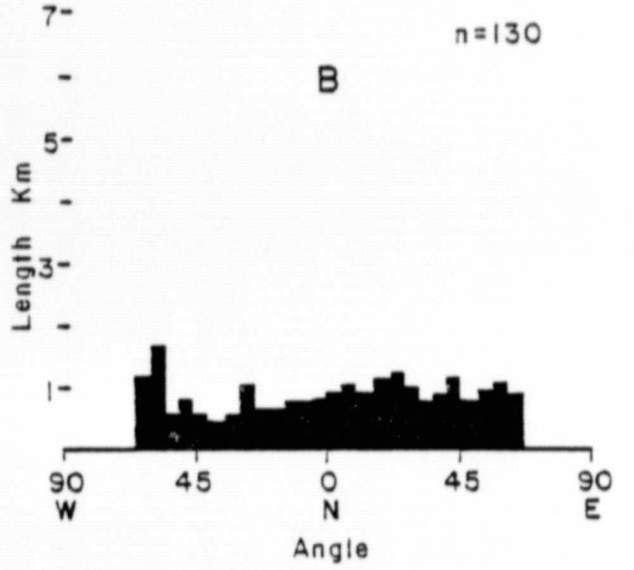
n = 130
B
Length Km
7
5
3
1
90 W
45
0 N
45
90 E
Angle

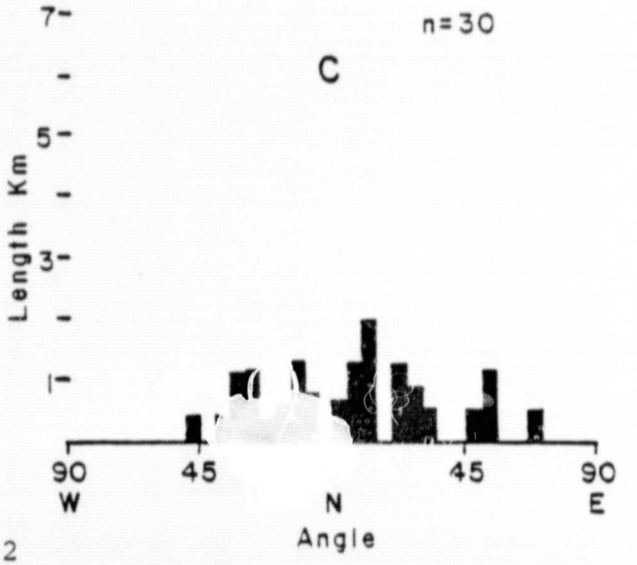
n = 30
C
Length Km
7
5
3
1
90 W
45
N
45
90 E
Angle